Membrane Based Separation of Oily Wastewater, Coal-solvent Mixture and Fruit Juice

A Thesis Submitted for the Award of the Degree

of

DOCTOR OF PHILOSOPHY

By

Vijay Singh

Department of Chemical Engineering
Indian Institute of Technology Guwahati
Assam – 781 039, INDIA

Membrane Based Separation of Oily Wastewater, Coal-solvent Mixture and Fruit Juice

A Thesis Submitted for the Award of the Degree

of

DOCTOR OF PHILOSOPHY

By

Vijay Singh
Roll No.: 09610716

Department of Chemical Engineering
Indian Institute of Technology Guwahati
Assam – 781 039, INDIA

May 2014

Dedication

To My Family Members

Department of Chemical Engineering
Indian Institute of Technology Guwahati
Guwahati, Assam-781 039, India

CERTIFICATE

This is to certify that the thesis entitled "***Membrane Based Separation of Oily Wastewater, Coal-solvent Mixture and Fruit Juice***", being submitted by ***Mr. Vijay Singh*** for the award of Ph.D. degree, is a record of bonafide research carried out by him at the Department of Chemical Engineering, Indian Institute of Technology Guwahati, under my guidance and supervision. The work embodied in this thesis has not been submitted to any other University or Institute for the award of any other degree or diploma.

Date:

Dr. Chandan Das
Associate Professor
Department of Chemical Engineering
Indian Institute of Technology Guwahati

ACKNOWLEDGEMENT

I take this opportunity to express my deep sense of respect and gratitude to my thesis supervisor, Dr. Chandan Das, for providing inspiration and valuable guidance throughout the course of this investigation. I am also indebted to them for their constant suggestions and encouragements. The experience of working with them, I strongly believe, will have far reaching influence in my future life. It has really been a remarkable experience working with him.

I express my sincere gratitude and indebtedness to the chair of doctoral committee, Dr. Bishnupada Mandal, for his critical comments and valuable suggestions at various stages of my work. His observations and comments helped me to establish the overall direction of the research and move forward within depth studies.

I would like to express my sincere thanks to Dr. Animes Kumar Golder, for serving as a member of my doctoral committee and generously sharing knowledge on experimental technique.

Furthermore, I am very grateful to another member of the doctoral committee, Dr. Saswati Chakraborty, Department of Civil Engineering, for providing insightful comments both of my work as well as on the thesis.

I would like to express my gratitude and indebtedness to Professor Vijay S. Moholkar, Head, Chemical Engineering Department.

I am obliged to Dr. Mihir Kumar Purkait and Dr. Ramagopal Uppaluri, of Chemical Engineering Department for their valuable suggestions.

I must also thank to all the faculty member, staff members and scientific officer of the Chemical Engineering Department for their genuine help during my entire research period.

I am grateful to Central Instruments Facility (CIF) for providing the analytical facilities towards this work. I am grateful to Indian Institute of Technology Guwahati, for providing the research fellowship.

I am thankful to Oil and Natural Gas Corporation Limited, Eastern region, Nazira, Assam, India and M/s TATA steel R&D, Jamshedpur, India for providing the oil water emulsion, coal and iron ore slime to research purpose.

I am happy to oblige my friends, Mr. Mahesh Kumar Garrai, Mr. Venkata Swamy Nalajala, Mrs Anjali Dasari, Mr. Ananth Praveen Kumar, Mr. Ardhendu Sekhar Giri, Mr. Naresh Kumar Meena, Mr. Arijit Das, Mr. Sujoy Bose, Mr. Sankar Chakma, and Mr. Suman Saha for their enriching friendship and friendly assistance in the experimental run. I am also thankful to my senior research scholars, Mr. Barun Kumar Nandi, Mr. Monash Purushothaman, Mr. Somen Jana and Mr. Debasish Ghosh for their friendly behaviour and assistance.

I greatly appreciate to Mr. Punit Kumar Jain, Mr. Abhijit Saurav, Mr. Harendra Rathore and Mr Sandup Tshering Bhutia for their support at several stages of the experiment and analysis.

Finally, I express my humble regards and respect to my parents, my wholehearted appreciation to my sisters and beloved wife. They have always encouraged me throughout this work with their selfless love and affection.

Indian Institute of Technology Guwahati ***Vijay Singh***

May 2014

CONTENTS

		Page No.
Nomenclature		i
List of Figures		iii
List of Tables		vii
Abstract		ix
CHAPTER 1	**INTRODUCTION AND OBJECTIVES**	**1-24**
1.1	Introduction	1
1.1.1	Membrane separation technology	5
1.1.2	Membrane fouling	11
1.1.3	Membrane cleaning	13
1.1.4	Applications of membrane separation technology	14
1.1.4.1	Cross flow microfiltration of industrial oily wastewater	14
1.1.4.2	Separation of coal-solvent mixture by membranes	17
1.1.4.3	Clarification of fruit juice	19
1.1.5	Merits and demerits of various separation processes	22
1.1.6	Selection of membrane module for oily wastewater treatment, coal-solvent mixture separation and clarification of fruit juice	22
1.2	Objectives of the current research	23
1.2.1	Cross flow microfiltration of industrial oily wastewater	23
1.2.2	Separation of coal-solvent mixture by membranes	24
1.2.3	Clarification of fruit juice	24
CHAPTER 2	**CROSS FLOW MICROFILTRATION OF INDUSTRIAL OILY WASTEWATER**	**25-49**
2.1	Experimental	25
2.1.1	Oily wastewater	25
2.1.2	Membrane	26
2.1.3	Procedure	26
2.2	Analysis	29

2.2.1 Particle size analysis 29
2.2.2 Chemical oxygen demand (COD) 30
2.2.3 Quantitative analysis 31
2.2.4 Measurement of oil concentration 31
2.3 Theoretical consideration 31
2.3.1 Concentration polarization model 32
2.3.2 Brownian diffusion model 34
2.3.3 Shear induced diffusion model 35
2.3.4 Proposed model 36
2.4 Results and discussion 38
2.4.1 Transient flux decline 38
2.4.2 Steady state permeate flux with the variation of Reynolds number and TMP drops 39
2.4.3 Steady state permeate concentration with the variation of Reynolds number and TMP drops 40
2.5 Model consideration 42
2.5.1 Variation of permeate flux with TMP drops for laminar and turbulent flow regime 42
2.6 Permeate quality 47
2.7 Summary 48

CHAPTER 3 MEMBRANE BASED SEPARATION OF COAL-SOLVENT MIXTURE 51-89

3.1 Experimental 52
3.1.1 Materials 52
3.1.2 Membrane preparation and characterization 53
3.1.3 Extraction experiments 57
3.1.4 Experimental set up 59
3.1.5 Coal extraction and solvent recovery mechanism 61
3.1.6 Analysis 62
3.2 Development of membrane based technology for the separation of coal from organic solvent 64

3.2.1 Results and discussion 64
3.2.1.1 Effect on pore size distribution with sintering temperatures 64
3.2.1.2 Chemical stability 66
3.2.1.3 Solvent recovery after extraction 67
3.2.1.4 Solvent recovery at different extraction stages 68
3.2.1.5 Microfiltration results 70
3.2.1.6 Fourier transforms infrared spectroscopy (FTIR) analysis 74
3.2.2 Summary 75
3.3 Fabrication of cost effective IOS ceramic membrane for the recovery of organic solvent used in coke production 77
3.3.1 Results and discussion 77
Membrane fabrication and characterization
3.3.1.1 Selection of membrane compositions 77
3.3.1.2 Pore size distribution, porosity, hydraulic permeability and corrosion stability 78
3.3.1.3 SEM and EDX analysis 81
Coal extraction followed by membrane separation
3.3.1.4 Effect of solvent on coal extraction 83
3.3.1.5 Proximate and ultimate analysis of raw and extracted coal (coke) 84
3.3.1.6 Fourier transform infrared spectroscopy (FTIR) analysis 85
Membrane cleaning study and preliminary cost estimation
3.3.1.7 Membrane cleaning 87
3.3.1.8 Preliminary cost estimation 88
3.3.2 Summary 89

CHAPTER 4 FRUIT JUICE CLARIFICATION 91-161

4.1 Materials and methods 92
4.1.1 Materials 92
4.1.2 Systematic scheme of pretreatment 92
4.1.3 Experimental set up 94
4.1.4 Experimental methods 97
4.1.5 Sample analysis 100

4.1.6 Pretreatment methods 102
4.1.6.1 Pretreatment through packed beds 102
4.1.6.2 Pretreatment with fining agents 102
4.1.6.3 Pretreatment by centrifugation 104
4.1.6.4 Pretreatment by combination of centrifugation and fining agent addition 104
4.1.7 Process evaluation 105
4.1.7.1 Theory for membrane transport equation at laminar flow regime 106
4.1.7.2 Theory for membrane transport equation at turbulent flow regime 111
4.2 Pretreatment of mosambi juice 113
4.2.1 Results and discussions 113
4.2.1.1 Effect on relative viscosity and clarity of clarified juice with variation of feed flow rate through packed column, supported with glass beads (0.0035 m) 113
4.2.1.2 Effect on relative viscosity and clarity of clarified juice with variation of feed flow rate in packed column, supported with molecular sieve (0.013×0.0015 m) 115
4.2.1.3 Effect on viscosity and clarity of clarified juice passing through two packed columns in series 117
4.2.1.4 Variation of relative viscosity and clarity on fining agent addition 119
4.2.1.5 Effects of centrifugation 121
4.2.1.6 Effects on physicochemical properties of treated raw juice for combined pretreatment operation (fining agent addition and centrifugation) 122
4.2.1.7 Quality analysis and cost estimation of juice pretreated with different methods 123
4.2.2 Summary 125
4.3 Performance of spiral wound UF membrane module in laminar flow regime 126
4.3.1 Results and discussions 126
4.3.1.1 Variation of permeate flux with time for with and without permeate recycle 126
4.3.1.2 Variation of VRF with time for with and without permeate 128

recycle
4.3.1.3 Resistance variation during membrane filtration for with and without permeate recycle 130
4.3.1.4 Variation of J_{exp} with J_{cal} using different diffusion models for with and without permeate recycle 132
4.3.1.5 Permeate quality 135
4.3.2 Summary 137
4.4 Performance of spiral wound UF membrane module in turbulent flow regime 139
4.4.1 Results and discussion 139
4.4.1.1 Variation of permeate flux with time for with and without permeate recycle 139
4.4.1.2 Variation of VRF with time for with and without permeate recycle 141
4.4.1.3 Resistance variation during membrane filtration for with and without permeate recycle 144
4.4.1.4 Variation of J_{exp} with J_{cal} using different diffusion models for with and without permeate recycle 146
4.4.1.5 Permeate quality 149
4.4.2 Summary 151
4.5 Comparison of spiral wound UF membrane performance at laminar and turbulent flow regime 153
4.6 Cleaning of fouled membranes 156
4.6.1 Effects of cleaning agent type on membrane permeability recovery 156
4.6.2 Optimization study of cleaning dose 158
4.6.3 Summary 161

CHAPTER 5 FINAL CONCLUSIONS 163-165

References 167-180

Appendix 181-183

List of publications from this work 185-187

NOMENCLATURE

u	Average fluid velocity (m/s)
d_s	Average pore diameter (µm)
K	Boltzman constant (1.38×10^{-23}, J/K)
D_B	Brownian diffusivity (m^2/s)
R_C	Cake resistance (m^{-1})
J_{cal}	Calculated flux ($m^3/m^2.s$)
L	Channel length (m)
D_c	Combined diffusivity (m^2/s)
ρ_w	Density of water (kg/m^3)
dt	Differential time (s)
D	Diffusivity (m^2/s)
d_e	Equivalent diameter (m)
J_{exp}	Experimental flux ($m^3/m^2.s$)
V_o	Feed volume (m^3)
$J(x)$	Flux ($m^3/m^2.s$)
J_f	Fouled membrane flux ($m^3/m^2.s$)
R_F	Fouling resistance (m^{-1})
k	Mass transfer coefficient ($m^2/m.s$)
Δ_{Pmax}	Maximum transmembrane pressure drop (kPa)
A_m	Membrane cross-sectional area (m^2)
L_p	Membrane permeability (m/Pa.s)
L_{pc}	Membrane permeability, after cleaning (m/Pa.s)
L_{pi}	Membrane permeability, initial (m/Pa.s)
R_M	Membrane resistance (m^{-1})
V_m	Membrane volume (m^3)
w_1	Membrane weight dry (kg)
w_2	Membrane weight wet (kg)
w	Module width (m)
M	Molecular weight
n	Number of pores
T	Operating temperature (K)
a	Particle diameter (m)
V_P	Permeate volume (m^3)
d_i	Pore diameter (µm)

V_R	Retentate volume (m^3)
R_o	Retention coefficent
D_s	Shear induced diffusivity (m^2/s)
C_b	Solute concentration in feed (mg/L)
C_p	Solute concentration in permeate (mg/L)
C_m	Solute concentration on membrane surface (mg/L)
h	Spacer thickness (m)
J_{ss}	Steady state flux ($m^3/m^2.s$)
R_T	Total membrane resistance (m^{-1})
ΔP	Transmembrane pressure drop (kPa)
R	Universal gas constant (8.314 J/mol.K)
J_w	Water flux ($m^3/m^2.s$)

Greek Symbols

ρ_m	Apparent density (kg/m^3)
ρ	Density of solvent (kg/m^3)
δ	Film thickness (m)
$\Delta\pi$	Osmatic pressure (kPa)
γ_0	Shear rate (s^{-1})
μ	Viscosity of fluid (Pa.s)
μ_w	Water viscosity (Pa.s)

Abbreviation

Re	Reynolds number
Sc	Schmidt number
Sh	Sherwood number
TMP	Transmembrane pressure
VRF	Volume reduction factor

List of Figures

Figure No.	Title	Page No.
Figure 2.1	Schematic diagram of cross flow membrane module.	27
Figure 2.2	Droplet size distribution in oily wastewater. Inset: Pore size distribution of polyamide membrane used for microfiltration.	30
Figure 2.3	Schematic for concentration polarization over the membrane surface.	32
Figure 2.4	Transient flux decline profile for MF at 69 kPa TMP drops	39
Figure 2.5	Variation of steady state permeate flux with TMP drops at different Reynolds numbers.	40
Figure 2.6	Variation of oil concentration in permeate with Reynolds number.	41
Figure 2.7	Variation of steady state permeate flux with Reynolds number for various TMP drops.	45
Figure 2.8	Variation of steady state permeate flux with TMP drops at Reynolds number of 4487.	45
Figure 2.9	Variation of steady state permeate flux with TMP drops at Reynolds number of 5769.	46
Figure 3.1	Apparatus for the extraction of coal under total reflux condition.	58
Figure 3.2	Flow sheet diagram of experimental schemes: (1) E1, E2, E3: Extraction stages 1, 2 and 3; (2) M: microfiltration membrane cell; (3) SS: Two 500 mesh stainless steel screens.	59
Figure 3.3	Schematic of the batch experiment set up: (1) nitrogen cylinder, (2) pressure gauge, (3) control valve, (4) inlet feed, (5) membrane cell, (6) mechanical stirrer, (7) ceramic membrane, (8) recovered solvent.	60
Figure 3.4	SEM photographs of the prepared ceramic membrane sintered at (a) 900ºC, (b) 950ºC and (c) 1000ºC.	65

Figure 3.5	Pore size distribution of the prepared membrane sintered at different temperatures.	65
Figure 3.6	Effect on solvent recovery (%) for the variation of solvent/coal ratio.	68
Figure 3.7	Variation of residual coal collected on 500 mesh SS surface and dissolved coal with solvent/coal ratio.	70
Figure 3.8	Transient flux decline with time for variation of coal/solvent (1:9 and 1:10) for three extraction stages.	71
Figure 3.9	Development of cake and fouling resistance with time at coal/solvent (1:9 and 1:10) for three extraction stages.	72
Figure 3.10	Variation of solvent (NMP) recovery with optimum solvent/coal ratios for three extraction stages.	73
Figure 3.11	FTIR analysis of coal, pure NMP and permeate.	75
Figure 3.12	Membrane pore size distribution at different sintering temperatures.	79
Figure 3.13	SEM images of the synthesized membrane surface at different sintering temperature (°C): (a) 700; (b) 800 and (c) 900.	81
Figure 3.14	FTIR spectra of coal samples, pure and recovered (permeate) NMP.	85
Figure 4.1	Flowchart for extraction of mosambi juice by different pretreatment methods.	93
Figure 4.2	Schematic flow diagram of packed bed column filled with packing materials.	95
Figure 4.3	Schematic diagram of spiral wound ultrafiltration membrane: (1) feed tank, (2) UF spiral wound membrane module, (3) cooling tank, (4) measuring cylinder, (5) plunger pump, (6) inlet pressure gauge, (7) outlet pressure gauge, (8) retentate flow rate, (9) permeate flow rate, (10) retentate control valve, (11) feed control valve, (12) drainage valve.	96
Figure 4.4	Variation of relative viscosity (a) and clarity (b) with operating time for different flow rates in a glass bead loaded column.	114

Figure 4.5	Variation of relative viscosity (a) and clarity (b) with operating time at different flow rates in a packed bed column supported with molecular sieve.	116
Figure 4.6	Effect on viscosity and clarity with time in series of glass and molecular sieve packed beds at 50 cm^3/hr.	118
Figure 4.7	Particle size distribution of fresh mosambi juice and pretreated juice with packed column.	119
Figure 4.8	Variation of (a) relative viscosity and (b) clarity with fining agents dose.	120
Figure 4.9	Variation of steady state viscosity and clarity with rpm.	122
Figure 4.10	Transient flux decline (a) with and (b) without permeate recycle.	127
Figure 4.11	Variation of VRF with operating time (a) with and (b) without permeate recycle.	129
Figure 4.12	Variation of total resistance with operating time for (a) with and (b) without permeate recycle.	131
Figure 4.13	Particle size distribution of pectin in feed.	133
Figure 4.14	Variation of J_{exp} with J_{cal} using Brownian, shear induced and combined diffusion models for (a) with and (b) without permeate recycle.	134
Figure 4.15	Transient flux decline (a) with and (b) without permeate recycle.	140
Figure 4.16	Variation of VRF with operating time (a) with (b) without permeate recycle.	142
Figure 4.17	Variation of total resistance with operating time for (a) with and (b) without permeate recycle.	145
Figure 4.18	Variation of J_{exp} with J_{cal} using Brownian, shear induced and combined diffusion models for (a) with and (b) without permeate recycle.	147
Figure 4.19	Variation of cleaning efficiency with cleaning agent type.	158
Figure 4.20	Optimization of SDS and EDTA concentrations to recover the original permeate flux.	160

List of Tables

Table No.	Title	Page No.
Table 1.1	Merits and demerits of various separation processes	22
Table 2.1	Physical properties of industrial oily wastewater	26
Table 2.2	Operating conditions for cross flow microfiltration of industrial oily wastewater	28
Table 2.3	Model constants for laminar and turbulent flow conditions	43
Table 2.4	Variation of retention oil with TMP drops and cross flow velocity	47
Table 3.1	Composition of raw materials used for fabrication of inorganic membrane	54
Table 3.2	Variation of membrane porosity in HCl, NaOH and NMP at different sintering temperatures	66
Table 3.3	Comparison of EDX analysis of fresh membrane, pH=2, pH=12 and pure NMP dip membrane sintered at 1000ºC after seven days	67
Table 3.4	Selection of suitable membrane compositions	78
Table 3.5	Variation of porosity, pore size and hydraulic permeability with sintering temperature	80
Table 3.6	EDX analysis results of the fabricated membrane (sintered at 900ºC) before and after the corrosion test	82
Table 3.7	Results of solvent extraction and membrane separation of the extract phase	83
Table 3.8	Proximate and ultimate analysis of raw coals and after extracted coals (coke) in Expt. No. 1	84
Table 3.9	Preliminary cost estimation of the synthesized IOS ceramic membrane	88
Table 4.1	Physiochemical properties of raw mosambi juice	93
Table 4.2	Operating conditions for clarification of mosambi juice by different pretreatment methods	98
Table 4.3	Operating conditions for clarification of juice through spiral	100

	wound UF membrane	
Table 4.4	Variation in physicochemical properties of mosambi juice and cost estimation after applied different pretreatment methods	124
Table 4.5	Comparison of physiochemical properties of permeates at steady state with and without permeate recycle (laminar)	136
Table 4.6	Comparison of physiochemical properties of permeates at steady state with and without permeate recycle (turbulent)	150
Table 4.7	Comparison results for with and without permeate recycle at laminar and turbulent flow regime	153

ABSTRACT

The work reported in this thesis can broadly be classified into three distinct studies. In the first study, treatment of industrial oily wastewater for onshore oil production supplied by Oil and Natural Gas Corporation (ONGC) Eastern region, Nazira, Assam, India is done by cross flow filtration cell. Membrane performance and permeate quality are compared at laminar and turbulent flow regime with variation of transmembrane pressure drops. Different diffusion models are assumed to predict the theoretical flux and compared with experimental flux values. In the second study, a membrane based technology for recovery of organic solvent from coal-solvent mixture is developed. Membrane performance is analysed in terms of transient flux decline. The dose of solvent/coal (v/w) is optimized to achieve maximum solvent recovery (%). Recovered organic solvent is again reused for improvement of coal properties in subsequent extraction stages. Fourier transform infrared spectroscopy analysis of permeate, coal and organic solvent are done to confirm the absence of coal in permeate. A low cost ceramic membrane is developed from steel industry waste iron ore slime (IOS) and is applied to recover of organic solvent from coal-solvent mixture. Prepared membranes are sintered at three different temperatures (700, 800 and 900ºC) and are characterized. Two different coals, such as, sub-bituminous coal (A) and bituminous coal (B) are used for extraction purpose. Proximate and ultimate analyses of coals are done before and after extraction to verify the moisture, ash, mineral matter, sulphur, carbon, and gross calorific content. Fourier transform infrared spectroscopy analysis of both coals (A and B), permeate and organic solvent are done separately to verify the

absence of coal particle in permeate sample. Last study is the fruit juice clarification through membrane. Before juice clarification, pretreatment is necessary. Different pretreatment methods are applied for clarification of juice and physicochemical properties are compared. During juice clarification, the spiral wound ultrafiltration membrane performance is evaluated at laminar and turbulent flow regimes for with and without permeate recycle.

***Keywords*:** Cross flow filtration; Transmembrane pressure drops; Membrane performance; Diffusion model; Theoretical flux; Solvent/coal; Extraction stage; Iron ore slime; Proximate and Ultimate analyses; Pretreatment; Physicochemical properties

Chapter 1

INTRODUCTION AND OBJECTIVES

Chapter 1

INTRODUCTION AND OBJECTIVES

In this chapter, a brief summary on the basic fundamentals, various terminologies and application involved in membrane technology along with the research problems is presented. The subsequent sections of this chapter present detailed literature review that include separation of oil-water emulsion, coal solvent recovery and fruit juice clarification by using polymer and ceramic membranes.

1.1 Introduction

Separation is a process to remove the undesired compounds from solute solvent mixture. Separation is based on size, vapour pressure, charge, density and freezing point [1]. Main objective of separation is concentration, purification, fractionation and reaction mediation. During concentration, preferred component present in low concentration and solvent are separated. In purification, unwanted product has been removed from solution. Mixture is separated from binary components by fractionation. In reaction mediation, chemical reaction is involved with a continuous removal of product. Various separation processes are applied such as, electrocoagulation [2], electrofloation [3], centrifugation [4], adsorption [5], absorption [6], leaching/ extraction [7], precipitation [8], crystallization [9], drying [10], sedimentation [11], ion

exchange [12], chromatography [13] and biological (aerobic/anaerobic) [14]. A brief overview of each process is cited here.

Electrocoagulation

Electrocoagulation (EC) generally refers to a group of technologies which uses an electrical current that coagulates suspended solids in wastewater due to charge neutralization. EC process has some limitations, such as, regular replacement of electrodes due to dissolution, coagulant generation and hydrogen gas evolution at the cathode/formation of hydroxyl ions.

Electro floatation

Electro floatation (EF) is preferred for the treatment of sewage as the density of suspended particles is low and also hydrophobic in nature. Its main applications are recovery of valuable ions such as, gold and silver from pollutant. Its main disadvantage is electrode maintenance and high replacement cost.

Centrifugation

Centrifugation is used to separate two immiscible liquids. During centrifugation, driving force is higher, resulting from the rotation of the liquid. Main disadvantage is high power consumption.

Adsorption

Adsorption may be defined as selective concentration or retention of one or more components on a solid surface. Common adsorbents are activated carbon, silica gel and activated alumina. During adsorption regeneration is the main problem.

Absorption

Absorption is the unit operation where one or more components of a gas stream are removed by being taken up (adsorbed) in a non-volatile liquid (solvent). Absorption can be either physical or chemical. Main drawback is high operating cost.

Precipitation

Precipitation is the formation of a solid in a solution, during a chemical reaction or by diffusion in a solid. Precipitation may occur rapidly from a supersaturated solution.

Leaching/ Extraction

Leaching is the process by which inorganic, organic contaminants are released from the solid phase. It is affected by pH and dissolved organic. Extraction involves physicochemical mechanism depends upon the characteristics of the solid and solvent.

Crystallization

The process of formation or production of crystals from a solution or a melt is called crystallization. Crystallization process consists of two major things such as,

nucleation and crystal growth. Crystal growth is the subsequent growth of the nuclei that succeed in achieving the critical cluster size.

Sedimentation

Sedimentation is the tendency for particles in suspension to settle out of the fluid in which they are entrained, and come to rest against a barrier. Different parameter affected the sedimentation, such as, particle size, temperature and currents.

Drying

Drying is a mass transfer process to remove solvent from any streams. Production of condensed milk involves evaporation, but production of milk powder involves drying. Main drawback is high power consumption.

Ion Exchange

Ion exchange is a separation process in which a solid containing mobile, replicable ion is contacted with solution of an ionizable species, when the mobile ions of solid are exchanged by charge (positive or negative) in the solution.

Chromatography

Chromatography technique is used for the separation of a mixture. Major common techniques are gas, liquid and supercritical fluid chromatography. They differ in the types of stationary and mobile phases.

Biological Treatment

During biological treatment, microorganisms mostly bacteria are used. Generally, biological treatment can be divided into aerobic and anaerobic methods, based on availability of dissolved oxygen. Its main applications are municipal sewage and industrial waste water treatment.

Each separation process has some merits and demerits. Membrane based separation is an attractive technology for removal of solute particles from solvent. Membrane market has been steadily growing in the last 25 years. It is fastest growing and fascinating fields in separation technology. Even in modern energy recovery techniques membranes are increasingly used. Global demand of different membrane modules was approximately US $15.6 billion in 2012. Driven by new development and innovations in material science, global demands are increasing continuously. It is expected that the market will grow around by 8% annually in next years. It is expected to approach upto US $21.22 billion by 2016 and reach US $25 billion by 2018 [15].

1.1.1 Membrane Separation Technology

Membrane plays an important role for treatment of industrial and domestic wastewater. Major advantages are [16-18]:

- Physical separation process
- Moderate operating temperature suitable for heat sensitive substances, i.e., separation at room temperature
- No change of phase
- Non-requirement of any chemical addition

- The capability of generating permeate of acceptable quality
- Easy to scale up
- Less energy requirement relative to conventional separation technologies

Membrane industry has been performing an excellent research and development work in this field. Membrane based separation process is successfully applied in various fields such as [19]:

- Treatment of industrial effluent such as tannery and oil-water emulsion
- Fruit juice clarification
- Desalination of sea water
- Biological application such as fat and protein recovery from milk
- Pharmaceutical industry waste

Membrane performance depends on several factors, such as, selectivity and flux [20, 21]. Selectivity of membrane is generally expressed in terms of retention and independent of transmembrane pressure (TMP) drops. Classification of membrane on based of pore size or the size of species separated are microfiltration, ultrafiltration, nanofiltration and reverse osmosis [22].

Microfiltration Membrane

Microfiltration (MF) membrane having the pore diameter in the range from 0.1 to 10 µm operated at TMP drops at 0.1 to 2.5 bar. It has ability to remove all bacteria, even though virus passes due to smaller size. Their main applications are biological waste water treatment and fruit juice clarification [23].

Ultrafiltration Membrane

Ultrafiltration (UF) membrane is used for the separation of suspended solids, colloids and bacteria. For completely removal of virus from waste streams, ultrafiltration membrane is used. The pore size of ultrafiltration membrane is in the range of 10 to 100 nm and operating TMP drops are 2 to 10 bar. Its main application is in dairy, food, textile, pharmaceutical and paint industry [24].

Nanofiltration Membrane

Pore diameter of nanofiltration (NF) fall in range of 1 to 10 nm and operating TMP drops are 10 to 25 bar. Divalent and larger ions can be removed and monovalent ions are passed through membrane pores. Its applications are pesticide elimination and colour retention from wastewater of dye industry [24].

Reverse Osmosis

Reverse osmosis (RO) is applied to demineralize water. Pore size of membrane is less than 2 nm and operating TMP drops is 30 to 100 bar. Its main application is purification of drinking water from mainly sea and brackish water. The membrane has certain limitations, such as fouling. To enhance the membrane performance pretreatment is require [25].

Membrane Modules

Membrane modules, such as, tubular, hollow fiber, flat sheet, spiral wound, spinning basket and rotating disk are available for various membrane applications.

Tubular module is assembled in a shell and tube arrangement. These membranes can be operated at a high cross flow velocity. Tubular membrane have a diameter of about 5 to 15 mm. Pumping capacity is more because these usually operated at turbulent flow regime. Packing density is low, which results in high prices per module. Tubular module is used for microfiltration and ultrafiltration application [26].

Hollow fiber is usually composed of 50 to 3000 individual hollow fiber tubes sealed together in a shell system. These tubes are having diameter less than 0.5 mm. Filtration can occur from inside the fiber to the outside. Mostly it operates at laminar flow regime and low TMP drops. Module packing density (specific surface area) is 750-1700 m^2/m^3 [26].

Flat sheet module occupies a lot of space and permeate collection rate is less compared to other modules. Low quantity of feed volume is treated and used in laboratory scale. The packing density of module is about 100-400 m^2/m^3 [27].

Membrane modules, such as, tubular, hollow fiber and flat sheet operate at low quantity of feed volume and consist of small membrane area with low permeate flux. To reduce the concentration polarization, enhance permeate rate and huge feed volume operation, spiral wound module is used. Module packing density is varying from 700 to 1000 m^2/m^3 [26].

Membrane Characterization

The type of membrane is chosen for a particular application is very important. Following properties are consider for any membrane such as, fabricated materials of a membrane can stand at different operating conditions such as, pH, temperature and solvent. The membrane structure is not degrading with acidic and alkaline solution. Temperature is another important factor, membrane surface not deteriorate to treat the high temperature feed. Others important factor is type of solvent such as organic solution and highly viscous solution also affected the membrane surface. Membrane morphology including surface structure, porosity, pore structure, pore size distribution, hydraulic permeability and membrane thickness are important characteristics for selection of particular membrane.

Membrane pore structure can be analysed by scanning electron microscopy (SEM). Crack formation is also studied by SEM image. The membrane porosity is determined by the psychometric method using deionized (DI) water as the wetting liquid. Other instrument mercury porosity meter is used for measure the porosity. Pore size distribution can be estimated by using imagej software. Pore size distribution is commonly presented by graph as a number of pores vs corresponding diameter. Pore size distribution may be unimodal or multimodal. Hydraulic permeability of a porous membrane can be determined by measuring pure water flux through the membrane at different TMP drops. The hydraulic membrane permeability (m/Pa.s) is determined from the slope of steady state permeate flux with different TMP drops [28].

Membrane Materials

Membrane materials make them a wide variety of application and extended life. Two different materials, such as polymeric and ceramic are used for symmetric and asymmetric membrane. Asymmetric membrane is fabricated from symmetric polymeric and ceramic, polymer support provides an extra strength on membrane surface.

Polymeric

Polymeric membrane is thin films of thickness 10-100 µm. Different type of polymer such as, polyamide (PA), polysulphone (PSF), polyvinyl pyrrolidone (PVP), polyacyrlonitrile (PAN) and polycarbonate (PC) materials are widely used for fabricate of polymer membrane by track etching and film stretching methods. Common advantages of polymeric membrane are, (i) availability of wide range of pore size; (ii) both hydrophobic and hydrophilic; (iii) easily fabricated and manufacturing cost is lower compared to ceramic and (iv) easily cleaned and replaceable [28].

However some basic disadvantages of polymer membranes such as, (i) temperature limitation; (ii) lower life time; (iii) low solvent resistance and (iv) low applicable range of pH and low corrosion strength.

Ceramic

Ceramic membranes are produced from inorganic materials such as aluminum oxides, titanium oxides, silicon carbide, zirconium oxide or some glassy materials. Good stability with chemically, thermally, and mechanically. Thickness of the membrane is varying in the range of 2-5 mm. Its common applications are in food and beverages, textile and chemical. Common advantages of ceramic membrane are [29].

- Good chemical, mechanical and thermal stability
- Applicability to wider pH range (0.5-14)
- Good bacteria resistant and less fouling tendency
- Longer life span (5-10 years)
- High abrasion resistance

However there exist few draw backs of ceramic membranes. They are presented as follows:

- It is available within microfiltration and ultrafiltration range. Not available for reverse osmosis and nanofiltration range
- Higher fabrication cost compare to polymer membrane

1.1.2 Membrane Fouling

Fouling is defined as a decrease in permeation flux over processing time. During membrane fouling absorption of solute molecules onto the membrane surface and the solute particle aggregates inside the pores. Hydrophobic interaction and electrostatic interactions have been identified to interpret the fouling mechanisms. These interactions are generally affected by the membrane properties such as hydrophilicity, surface topography, roughness, pore size, pore distribution and solution properties such as solute type, concentration, pH and ionic strength. The fouling mechanism has been investigated in order to improve permeation flux and reduce membrane fouling [30]. Membrane fouling is traditionally visualized as occurring through three mechanisms such as, pore blocking, pore constriction, and cake formation.

Pore blocking occurs when the entrance to a pore is completely sealed by a particle. For this mechanism, the membrane is viewed as a plate with orifices in it, and

hydraulic resistance to flow is proportional the net area of open pores. As a portion of the pore area is blocked at the surface, flow declines by a commensurate amount [31].

Pore constriction is the reduction of the void volume within a membrane due to adsorption of materials within the pores. Several essential elements must take place for pore constriction to occur. First, the materials must be smaller than the pore size of the membrane so they can penetrate into the membrane. Second, they must be transported to the pore walls either by diffusion or hydrodynamic conditions. Third, materials must have an affinity for attaching to the pore walls, without which they would pass right through the membrane [32].

Particles that are too large to enter the pores collect on the membrane surface in a porous matrix define a filter cake. The cake layer acts as a ‘‘dynamic’’ filter and can retain additional smaller material, but also generates hydraulic resistance to flow as it does so. The cake layer can prevent particles smaller than the retention rating from reaching the membrane, improving filtration effectiveness and possibly minimizing fouling from pore constriction [31]. Different types of fouling are there such as,

Colloidal Fouling

Colloidal fouling is pressure driven membranes. Colloids cover a wide size range, from a few nanometers to a few micrometers. Examples of aquatic colloids are clay minerals, colloidal silica, aluminium oxides and suspended matter. During membrane fouling, colloids accumulate on the membrane surface or within the membrane pores and adversely affect both the quantity (permeate flux) [33].

Organic Fouling

Organic fouling is applied for those substances that are dissolved in the feed solution and that tend to stick to the membrane surface. Foulants like oil, macromolecules, proteins, anti-foaming agents are contributing to an organic gel layer on top of the membrane or in pores [34].

Scaling

Scaling or precipitation fouling involves crystallization of solid salts, oxides and hydroxides from solutions. Through changes in temperature or water removal (as in reverse osmosis), the concentration of salts may exceed the saturation, leading to a precipitation of salt crystals [34].

Biofouling

The formation of biological foulants or slimes on the membrane surface is undesirable because it reduce the flux through the membrane and reduces the effective salt rejection of the membrane. For e.g., RO membrane is damage by chlorine. There for feed must be dechlorinated, usually with sodium bisulfite [35].

1.1.3 Membrane Cleaning

Fouling can be characterized as irreversible or reversible. Permeate flux is recover by circulating water or backwashing is called reversible fouling. Membrane cleaning usually performs in three forms: physical, chemical and biological. In physical cleaning, ultrasonic technique has been used to remove foulants of ultrafiltration and microfiltration membrane. In chemical cleaning acid, alkaline solutions, surfactant

(cationic and anionic) and metal chelating agent have been used as a cleaning agent. In biological cleaning, sodium bisulphite addition and enzyme is used [36].

1.1.4 Applications of Membrane Separation Technology

Polymeric as well as ceramic membranes have been found to be suitable in various pressure driven membrane (MF, UF, NF and RO) applications such as, industrial wastewater desalination, solvent recovery and food processing. Three major applications, such as, oily wastewater treatment, coal-solvent recovery and fruit juice clarification have been chosen for removal of solutes from feed streams.

1.1.4.1 Cross flow Microfiltration of Industrial Oily Wastewater

A large volume of oil-in-water or water-in-oil emulsion is generated in different process industries such as petrochemical, metallurgical, transportation, onshore and offshore oil and gas exploration. This produced wastewater cannot be re-injected to oil wells as it has a high concentration of oil and suspended particles which can lead to change in dissolved oxygen level and change in stream temperature. Impurities must be removed so that water can be reused safely for oil and gas production, washing or laundering purpose.

Most of the reported investigations have focused on treatment of oily wastewater having oil concentration equal to or higher than 1000 mg/L [37-39]. Oily water with emulsion droplets size higher than 50 µm is in unstable state and less than 10 µm is considerable to be highly stable and so is very difficult to separate particularly when oil concentration is in lower range [40]. Therefore, oil content in water collected from the

effluent treatment plant of most industries is well above the discharge standard (10 mg/L) [41].

Several conventional techniques are used to treat oil water emulsion, namely chemical emulsification [42], gravity settling [43], centrifugal settling [44], filter coalesce [45], heat treatment [46], electrostatic coalesce [47] and membrane filtration [48]. All these treatment techniques are energy intensive. Membrane separation processes are especially suited for solute removal from dilute solution. These technologies have certain advantages, e.g., non-requirement of any chemical addition, reduction of COD values, the capability of generating permeate of acceptable quality and less energy requirement relative to conventional separation technologies (e.g. Distillation, extraction and even adsorption processes). Typical examples include the dehydration of oil emulsion via pervaporation [49], reverse osmosis [50], microfiltration [51, 52] and ultrafiltration [53, 54].

Many investigations attempt the use of microfiltration membrane for treating oily waste water in the past [55, 56]. The membranes used were either polymeric ones such as polyamide or polyethersulfone or inorganic ones such as alumina with a molecular weight cut-off 20-50 kDa. Membrane fouling in cross flow microfiltration is a key factor affecting the economic and technological viability of microfiltration processes, which essentially depend on the permeate fluxes obtained and their stability with time [57]. The decline in permeate flux is consequence of membrane fouling.

During the past decades, many theoretical models have been developed to explain or predict the flux performance for cross flow microfiltration. In particular, the variation in steady state flux with hydrodynamic conditions has been intensely studied due to its importance in industrial processes.

Microfiltration models can be classified into resistance model and back flux transport model. The resistance model is based on different mode of membrane fouling theory. Fouling of the membrane can be analyzed using different pore blocking models namely complete pore blocking model, standard pore blocking model, intermediate pore blocking model and cake filtration model [58]. The back flux models are mainly based on the concentration polarization model [59] which describes the flux behaviour at steady state where the rate of convection to the membrane is balanced by diffusion back into the bulk. Baruah et al., have developed a global model for optimization of cross flow microfiltration and ultrafiltration processes [60]. Pospisil et al., have applied shear stress-based modeling of steady state permeate flux in microfiltration enhanced by two-phase flow [61]. An artificial neural network model for transient cross flow ultrafiltration of polydispersed suspensions has been developed by [62]. Aydiner et al., also have modeled flux decline using neural networks for the case of phosphate removal in cross flow mode of filtration [63]. Kim and Park have developed a model using the effective diameter for shear-induced diffusion for characterizing cake formation in cross flow filtration at polydispersed conditions [64]. Kronkamp et al., have produced a suspension flow model for hydrodynamics and concentration polarization in cross flow microfiltration [65]. Malack et al., have considered the fouling mechanism in cross flow microfiltration of electro coagulated kaolin suspension [66].

It is well-known that when the steady state flux is obtained during cross flow microfiltration of stable emulsion, particle transport towards the membrane due to the permeation flux must be balanced by the particles transport away from the membrane. Keeping this in mind, four different models viz. Brownian diffusion, shear induced

diffusion, inertial lift and surface transport have been widely used to analyse flux behaviour.

The back transport models may be more suitable, since the oil water emulsion exists with a mean droplet size in the range of 0.1 to 60 μm and the emulsion droplets are also highly deformable and compressible [67-70]. The inertial lift and surface transport models are probably not appropriate because the former is valid for large particles greater than 20 μm and latter is applicable when a thick stagnant cake forms. These conditions do not exist during microfiltration of oily wastewater. Again, emulsion bears in a wide range droplets size for which a particular model may not responsible for permeate flux decline. Thus selection of suitable model for the microfiltration of oily waste water may be a further scope of research.

1.1.4.2 Separation of Coal-solvent Mixture by Membranes

Coal is the most important and abundant fossil resource in the world. Coal contains a high level of inorganic impurities (approximately 10% combustible hydrocarbons). These create a problem in the uncontrolled ash deposition in the boiler wall and tubes. These impurities deteriorate the efficiency of the boiler. Various methods, namely, Soxhlet extraction, microwave-assisted extraction, supercritical fluid extraction, chemical leaching are employed to reduce the ash content in coal. These techniques demonstrate high effectiveness for the production of ultra clean coal (ash <1%). But these methods have several drawbacks. Soxhlet extraction process is a time consuming process and large amount of solvent is required [71]. Microwave-assisted extraction requires a huge time [72]. Due to the usage of excess energy in supercritical fluid extraction, it is not cost effective [73]. In chemical leaching methods with alkali

and acids, recovery is very low [74, 75]. Another option for the removal of inorganic mineral component is to extract the organic part of the coal with solvents. Different solvents, such as potassium hydroxide, pyridine and aliphatic primary amines (hexylamine, ethylediamine and monoethinalamine) have ability of conversion from some medium to high rank coal [76]. This conversion was observed due to the removal of mineral matters, e.g., kaolinite and quartz and reduction of ash content in coal. Thermal extraction yield of some low rank coals were improved by treating with the inorganic acid, such as HCl, before thermal extraction. But the extraction yield was also dependent on acid concentration, extraction time and extraction temperature [77]. The typical extraction time was 30-40 min and temperature was 400°C for the removal of maximum impurities in coal. Extraction yield was found to depend on the properties of solvent, i.e., coordination with the acidic surface group, thus breaking the secondary structure and swelling the coal. But, single solvent was not enough to remove all the inorganic impurities and to obtain the desired extraction yield [78]. Solvent mixture e.g., blends of CS_2 and NMP have also been to be proven useful [79, 80]. CS_2-NMP mixed solvent (1:1, v/v) were used for extraction purpose and extraction yield was increased from 31 to 63% at room temperature. These are in particular, effective upto 65% of the organic part of some coal at room temperature and 85% at elevated temperature [81]. In all the processes, solvent recovery is very low; time consuming; highly expensive.

Clay materials mixed with inorganic materials were used for the fabrication of ceramic membrane in microfiltration range. Jana et el., have shown that the prepared ceramic membrane had good chemical stability and used for chromate removal [82]. Higher flux in ceramic membrane was achieved by increasing the average pore diameter

and the prepared membrane were used for de-emulsification of soybean oil/water filtration in cross flow filtration. Maximum rejection of oil was achieved as 99% [83]. Inorganic materials were also used for fabrication of ceramic membrane in microfiltration range. Membrane was sintered in different temperatures and the effects of sintered temperature on membrane preparation were studied in detail [84]. To reduce the cost of ceramic membrane in microfiltration range, non-expensive natural zeolite was used [85].

Iron ore slime (IOS) is one of the waste materials formed in the steel production unit. It contains around 35 to 40% iron. IOS is not normally suitable for steel production for extremely fine particle size less than 50 µm containing a significant amount of Fe along with SiO_2 and Al_2O_3. IOS has good thermal stability and could be a suitable raw material for low cost ceramic membrane fabrication upon appropriate blending with other components. These waste materials cannot directly be used for land filling purpose because of potential threat of heavy metal transportation in surface runoff. The waste IOS is collected from this steel production unit of M/s TATA steel Jamshedpur (India) for fabrication of low cost membrane and its subsequent application in solvent-coke separation.

1.1.4.3 Clarification of Fruit Juice

During non-seasoning time, citrus fruit especially mosambi are made available by storing them after clarification and depectinization. There is no direct method to store the juice after extraction process due to the presence of pectin and carbohydrate in the raw juice. So the clarification of raw juice is necessary to store the extracted juice for a long time. Membrane treatment is one of the best processes to remove all pectin

materials from raw juice due to several advantages, such as, non-chemical requirement; low operating cost compared to other treatment processes. Membrane process cannot be directly used for clarification of raw juice due to fouling and flux decline with operating time [86]. Before membrane separation process, pretreatment is required for removing suspended materials from raw juice. Different pretreatment methods e.g., centrifugation, fining agents such as gelatin, bentonite and enzyme treatments are there to remove impurities from raw juice. Each process has some merits and demerits. Centrifugation process consumes more power. In centrifugation, heavy suspended materials are removed, but some colloidal particles remain in clarified juice. Clarification of juice with fining agents depends on its dose. Single fining agent is not enough to remove all suspended materials from the raw juice. Gelatin-bentonite (1:5) combined dose is used to remove the maximum suspended impurities and removal efficiencies are compared with single fining agents [87]. Maximum impurities can be removed by using enzyme treatment such as pectinase. Enzyme pretreatment method is costly compared to other pretreatment techniques.

Major constituent of citrus fruit juice is sucrose, pectin and water. Presence of pectin clarified juice turned into haziness and highly viscous. Haze formation of juice also affects the quality of clarified juice and decrease the shelf life of clarified juice. Thermal treatment is widely used for preserve the juice [88]. During thermal treatment qualities of juice such as, nutrient and antioxidant property degraded during storage. These antioxidant properties provide protection with several diseases [89]. To preserve antioxidant and nutrient, membrane based separation is used [90].

In membrane operations, different membrane modules are available for clarification of juice such as tubular [91], hollow fiber [92], flat sheet [93] and spiral

wound [94]. Spiral wound has an extra advantage compared to other membrane module, such as, high packing density, low cost per unit area, easy replacement of module and low energy consumption [95]. With an extra advantage compared to others membrane modules, it can operate at high TMP drops and turbulent flow regimes, due to the presence of feed spacer. Spacer enhances the mass transport (back mixing) in feed channel of spiral wound module, but it increases the flow resistance [96]. Spacer develops the turbulence at the membrane surface and reduces the concentration polarization. Hence, it enhances flux and minimizes the TMP drops. It directly reduces the pumping power consumption cost [97]. It can easily be cleaned by different processes such as, circulation of deionized water or cleaning with different chemical dose concentration. Microfiltration (MF), ultrafiltration (UF) and reverse osmosis (RO) processes were used for the clarification of juice [98]. Ultrafiltration membrane was found to retain more than 80% flavour compounds in the fruit juice [98]. Pectin and microorganism retentate during UF process only small amount of sucrose and vitamins flow with water [99]. During UF clarification, with permeate recycle is favourable operating condition in terms of reduction of concentration polarization, improvement of membrane performance and final quality of the product due to high dilution rates [100]. While without permeate recycle has increased the concentration polarization and enhances the cleaning cycle of membrane module [101]. Permeate recycle would save cost of cleaning agent dose and operating time. UF treatment could be used as a pretreatment process for the next stage of membrane operations.

1.1.5. Merits and Demerits of Various Separation Processes

Every separation processes has its merits and demerits. Following are major advantage of membrane separation processes over conventional processes; i) physical separation process; ii) no chemical are used; iii) generally less energy requirement; iv) treatment of heat sensitive materials e.g., fruit juice; v) mild operating (operable under ambient temperature); vi) almost no damage to the species under processing; vii) no phase change; viii) less capital and running cost; ix) easy to scale up (modular in nature) and x) process management simple (low man power). Merits and demerits of other conventional processes with membrane separation processes are shown in **Table 1.1**.

Table 1.1. Merits and demerits of various separation processes.

Processes	Merits	Demerits
Chemical emulsification	Precise control of chemical reaction, heat and viscosity	Demulsification
Gravity settling	It is effective of size greater than 80 μm	Temperature dependent and time consuming
Centrifugation	Effective with high oil concentration	High power consumption
Heat treatment	Easy oil removal from oil-water emulsion	Precise temperature control is needed
Filter Coalesce	High efficiency and low capital investment	Life time is less
Membrane	Low energy consumption and COD value reduce	Concentration polarization and pore blocking

1.1.6 Selection of Membrane Module for Oily Wastewater Treatment, Coal-solvent Mixture Separation and Clarification of Fruit Juice

Cross flow membrane filtration unit has an extra advantage, such as, low concentration polarization compared to batch cell for long operating time. During microfiltration, oil droplets are stacked on membrane surface resulting membrane fouling and decline of permeate flux. Fouled polymeric membranes can be cleaned easily and are replaceable. It is difficult to fabricate a ceramic membrane for high

surface area with proper strength. During repeated cleaning, there is a possibility of membrane surface damage. Spiral wound can also be used for oil-water filtration, but cleaning will not be easy due to wound of membrane structure. So, flat sheet polyamide microfiltration membrane in rectangular cross flow cell is most suitable for oil-water separation.

After coal extraction using organic solvent like NMP, the extract at 180°C is placed in membrane filtration (stirred batch cell) and organic solvent is recovered from permeate side. Polymer membrane is not suitable at such high temperature (180°C) and has chance to be dissolved in organic solvent. Hence, the ceramic membrane is most suitable for coal-solvent mixture separation.

For fruit juice clarification, both polymeric and ceramic membrane can used in various modules, such as, flat sheet, batch cell and spiral wound. For industrial application, spiral wound is most suitable due to high surface to volume ratio and high permeate rate compared to other membrane modules. It can be cleaned easily by different cleaning agents without tampering the membrane surface.

1.2 Objectives of the Current Research

The following objectives are accomplished from the lacuna in current research.

1.2.1 Cross Flow Microfiltration of Industrial Oily Wastewater

1. Evaluation of cross flow microfiltration membrane performance for the treatment of industrial oily wastewater.
2. Studies on permeate quality with variation of TMP drops and cross flow velocities.

3. Development of a combined diffusion model based on Brownian and shear induced diffusion models for predicting the permeate flux.

1.2.2 Separation of Coal-solvent Mixture by Membranes

1. Removal of inorganic impurities from typical Indian coal by solvent extraction process using NMP and EDA at different coal/solvent ratios.
2. Development of a ceramic membrane and its characterization in terms of pore size distribution, chemical stability and porosity.
3. Utilization of steel industry waste iron ore slime (IOS) to fabricate low cost ceramic membrane.
4. Studies on cleaning of fouled membranes with cleaning agents to regain permeate flux.

1.2.3 Clarification of Fruit Juice

1. Investigation on raw mosambi juice pretreatment using a packed column supported with glass beads and molecular sieves.
2. Performance of spiral wound ultrafiltration membrane module for juice clarification both in laminar and turbulent flow regimes at two different operating conditions, namely, with and without permeate recycle.
3. Studies on the selection of suitable model, i.e., Brownian, shear induced and combined diffusion model for prediction of permeate flux values.
4. Cleaning study of fouled ultrafiltration membrane in terms of optimization of cleaning agent dose in detail using different cleaning agents, namely, SDS, EDTA and deionized water.

Chapter 2

CROSS FLOW MICROFILTRATION OF INDUSTRIAL OILY WASTEWATER

Chapter 2

CROSS FLOW MICROFILTRATION OF INDUSTRIAL OILY WASTEWATER

In this chapter, removal of oil from oil-water emulsion through cross flow microfiltration was discussed. Permeate qualities were studied in details with variation of TMP drops and cross flow velocities. A model was proposed by combining Brownian diffusion and shear induced diffusion to predict the steady state permeates flux data at different cross flow velocities and TMP drops.

2.1 Experimental

2.1.1 Oily Wastewater

Oil and Natural Gas Corporation Limited (ONGC) supplied the industrial oily wastewater for onshore oil production, Eastern region, Nazira, Assam, India. The supplied industrial oily wastewater was a stable emulsion due to the presence of natural surfactant. It enhances the membrane separation performance by reducing fouling layer thickness as well as stickiness of oily layer over membrane surface. The average oil

The work presented in this chapter is published at ***Separation Science and Technology***, 46 (2011), 1213-1223.

droplet size range was 0.01 to 47 µm. All other properties of oily effluent were shown in **Table 2.1**.

Table 2.1. Physical properties of industrial oily wastewater

Properties	**Values**
Oil concentration (mg/L)	192
Oil droplet size range in feed (µm)	0.01-47
COD (mg/L)	2000
TDS (mg/L)	2500
Ionic conductivity (mho/cm)	5

2.1.2 Membrane

An organic polyamide membrane (thin film composite) with average pore size 1.16 µm and average thickness 50 µm was obtained from Permionics Membrane Pvt. Ltd, Gujarat, India was used to conduct all the cross flow experiments using a rectangular cell. Permeability of membrane was measured using standard technique and was found to be 12.66×10^{-11} m/Pa s. Polyamide is the most common material used in MF and UF membrane due to outstanding properties, such as, good thermal stability, chemical resistance and high mechanical strength. Polyamide membranes are usually fabricated using a phase inversion process which results in a porous polymer films.

2.1.3 Procedure

A rectangular cross-flow cell, made of stainless steel, was designed and fabricated. The oily effluent was placed in a stainless steel feed tank of 10×10^{-3} m^3 capacity. The schematic of the experimental setup is shown in **Figure 2.1**. A

reciprocating pump was used to feed the effluent into the cross flow cell. The retentate stream was recycled back to the feed tank. The permeate stream was also recycled to maintain a constant concentration in the feed tank. A by-pass from the pump delivery to the feed tank was provided. The two valves in the bypass and the retentate lines were used to vary the TMP drops and the flow rate through the cell, independently. The cell consisted of two matching flanges which dimension was 0.05 m×0.14 m. The bottom flange consists of internal grid structure. A porous stainless steel plate was placed on lower plate that provides the mechanical support of the membrane. Neoprene rubber gasket of 0.2×10^{-3} m thickness was placed over the membrane surface. The two flanges were tightened to create a leak proof channel.

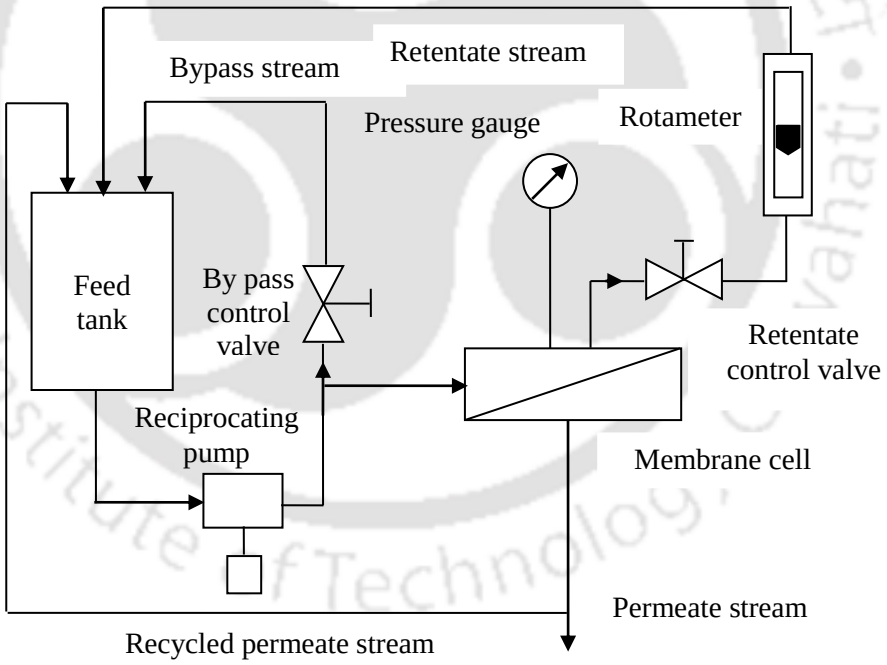

Figure 2.1. Schematic diagram of cross flow membrane module.

A fresh polyamide membrane was compacted at a TMP drop of 690 kPa for three hr using distilled water. During these processes, the porous structure was

compacted and as a result, the flux was decreased. After relaxation (effected by reducing the TMP drops), the flux values should not return to its original value since the deformation process was irreversible. A steady state flux value of distilled water at different operating pressures was plotted against applied TMP drops. The average value of membrane permeability was determined from the slope and was found to be 12.66×10^{-11} m/Pa.s. The operating conditions for the cross flow experiments were given in **Table 2.2**. The duration of a cross flow experiment was one hour.

Table 2.2. Operating conditions for cross flow microfiltration of industrial oily wastewater

TMP drops (kPa)	Reynolds number	Flow rate (lpm)	Cross flow velocity (m/s)
69, 138, 207	897	1.6	0.26
	1282	2.0	0.33
	1923	3.0	0.50
	4487	7.0	1.16
	5769	9.0	1.50

After each experiment, the setup was cleaned with distilled water and 0.1% (w/v) SDS (sodium dodecyl sulfate) solution for 30 min at TMP drops of 690 kPa. After that, the setup was run continuously with fresh distilled water for 2 to 3 times for 15 min at the same TMP drops. After that the cross flow channel was dismantled and the membrane was dipped in distilled water for 30 minutes to remove traces of oil droplets. The cross flow cell was reassembled and the membrane permeability was measured again. It was observed that the membrane permeability remains almost

constant between successive runs. All the experiments were conducted at temperature of 30±2°C. The observed retention of each solute was defined as $R_0=1-(C_p/C_0)$ where, C_p and C_0 were the oil concentrations in the permeate and feed, respectively.

2.2 Analysis

2.2.1 Particle Size Analysis

The particle size distribution (PSD) of a particle dispersed in a fluid represents the value that defined the relative amount of particle present, sorted according to size. Scanning electron microscope (SEM) images from different sections of the polyamide membrane were considered and around 200 pore diameters were measured using the imagej software. Average pore diameters (d_s) were calculated using following equation:

$$d_s = \left[\frac{\sum_{i=1}^{n} n_i d_i^2}{\sum_{i=1}^{n} n_i} \right]^{0.5}$$

where n is the number of pores, and d_i is the pore diameter (µm) of the i-th pore. The average pore size of polyamide membrane was 1.16 µm and the average oil droplet size in the feed ranges from 0.01 to 47 µm, which is greater than the average pore size of polyamide membrane. The range of the oil droplets was obtained from Laser Particle Size Analyzer (LPSA), Mastersizer 2000 of M/s Malvern Instrument Ltd., UK. Hence, maximum oil droplets should be retained by the membrane surface (refer **Figure 2.2**)

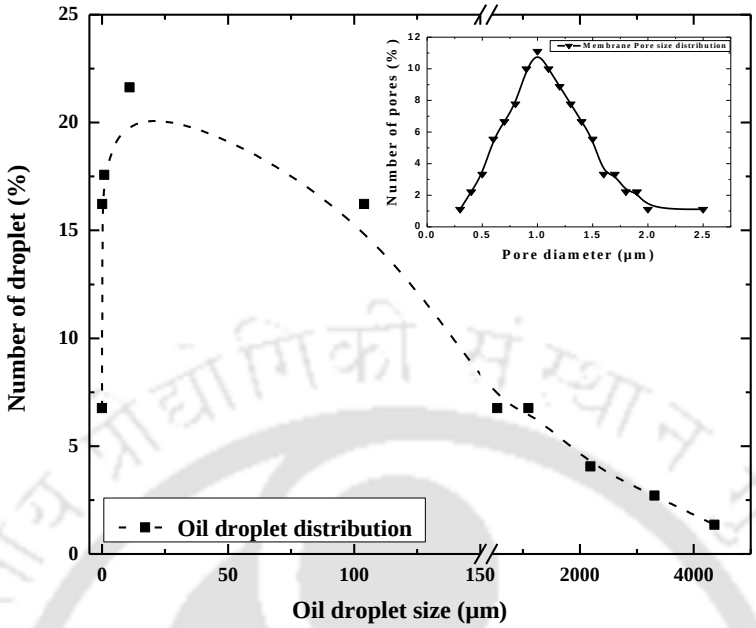

Figure 2.2. Droplet size distribution in oily wastewater. **Inset**: Pore size distribution of polyamide membrane used for microfiltration.

2.2.2 Chemical Oxygen Demand (COD)

COD test was commonly used to measure the amount of organic compound present in water. It indicated the mass of oxygen consumed per liter of solution. The sample (feed, permeate and retentate stream at each operating condition) was refluxed with potassium dichromate and sulphuric acid in presence of mercuric sulphate (to neutralize the effect of chlorides), and silver sulphate (catalyst). The excess of potassium dichromate was titrated against ferrous ammonium sulphate (FAS) using ferroin as an indicator. The amount of potassium dichromate used was proportional to the oxidizable organic matter present in the sample [102]. COD was measured using the following relation.

$$COD = \frac{(b-a)\times(N)\ of\ FAS\times 8000}{volume\ of\ sample}$$

where *b*, ml of titrate using blank and *a*, ml of titrate using sample.

2.2.3 Quantitative Analysis

The total dissolved solids concentration, TDS (mg/L), ionic conductivity (mho/cm) of feed, permeate and retentate streams at each operating conditions were measured by digital portable water/soil analysis kit provided by Vsi Electronics Pvt. Ltd., Punjab (India). All the properties were measured thrice.

2.2.4 Measurement of Oil Concentration

Feed and permeate oil concentration were measured by a UV spectrophotometer (Perkin-Elmer Precisel, Lamda-35, Canada) (refer Appendix). The wavelength at which maximum absorption occurred were obtained from the measurement of pure component was 390 nm. The standard method was used to calculate the concentration of different oil from the mixture [103].

2.3 Theoretical Consideration

In cross flow microfiltration, it is well known that when the steady state flux is obtained, particles transport towards the membrane due to the permeation flux must be balanced by the particles transport away from the membrane. For laminar flow and turbulent flow, three basic models have been widely applied, namely, concentration polarization model [104], Brownian diffusion model [105] and shear induced diffusion model [69]. Combined diffusion model is based on the diffusion of oil particle from

feed to permeate side and diffusivity is dependent on oil particle diameter, viscosity and cross flow velocity.

2.3.1 Concentration Polarization Model

In this model, the rejection of solute particles carried toward the membrane by the permeate flow gives rise to a thin fouling layer δ on the membrane surface, overlaid with a flowing concentration polarization layer in which particles diffuse away from the membrane surface. Initial permeate flux *J(x)* is higher because the membrane surface is free of solute deposition. After a certain time, the permeate flux *J(x)* value decreases as more solute particles transfer toward the membrane surface and increase the membrane fouling layer thickness, δ (refer **Figure 2.3**). At a lower emulsion concentration, the concentration polarization is not obvious, the permeate flux increase with the increase in TMP drops. At higher emulsion concentration, the flux is controlled by the gel layer [106].

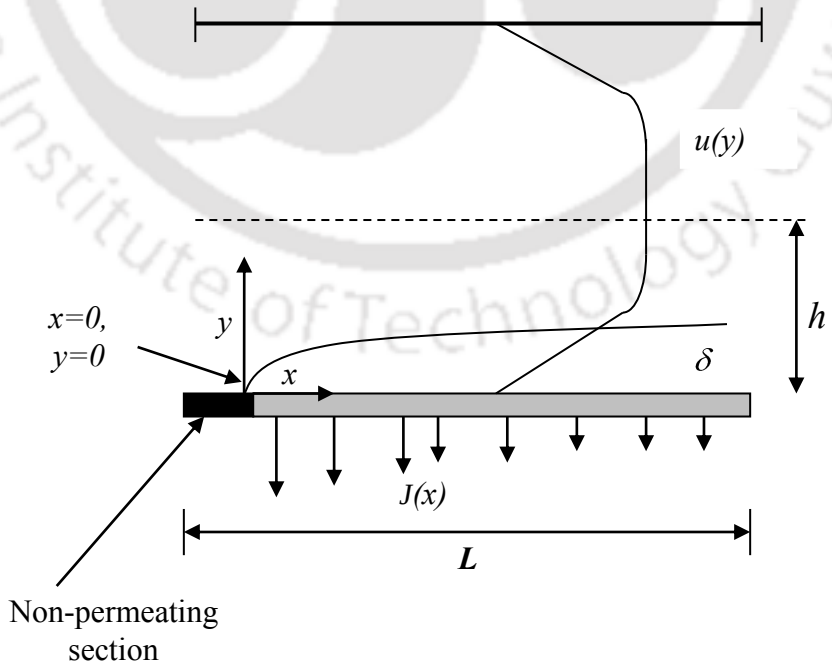

Figure 2.3. Schematic for concentration polarization over the membrane surface.

The simple concentration polarization model is expressed as

$$J(x)C = D\frac{dC}{dy} \tag{2.1}$$

where *J(x)* is the local filtrate flux or velocity, *C* is the particle concentration, *D* is the particle diffusion coefficient, and *y* is the perpendicular distance from the membrane. Integrate Eq. (2.1) with in limit at $y = 0$ then $C = C_m$

$y = \delta$ then $C = C_o$

$$J(x) = \frac{D}{\delta}\ln\frac{C_m}{C_o} = k\ln\frac{C_m}{C_o} \tag{2.2}$$

where *k*, which is equal to D/δ, represent the local particle mass transfer coefficient between the bulk suspension and membrane surface, δ is the film thickness, C_m and C_o are particle concentration, at the edge of the polarized layer and in the bulk suspension, respectively. For laminar flow when only a thin boundary layer is formed, the length average mass transfer coefficient is determined, by solution of the Leveque equation as

$$k = 0.81\left(\gamma_0 D^2/L\right)^{1/3} \tag{2.3}$$

where *L* is the channel length, γ_0 is the shear rate at the surface of membrane due to the bulk laminar flow and *D* is the particle diffusivity.

Comparing with Leveque equation for laminar flow

$$\gamma_0 = \frac{12.1u}{d_e} \tag{2.4}$$

where d_e is the equivalent diameter. Put the value of γ_0 in Eq. (2.3) then

$$k(x) = 1.86\left(\frac{uD^2}{d_e L}\right)^{1/3} \tag{2.5}$$

Eq. (2.5) is used for laminar flow.

For turbulent flow through a conduit or a channel, the Dittus-Boelter equation can be applicable

$$Sh = 0.023\,(Re)^{0.8}\,(Sc)^{0.33} \tag{2.6}$$

where *Sh* is the Sherwood number, *Sc* is the Schmidt number and *Re* is the Reynolds number. Mathematically these are defined as:

$$Sh = \frac{k d_e}{D}, \quad Sc = \frac{\mu}{\rho D} \quad and \quad \mathrm{Re} = \frac{\rho u d}{\mu}$$

Putting the values of *Sh* and *Sc* in Eq. (2.6) and solving it for value of *k*:

$$k = 0.023(\mathrm{Re})^{0.8}\,\frac{\mu^{0.3} D^{0.67}}{\rho^{0.3} d_e} \tag{2.7}$$

J(x) is calculated by putting the value of *k* in Eq. (2.2).

2.3.2 Brownian Diffusion Model

Brownian diffusion is important for particles less than $0.1\,\mu m$ with the Brownian diffusivity given by Stokes-Einstein relationship [107].

$$D_B = KT/(6\pi\mu a) \tag{2.8}$$

where *K* is the Boltzman constant (1.38×10^{-23} *J/K*), *a* is the particle radius, *T* is the absolute temperature, μ is the viscosity of the particle free solution. Putting the value of D_B in Eq. (2.5), the average mass transfer coefficient is defined as:

$$k = 1.86\left[\frac{u D_B^2}{d_e L}\right]^{1/3}$$

The steady state permeate flux *J(x)* for laminar flow written as

$$J(x) = 0.2647\left[\frac{u K^2 T^2}{d_e \mu^2 a^2 L}\right]^{1/3} \ln\frac{C_m}{C_0} \tag{2.9}$$

Eq. (2.9) clearly shows that the predicted flux for the Brownian diffusion mechanism increases with feed velocity to the one-third power, and decrease with particle radius to the two-third power for laminar flow

$$J(x) \propto u^{1/3} \quad \text{and} \quad J(x) \propto \frac{1}{a^{2/3}}$$

For turbulent flow through a conduit or a channel, the Dittus-Boelter equation (Eq. (2.6)) can be applicable. Putting the values of *Sh*, *Sc* and $D=D_B$ in Eq. (2.6), the value of *k* may be written as:

$$k = 0.023(\mathrm{Re})^{0.8} \frac{\mu^{0.3} D_B^{0.67}}{\rho^{0.3} d_e}$$

or,

$$k = 0.00323(\mathrm{Re})^{0.8} \left(\frac{KT}{a}\right)^{0.67} \frac{1}{\mu^{0.4} d_e \rho^{0.3}} \tag{2.10}$$

Now, *J(x)* can be calculated by using the value of *k* in Eq. (2.2).

2.3.3 Shear Induced Diffusion Model

As a possible resolution of the flux paradox, the concentration polarization model could be applied to microfiltration, provided that the Brownian diffusivity was replaced by the shear induced diffusivity. Shear induced hydrodynamic diffusion of particles occurs because individual particles undergo random displacements from the streamlines in a shear flow as they interact with and tumble over other particles. Shear induced model is important for particles of 0.5 to 30 μm [108].

The shear induced diffusivity is expressed as:

$$D_s = 0.3\gamma_0 a^2 \tag{2.11}$$

where $\gamma_0 = 12.1\frac{u}{d_e}$

Substituting the value of shear rate

$$D_s = 3.63 u a^2 / d_e \tag{2.12}$$

The average mass transfer coefficient from Eq. (2.5) we have

$$k = 4.39\left(\frac{u}{d_e}\right)\left(\frac{a^4}{L}\right)^{1/3} \tag{2.13}$$

Putting the value of *k(x)* in Eq. (2.2) the expression for steady state flux is as follows:

$$J(x) = 4.39\left(\frac{u}{d_e}\right)\left(\frac{a^4}{L}\right)^{1/3} \ln\frac{C_m}{C_0} \tag{2.14}$$

The shear induced diffusion model is due to the combination of shear and concentration gradient. For turbulent flow through a conduit or a channel, the Dittus-Boelter equation can be applicable. Putting the value of *Sh*, *Sc* and $D=D_s$, in Eq. (2.6), the value of *k* may be written as:

$$k = 0.0545\frac{\rho^{0.5} u^{1.47} a^{1.3}}{\mu^{0.5} d_e^{0.87}} \tag{2.15}$$

Now, *J(x)* can be calculated by putting the value of *k* in Eq. (2.2).

2.3.4 Proposed Model

A model (combination of Brownian and shear induced) has been proposed on the basic of droplet size in the permeate. During microfiltration of oily wastewater having droplet size within the range of 0.01 to 47 µm in the feed, steady state flux data were analyzed. It is assumed that overall diffusivity, *D* is the combination of D_B and D_s

as both the models (Brownian and shear induced) come within the range of oil droplet size in the permeate considered in the present investigation.

For Brownian diffusion model, the steady state permeate flux is

$$J(x) = 0.2647\left[\frac{u K^2 T^2}{d_e \mu^2 a^2 L}\right]^{1/3} \ln\frac{C_m}{C_o} \tag{2.16}$$

when the shear induced diffusion (D_s) dominate the particles transport, $J_S(x)$ can be expressed as

$$J(x) = 4.39\left(\frac{u}{d_e}\right)\left(\frac{a^4}{L}\right)^{1/3} \ln\frac{C_m}{C_o} \tag{2.17}$$

In the proposed model both the diffusion models (Brownian and Shear induced) are considered, since the droplet size varies within the range of 0.01 to 47 μm. Therefore, a modified diffusion coefficient (sum of diffusion coefficients of Brownian and Shear induced) has been proposed and Eq. (2.2) has been modified as

$$J(x) = 1.86\left(\frac{u(D_s + D_B)^2}{d_e L}\right)^{1/3} \ln\left(\frac{C_m}{C_o}\right) \tag{2.18}$$

where $D_B = \dfrac{KT}{6\pi\mu a}$ *and* $D_s = 3.63\dfrac{u a^2}{d_e}$

Putting the values of D_B and D_S in Eq. (2.18) the modified permeate flux expression becomes

$$J(x) = 1.86\left(\frac{u}{d_e L}\right)^{1/3}\left[\frac{K^2T^2}{36\mu^2\pi^2a^2} + 13.17\frac{u^2a^4}{d^2{}_e} + 1.21\frac{KTua}{d_e\mu\pi}\right]^{1/3} \times \ln\left(\frac{C_m}{C_o}\right) \tag{2.19}$$

The Dittus-Boelter equation can be applicable for turbulent flow through a conduit or a channel. Putting the values of *Sh*, *Sc* and modified diffusion coefficient in Eq. (2.6), the expression for *k* becomes

$$k = 0.023(\mathrm{Re})^{0.8} \frac{\mu^{0.3} (D_B + D_S)^{0.67}}{\rho^{0.3} d_e}$$

Using the values of D_B and $D_{s,}$ we get

$$k = 0.023(\mathrm{Re})^{0.8} \frac{1}{d_e} \left(\frac{\mu}{\rho} \right)^{0.3} \left(\frac{KT}{6\pi\mu a} + \frac{3.63ua^2}{d_e} \right)^{0.67} \tag{2.20}$$

Now, *J(x)* can be calculated by putting the value of above *k* in Eq. (2.2).

2.4 Results and Discussion

2.4.1 Transient Flux Decline

Figure 2.4 shows the variation of permeate flux at different Reynolds numbers (varies from 897 to 5769) at 69 kPa. It can be observed from the figure that initial permeate flux is very high and after that it decreases sharply up to 200 s. Then the permeate flux value remains almost constant with time and thus steady state flux is achieved. The initial sharp decline is due to pore blocking of membrane porous structure and gel layer formation over the membrane surface by oil droplet present in the feed. At a Reynolds number of 5769, the permeate flux value declines from 8.74×10^{-6} $m^3/m^2.s$ to 4.71×10^{-6} $m^3/m^2.s$ in 138 s. Steady state permeate flux value in turbulent flow regime is higher than laminar flow condition for a particular TMP drops.

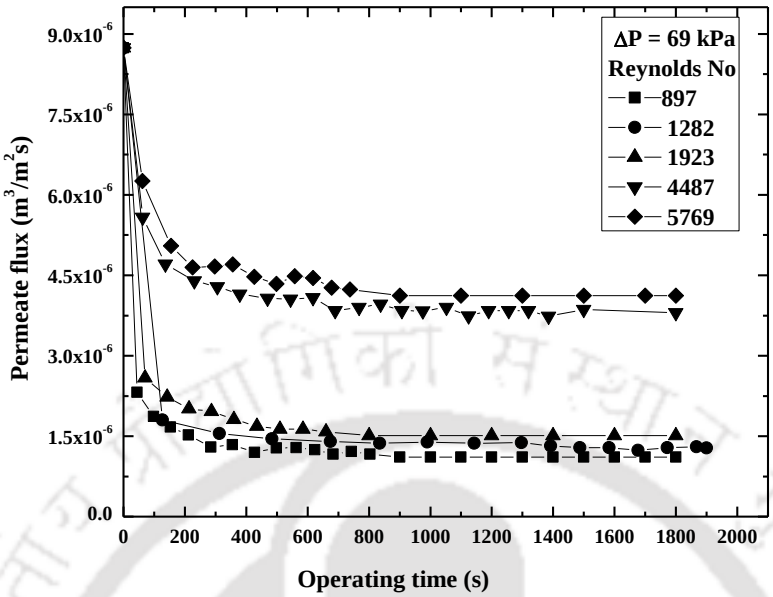

Figure 2.4. Transient flux decline profile for MF at 69 kPa TMP drops.

2.4.2 Steady State Permeate Flux with the Variation of Reynolds Number and TMP Drops

Steady state permeate flux increases with Reynolds number and TMP drops. It can be observed from **Figure 2.5** that at a TMP drops of 69 kPa, the permeate flux value increases from 1.11×10^{-6} $m^3/m^2.s$ to 4.12×10^{-6} $m^3/m^2.s$ when the Reynolds number increases from 897 to 5769. For any particular TMP drops, at higher Reynolds numbers the steady state flux value is higher. It indicates that the fouling layer decreases due to the development of high shear stress. **Figure 2.5** shows that steady state permeate flux values increase from 4.12×10^{-6} $m^3/m^2.s$ to 10.3×10^{-6} $m^3/m^2.s$ when TMP drops is increased from 69 to 207 kPa at a Reynolds number of 5769.

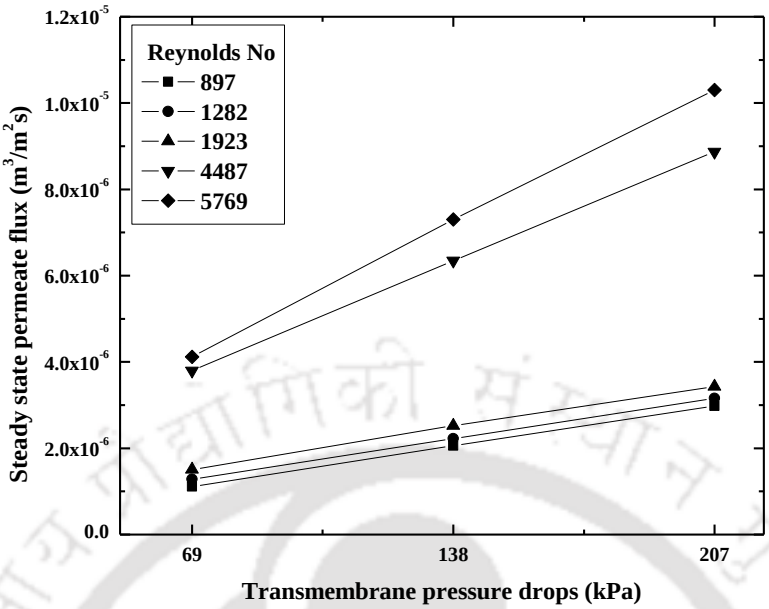

Figure 2.5. Variation of steady state permeate flux with TMP drops at different Reynolds numbers.

2.4.3 Steady State Permeate Concentration with the Variation of Reynolds Number and TMP Drops

Figure 2.6 shows the variations of oil concentration in permeate with varying Reynolds number at three different TMP drops. It may be seen from the figure that the steady state permeate concentration decreases with increase in Reynolds number for all the TMP drops considered here. The permeate concentration decreases from 9.75 to 4.5 mg/L when Reynolds number increases from 897 to 5769 at 207 kPa TMP drop. With increase in Reynolds number, the membrane surface concentration decreases due to high shear stress and as a result of which permeate concentration decreases. The steady state permeate concentration increases with TMP drops at a constant Reynolds number. For example, permeate concentration increases from 8 to 9.75 mg/L as TMP drops increases from 69 to 207 kPa at Reynolds number of 897. As TMP drops increases,

more numbers of smaller oil droplets are convected towards membrane surface and pass through the membrane pores. This is because of the fact that with increasing TMP drops, more solvents pass through the membrane leaving more number of oil droplets that increase the concentration polarization of oil droplet over the membrane surface. After a certain concentration, these droplets come closer and coalesces each other and may form a thin layer over the membrane surface. Under enhanced TMP drops, more number of oil droplet from the polarized and or thin layer passes through the membrane pore (increased forced convection) causing reduced rejection efficiency.

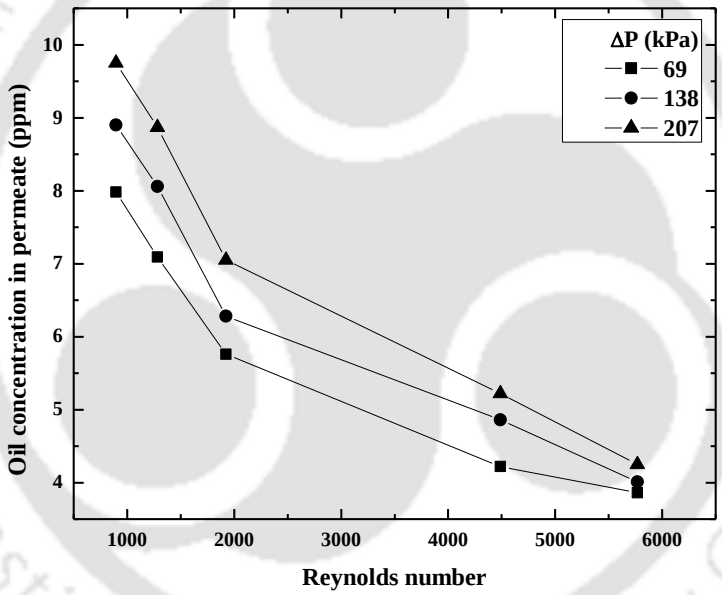

Figure 2.6. Variation of oil concentration in permeate with Reynolds number.

2.5 Model Consideration

2.5.1 Variation of Permeate Flux with TMP Drops for Laminar and Turbulent Flow Regime

Membrane surface oil concentration is calculated using the experimental data at steady state for various operating conditions (TMP drops and cross flow velocity, i.e., Reynolds number) for various models. The membrane surface oil concentration is correlated with the operating conditions as,

$$C_m = a\left(\frac{\Delta P}{\Delta P_{\max}}\right)^{n1}\left(\mathrm{Re}\right)^{n2} \tag{2.21}$$

Taking the logarithm in both the sides:

$$\ln C_m = \ln a + n_1 \ln\left(\frac{\Delta P}{\Delta P_{\max}}\right) + n_2 \ln\left(\mathrm{Re}\right) \tag{2.22}$$

where ΔP_{max} is the maximum TMP drops (207 kPa). Using multiple log linear regression analysis of Eq. (2.22), the values of *lna*, n_1, n_2 are obtained and presented in **Table 2.3** for different hydrodynamic conditions. The positive values of n_1 and negative values of n_2 confirm the trend of membrane surface oil concentration with the operating conditions. The higher value of R^2 corresponds to a better fit of the model. As seen from R^2 value at different model for laminar and turbulent flow (**Table 2.3**), the best fitting was obtained for the proposed model. However the proposed model plays a major role to describe the calculated steady state flux data with experimental steady state flux data. As TMP drops increases, more solutes are convected towards the membrane and this enhances the concentration polarization, resulting in increase in

membrane surface concentration. The increase in Reynolds number reduces the concentration polarization.

Table 2.3. Model constants for laminar and turbulent flow conditions

Model	Laminar flow				Turbulent flow			
	lna	n_1	n_2	R^2	***lna***	n_1	n_2	R^2
Concentration polarization	-1.65	7.6×10^{-5}	-5.5×10^{-5}	0.94	-1.65	8.5×10^{-6}	-2.4×10^{-5}	0.96
Brownian diffusion	0.39	1.07	-0.01	0.95	2.14	0.75	-0.27	0.96
Shear induced	0.97	0.37	-0.27	0.94	2.08	0.28	-0.37	0.97
Proposed model	0.81	0.35	-0.25	0.96	-1.39	0.85	-0.13	0.97

The membrane surface concentration is correlated with the operating conditions for the Eq. (2.21) using multiple regression analysis, as mentioned earlier. Steady state permeate flux values are calculated by using the Eqs. (2.9, 2.14 and 2.19), separately, considering C_m value from Eq. (2.21). **Figure 2.7** shows the variations of steady state permeate flux with Reynolds number at different TMP drops and **Figures 2.8** and **2.9** show the variation of permeate flux with TMP drops at different Reynolds numbers. The steady state permeate flux values are calculated for laminar and turbulent flow at different models such as Concentration polarization model (using Eqs. (2.5 and 2.7)), Brownian diffusion model (using Eqs. (2.9 and 2.10)), shear induced diffusion model (using Eqs. (2.14 and 2.15)) and proposed model (using Eqs. (2.19 and 2.20)). It is observed from these figures that calculated permeate flux values are within ± 10% of the experimental data. Brownian diffusion model is applicable for droplet size less than 1 µm. On the other hand, the shear induced diffusion model is valid for droplet size of

0.3 to 30 µm. In this case, the Brownian diffusion model diffusivity value is very less compared to shear induced model. To summarize the above models reviewed, it would be convenient to differentiate these by the working mechanism.

1. Brownian diffusion is due to Brownian motion diffusivity, which is temperature dependent.
2. Shear induced diffusion is due to the combination of shear and concentration gradient.

For Laminar Flow

For laminar flow region, the proposed model data for steady state permeate flux is much closer to the experimental steady state permeate flux data (**Figure 2.7**). But the deviation between steady state experimental flux data and other model e.g., Brownian, shear induced and concentration polarization model flux data gets wider as the TMP drops increases. The significance of particle size on back transport by the combined effect of Brownian and shear induced diffusion is represented. Brownian diffusion controls the back transport of very small droplets where as shear induced diffusion dominates of large particles. The proposed model Eq. (2.21) applies only to a feed suspension with uniform droplet size [109, 110]. But when the TMP drops is increased upto 207 kPa, the proportion of the droplet size was reduced in the permeate. The steady state permeate flux data predicted from proposed model is within the range ± 10% of experimental calculated steady state flux data.

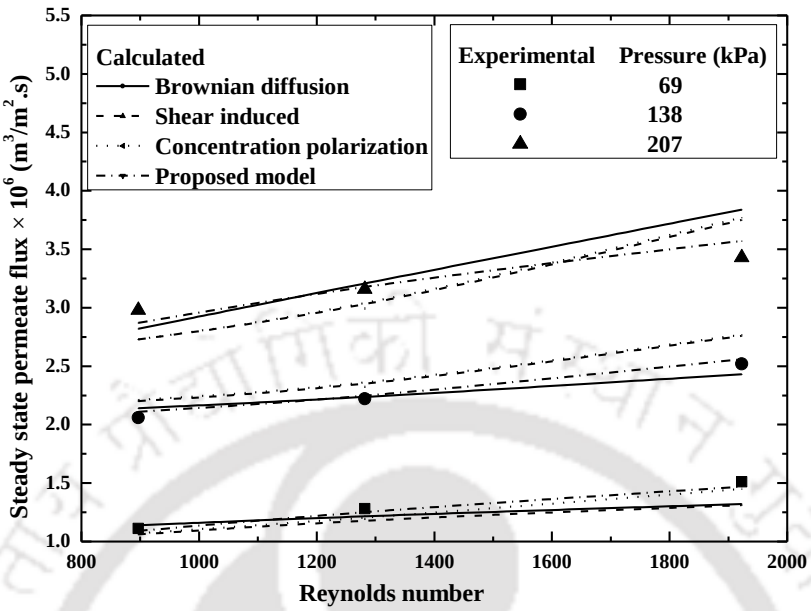

Figure 2.7. Variation of steady state permeate flux with Reynolds number for various TMP drops.

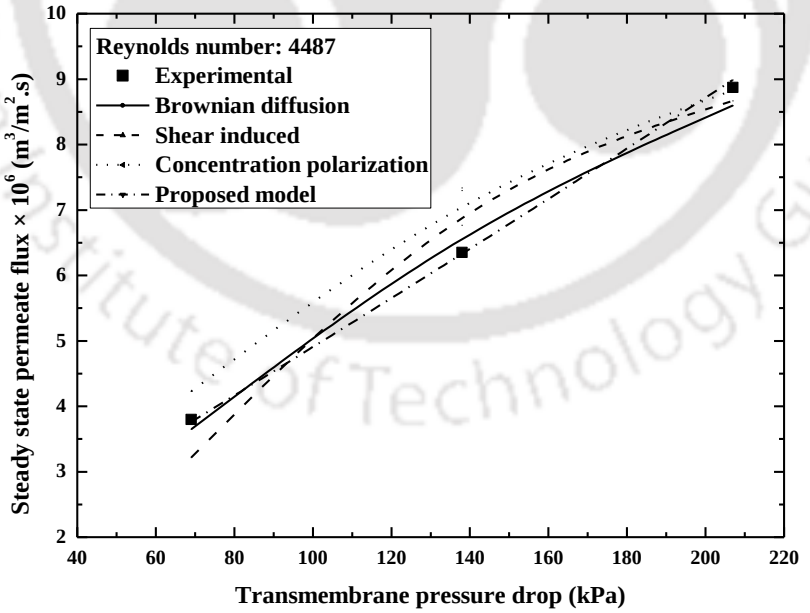

Figure 2.8. Variation of steady state permeate flux with TMP drops at Reynolds number of 4487.

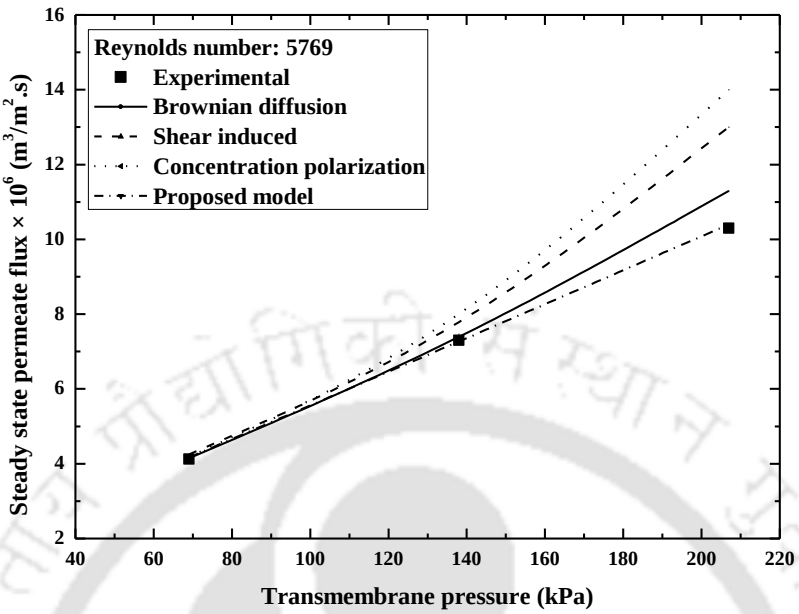

Figure 2.9. Variation of steady state permeate flux with TMP drops at Reynolds number of 5769.

For Turbulent Flow

The variations steady state permeate flux values for the Reynolds numbers of 4487 and 5769 in turbulent regime are presented in **Figures 2.8** and **2.9.** The model predicated steady state permeate flux data are much closer to the experimental data. Other models, i.e., Brownian, shear induced and concentration polarization model calculated flux deviate from experimental permeate flux data. The steady state permeate flux increases linearly with at lower TMP drops revealing the partial absence of concentration polarization or cake build up. But at higher TMP drops, steady state permeate flux data for different model deviate due to decrease the concentration polarization. The proposed model flux comes within the range ± 10% of experimental permeate flux.

2.6. Permeate Quality

The variations of oil retention with cross flow velocity at different TMP drops are shown in **Table 2.4.**

Table 2.4. Variation of retention oil with TMP drops and cross flow velocity

Feed		Cross flow velocity (m/s)	Reynolds number	Retention of oil (%)			Permeate COD (mg/L)
Oil conc. (mg/L)	COD (mg/L)			69 kPa	138 kPa	207 kPa	
192	2000	0.26	897	95.8	95.4	94.9	225
		0.33	1282	96.3	95.8	95.4	
		0.50	1923	97.0	96.7	96.3	
		1.16	4487	97.8	97.5	97.3	
		1.50	5769	98.0	97.9	97.8	

It is observed that with increase in TMP drops, the retention of oil decreases whereas increase in retention is observed with increase in cross flow velocity. With increase in TMP drops, the concentration of oil in permeate increases which causes the lower retention. On the other hand, with the increase of cross flow velocity, the extent of concentration polarization decreases that favors the retention. Also, an oil droplet at the membrane surface is less likely to enter a pore when the tangential velocity (Reynolds number) is increased and transverse (permeate) velocity is decreases due to decreased TMP drops. This is due to the skimming effect [111, 112]. The permeate quality is determined in terms of COD, TDS, ionic conductivity and oil concentration. It was found that the average COD, TDS and ionic conductivity of permeate remains at 225 mg/L, 1270 mg/L and 1.99 mho/cm respectively. The oil removal efficiency was

within the range of 94-98% depending on the experimental conditions. The oil concentration in permeate remains within the permissible limit (10 mg/L) for all the experimental conditions considered herein. For example, oil concentration in permeate remains at 4.5 mg/L at 207 kPa TMP drops and at Reynolds number of 5769. The alkali condition (pH=8) was more effective for oil removal than neutral one due to reduction of surface tension of treated waste [113].

2.7 Summary

The cross flow microfiltration process was applied to treat the oily wastewater using polyamide membrane. Characterization of oily wastewater and the membrane used was done. The average oil droplet size range was 0.01 to 47 µm and the average pore size of membrane was 1.16 µm respectively. The effects of cross flow velocity (Reynolds numbers) and TMP drops over steady state permeate flux and quality was investigated in detail. It was observed that transient flux declined with time due to the membrane fouling. Transient flux decline in turbulent flow was lower compared to laminar flow. The steady state permeate flux data increases with Reynolds number and TMP drops due to the increase of the shear stress and driving force. The fouling layer decreases due to the high shear stress development with Reynolds number. Solute concentration in the permeate decreases with Reynolds number and increases with the TMP drops. Three different models viz. Brownian diffusion, shear induced and concentration polarization models were used to quantify the steady state permeate flux data. It was observed that these models are not suitable enough to predict the experimental data. A proposed model based on Brownian diffusion and shear induced diffusion model was developed considering wide range of oil droplet sizes and used to

predict the accurate experimental flux data. The calculated flux data using the proposed model fit best within the range of $\pm 10\%$ of the experimental data point for both laminar and turbulent flow region.

Chapter 3

MEMBRANE BASED SEPARATION OF COAL-SOLVENT MIXTURE

Chapter 3

MEMBRANE BASED SEPARATION OF COAL-SOLVENT MIXTURE

In this chapter, organic solvent compatible ceramic membrane was prepared to recover solvent from extraction solution. The inorganic impurities of the Indian coal were removed by thermal extraction process using blended organic solvents, namely, n-methyl-2-pyrrolidinone (NMP) and ethylenediamine (EDA). Membrane characterization, extraction and microfiltration results were reported and discussed in detail. In another study, a low cost ceramic membrane was synthesized using industrial waste iron ore slime (IOS) of M/s TATA steel R&D, Jamshedpur (India) to separate the dissolved coking fraction from the solvent-coal mixture. Two different coals such as, sub-bituminous coal (A) and bituminous coal (B) were extracted using NMP and EDA.

The work presented in this chapter is published at ***Desalination*** 299 (2012), 123-128.

3.1 Experimental

3.1.1 Materials

Kaolinite ($Al_2Si_2O_5(OH)_4$), quartz (SiO_2), boric acid (H_3BO_3), calcium carbonate ($CaCO_3$), sodium carbonate (Na_2CO_3) and sodium meta silicate (Na_2SiO_3) were used for fabrication of ceramic membrane. N-methyl-2-pyrrolidone (NMP) and ethylenediamine (EDA) were used for coal extraction. All the chemicals were procured from Loba Chemie Pvt. Ltd., Mumbai, India and used without further purification. Sodium dodecyl sulphate was used as a cleaning agent. It was procured from Merck India Ltd. Steel industry waste iron ore slime (IOS) and Indian coal (coal A: sub-bituminous and coal B: bituminous, particle sizes below 100 µm) were supplied by TATA Steel R&D, Jamshedpur, India.

Physical and Chemical Properties of IOS

IOS is one of the waste materials formed in the steel production unit. It contains around 35 to 40% iron along with SiO_2 and Al_2O_3. It has good thermal stability and could be a suitable raw material for low cost ceramic membrane fabrication upon appropriate blending with other components. It is consisting of particle size less than 50 µm with a density of 5.1×10^3 kg/m^3. It is rich in iron oxides with rusty red color appearance. The elemental composition (wt %) of IOS is analysed by Energy dispersive X-ray spectroscopy (EDX) and is as follows: oxygen (41.80), iron (35.63), silicon (10.79), aluminium (10.47) and thallium (1.29). Iron in IOS acts as a binder for ceramic membrane fabrication providing strength and reduces the cost of synthesized

membrane. IOS was insoluble in de-ionized water and slightly soluble in acidic solution (pH 3-4).

3.1.2 Membrane Preparation and Characterization

The uniaxial die pressing method was employed to synthesis the membranes. All the membrane materials were heated for 3 hr at 100°C in a hot air oven (make: Reico Equipment & Instrument Pvt. Ltd., Kolkata, India) for moisture removal and then mixed thoroughly. The membrane disc (Ø 0.055 m, 0.005 m thick) was prepared by compacting the mixed materials in a rigid die under an applied load of 2 tons in a single axial direction with the help of a rigid piston for 2 min. A high speed energy efficient hydraulic deep drawing press (Make: Velan Engineering Coimbatore, India) was employed for this purpose. The compacted membrane weights about 22 g. The raw membrane was then sintered at different temperature in a programmable muffle furnace (Make: Reico Equipment & Instrument Pvt. Ltd., Kolkata, India) prior to membrane characterization and filtration test [82]. The disk was kept in hot oven furnace for two different sequential heat treatment processes. In the first heat treatment process, furnace temperature was increased from 25 to 250ºC at low heating rate of 1ºC/min for 4 hr. Low heating rate reduced the chance of crack formation in the membrane. The disk was kept at 250ºC for 20 hr. In the next heat treatment process, the temperature of hot oven furnace was increased from 250ºC to desired sintering temperature such as 900, 950 and 1000ºC at 2ºC/min. After that, membrane was kept for 6 hr in hot oven furnace to verify the effect of the membrane properties at desired sintering temperature. The sintered membrane was cooled at different cooling rate up to room temperature. The

prepared membrane was hard, rigid and porous texture. The composition of raw materials used for fabrication of inorganic membrane was shown in **Table 3.1**.

Table 3.1. Composition of raw materials used for fabrication of inorganic membrane

Material	**Composition dry basic (wt %)**
Kaolinite	50
Calcium carbonate	20
Sodium carbonate	10
Quartz	10
Boric acid	5
Sodium meta silicate	5

Morphological study of prepared ceramic membrane was done by scanning electron microscope (SEM, LEO 1430VP, Oxford, U.K.) to analyze the presence of possible defects in membrane. Imagej software (Version 1.37) was used to measure the pore size and the pore size distribution of membrane [113, 114]. SEM images were taken from various parts of the prepared membrane and magnified using software. The shapes of the pores were assumed to be circular and around 150 pores were considered to calculate the average pore diameter of a sample. Due to the limitation of the software, pores below 10 nm were not measured. Chemical stability of ceramic membrane was done with acidic, alkaline solution and NMP.

Membrane Porosity

Porosity of the membrane is determined by the pycnometric method using water as wetting liquid. The membrane was immersed in de-ionized water for two consecutive days and the porosity was determined by using Eq. (3.1).

$$porosity = \frac{\text{void volume}}{\text{bulk volume}} \tag{3.1}$$

$$Porosity = \frac{(w_2 - w_1)/\rho_w}{w_1/\rho_m} \tag{3.2}$$

or

$$Porosity = \frac{(w_2 - w_1)}{\rho_w \times V_m} \tag{3.3}$$

where, w_1 was the dry membrane weight, w_2 was membrane weight after 24 hr dipped in a water, ρ_w was the density of water, ρ_m was apparent density of membrane and V_m (w_1/ρ_m) was the membrane volume.

Pore Size Distribution

The pore size distribution of prepared ceramic membrane sintered at different temperatures was analysed by SEM/EDX technique. Small pieces of the prepared ceramic membranes were cut out without distorting the surface geometry and used for SEM/EDX analysis. The ceramic membrane samples were fixed to the SEM stub with conductive adhesive and a thin layer of gold coated using sputtering device. The top image of membrane active layers was recorded and the average pore diameter determined according to the Eq. (3.4) using the imagej software (Version 1.37).

$$d_s = \left[\frac{\sum_{i=1}^{n} n_i d_i^2}{\sum_{i=1}^{n} n_i} \right]^{0.5} \quad (3.4)$$

where, n is the number of pores and d_i is the pore diameter (μm) of the i^{th} pore [113].

Membrane Hydraulic Permeability

The water permeability measurements were performed at room temperature (25±2ºC) using 500 ml of deionized water in a membrane filtration cell. The effective membrane cross-sectional area was 2.38×10^{-5} m^2. According to Darcy's law, the steady state permeate flux, J_{ss} ($m^3/m^2.s$) is defined as Eq. (3.5):

$$J_{ss} = L_p(\Delta P - \Delta\pi) = \frac{dV_p}{A_m\, dt} \quad (3.5)$$

where, ΔP was TMP drops (kPa), $\Delta\pi$ was osmotic pressure (kPa), A_m was membrane cross-sectional area (m^2), dV_p was volume collected on permeate (m^3) side at particular time interval dt (seconds). Hydraulic permeability of ceramic membrane was determined from the steady state permeate flux value measured after stabilization at different TMP drops (after 35 min of water filtration experiment). It was seen that the steady state permeate flux increased linearly with TMP drops. The hydraulic membrane permeability L_p (m/Pa.s) was determined from the slope of steady state permeate flux with TMP drops (Eq. (3.6)) with $\Delta\pi$=0 for pure water [114].

$$L_p = \frac{J_{ss}}{\Delta P} \quad (3.6)$$

Chemical Stability Test

The membrane chemical/corrosion stability test was performed both at acidic (pH 2) and basic (pH 12) conditions with 500 mL corrosion liquid. The solution pH adjustment was carried out using 0.1M HCl and NaOH. The membrane was kept immerged in the solution for one week at atmospheric conditions, then washed with deionized water and dried at 80ºC for 2 hr. The porosity and EDX analysis before and after acid or alkalis treatment were conducted in order to study the membrane stability when exposed to corrosive environment [115].

3.1.3 Extraction Experiments

The measured amount of coal, NMP and EDA were placed in round bottom flask (5×10^{-4} m^3 capacity). The flask was connected to a reflux condenser and electrically heated by means of a heating mantle controlled by a variac. The apparatus was shown in **Figure 3.1**. The extraction experiment was carried out for one hour under total reflux condition at 180ºC. After extraction, the hot extracted mixture was passed through two 500 mesh stainless steel (SS) screens consecutively (refer Appendix). Non coking solid coal residue was retained on the 500 mesh SS screen surface and coking part of coal was suspended in organic solvent.

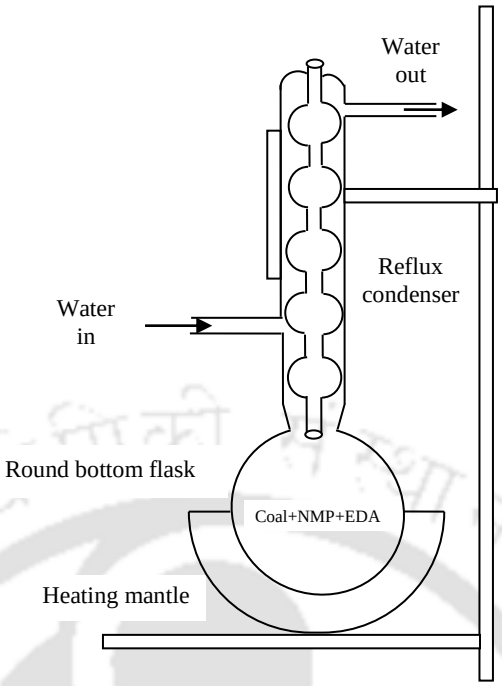

Figure 3.1. Apparatus for the extraction of coal under total reflux condition.

The detailed systematic scheme of coal extraction and solvent recovery was shown in **Figure 3.2**. The non coking coal was dried and weighted separately. Coking parts of coal was feed in first membrane filtration cell. Permeated organic solvent from first membrane filtration cell was used for the second stage extraction. In second membrane filtration cell, the solvent was recovered from coal organic solvent mixture. The separated solvent was reused in third stage extraction operation. After this, the extracted solvent was further recovered by third membrane filtration cell. The ratios of coal/organic solvent composition were kept constant for every extraction stages.

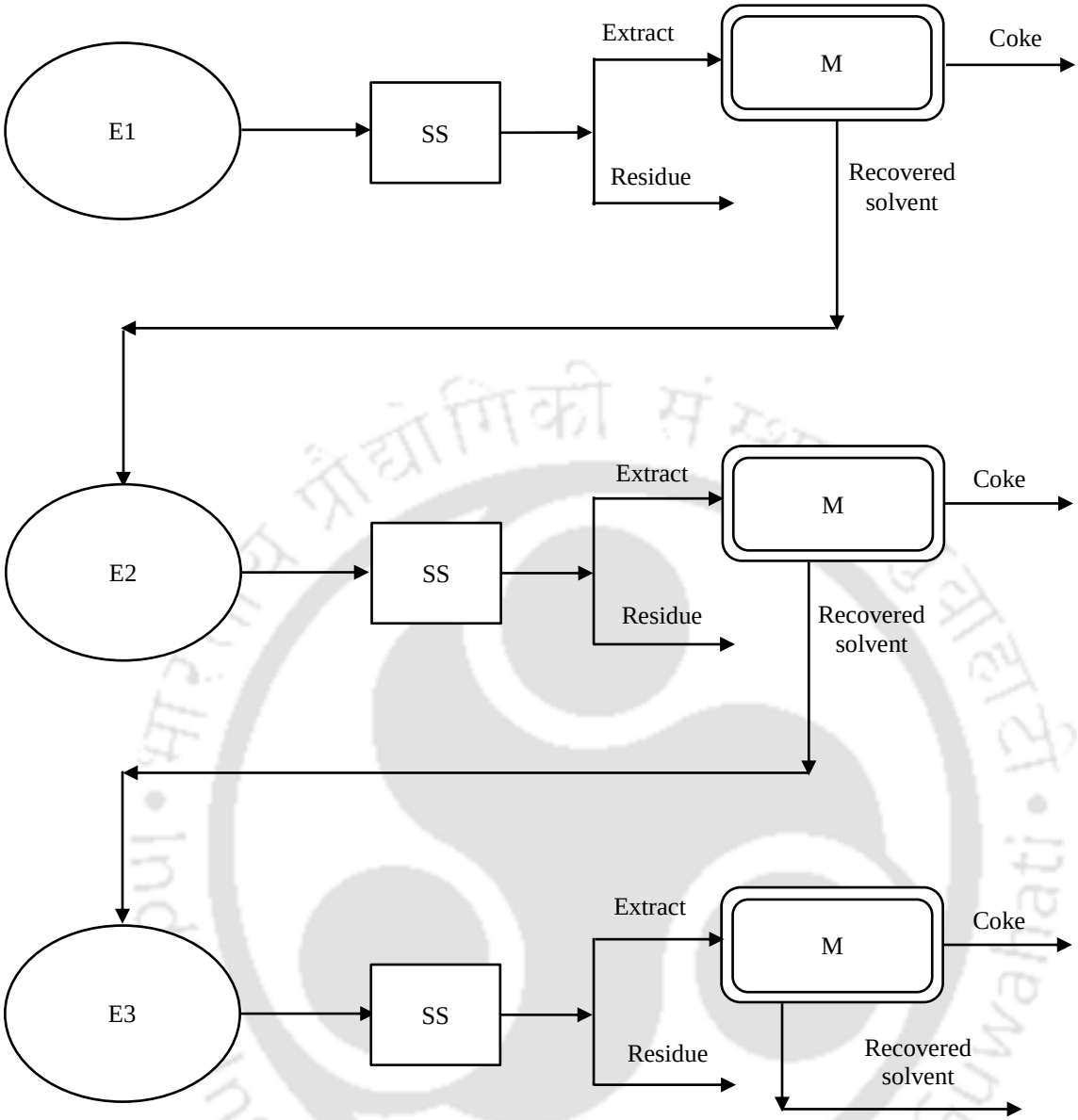

Figure 3.2. Flow sheet diagram of experimental schemes: (1) E1, E2, E3: Extraction stages 1, 2 and 3; (2) M: microfiltration membrane cell; (3) SS: Two 500 mesh stainless steel screens.

3.1.4 Experimental Set up

A cylindrical batch membrane filtration cell (capacity: 5×10^{-4} m^3) made of stainless steel was designed and fabricated at IIT Guwahati, India. The schematic of the experimental set-up was shown in **Figure 3.3**. One control valve was arranged in batch

cell to maintain the TMP drops (203 kPa) inside the system. The cell consisted of one matching flanges with diameter of 0.06 m. The bottom flange was consisted of internal grid structure. A porous stainless steel plate was placed on lower portion that provides the mechanical support of the ceramic membrane and was placed in the lower section. One gasket was provided in the bottom flange cell and tightened with bolt to create a leak proof cell. Permeate was collected from bottom of the cell. For uniform mixing, one stirrer was attached on the top of the membrane filtration cell. All membrane experiments were performed under nitrogen atmosphere. This was particularly important during the experiment, as trace of oxygen may inhibit the extent of coal dissolution.

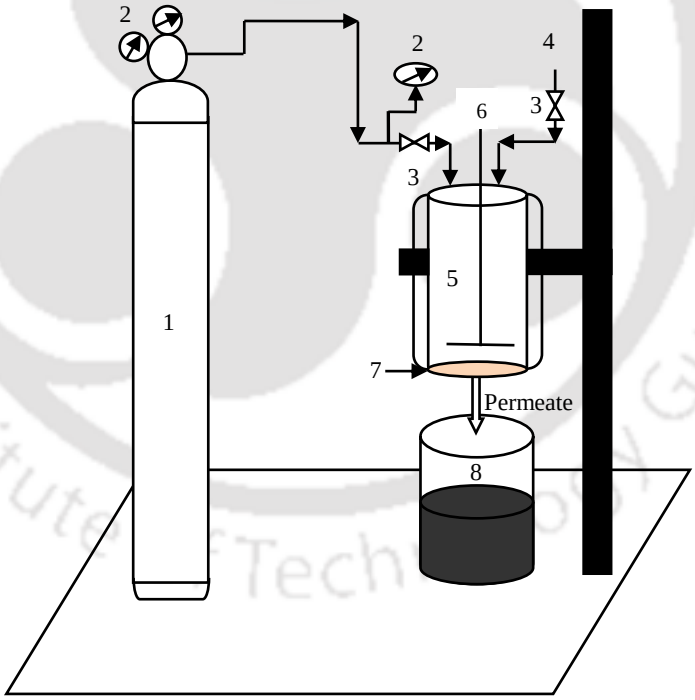

Figure 3.3. Schematic of the batch experiment set up: (1) nitrogen cylinder, (2) pressure gauge, (3) control valve, (4) inlet feed, (5) membrane cell, (6) mechanical stirrer, (7) ceramic membrane, (8) recovered solvent.

Membrane experiments were carried out until permeate flux remained almost zero (~2 hr). Permeate was free from coking coal for all the extraction stages. At the end of each experimental run, the membrane was dried and cleaned with an ordinary brush to remove coal particles deposited over the membrane surface. After that, the membrane was reversely placed on membrane cell and cleaned with cleaning agent to recover the membrane original permeability. Membrane cleaning did not increase additional cost except the negligible amount of membrane experimental cost.

3.1.5 Coal Extraction and Solvent Recovery Mechanism

Coal constitutes a network type structure. NMP is a suitable organic solvent for extraction of bituminous and sub bituminous coals. The extraction primarily occurs from the outer surface of coal particles due to high viscosity (1.81×10^{-3} Pa.s) and low penetration. For this reason, NMP alone has a low extraction yield. The solvent diffused inside the coal particles and soluble coal molecules comes out. During solvent extraction some of the solvent remain inside the porous structure of coal and resulting in swelling. The swelling results in loss of organic solvents during extraction process. Organic solvent breaks the intermolecular forces among coal molecules, such as, H-bonding, van der walls forces and other charge transfer π-π interaction and makes bonding with coal molecule resulting in coal extraction. EDA commonly is mixed with NMP to improve the extraction yield as it reduces viscosity and can easily penetrate inside the network like coal structure. A 9:1 NMP to EDA ratio could reduce the viscosity to 1.67×10^{-3} Pa.s from 1.81×10^{-3} Pa.s for pure NMP. EDA addition also reduces the cost of solvent.

A mixture of organic solvent and coal particles was collected after the extraction operation as filtrate and was permeated through a membrane filtration cell. In membrane filtration cell, organic solvent was recovered as permeate through membrane pores and suspended materials (coke) were collected on membrane surface.

3.1.6 Analysis

Proximate and Ultimate Analysis

Proximate analysis is the most often used coal characterization technique in connection with their utilization for a specific purpose. The proximate analysis was performed according to the ASTM D3172-07a method [116]. Ultimate analysis of a fuel provides the elementary composition of carbon, hydrogen, oxygen, nitrogen and sulfur (free from moisture and inorganic constituents). The ultimate analysis was carried out as per the ASTM D3176-89 method [117].

Fourier Transform Infrared Spectroscopy (FTIR) Analysis

In order to observe the absence of coal in permeate, Fourier transform infrared spectroscopy (FTIR) was performed for pure coal samples, pure NMP and the permeate using a PerkinElmer spectrum 65 FTIR spectrometer, USA. FTIR of pure EDA is not shown because of low EDA concentration in the blended solvent with respect to NMP and it gives synergistic effect only in coal extraction. Due to synergistic effect of organic co-solvent (EDA), total extraction yield of the coal is found to increase. The diffused reflectance spectra were recorded and analysed. The spectra were obtained with the KBr pellets (5:100 w/w).

Pore Formation Mechanism Ceramic Membrane

Calcium carbonate ($CaCO_3$) played an important role in the formation of pores in ceramic membrane. During calcination, $CaCO_3$ is decomposed into calcium oxide and carbon dioxide (Eq. (3.7)):

$$CaCO_3 \rightarrow CaO + CO_2 \quad (3.7)$$

CO_2 dispersion path creates the membrane pores. Similarly, high temperature calcinations with various forms of iron ores, such as, magnetite Fe_3O_4, hametite Fe_2O_3, goethite FeO(OH) or siderite $FeCO_3$ generating iron oxide and CO_2 could enhance membrane pore formation.

3.2 Development of Membrane Based Technology for the Separation of Coal from Organic Solvent

In this section, development of membrane based technology for the separation of coal from organic solvent was discussed in detail. Membrane characterization, extraction and microfiltration results were also reported.

3.2.1 Results and Discussion

3.2.1.1 Effect on Pore Size Distribution with Sintering Temperatures

The pore size distributions of prepared ceramic membranes at different sintered temperature were analysed by SEM/EDX technique. The SEM images were taken from top view of membrane active layers as shown in **Figure 3.4**. The average pore diameter of prepared membranes sintered at 900, 950 and 1000ºC was around 0.8 μm, which correspond to microfiltration range (refer **Figure 3.4**). It was observed that the pore size distribution was closely related to the sintering temperature. For all the sintering temperatures, the maximum numbers of pores (65-75%) were in the range of 0.75-0.78 μm and were shown in **Figure 3.5**. The average pore size of the membrane was increased with sintering temperature, and the pore size distribution curves were broadened simultaneously. This was partly due to the growth of grains leading to the formation of large pores and elimination of small pores [118, 119].

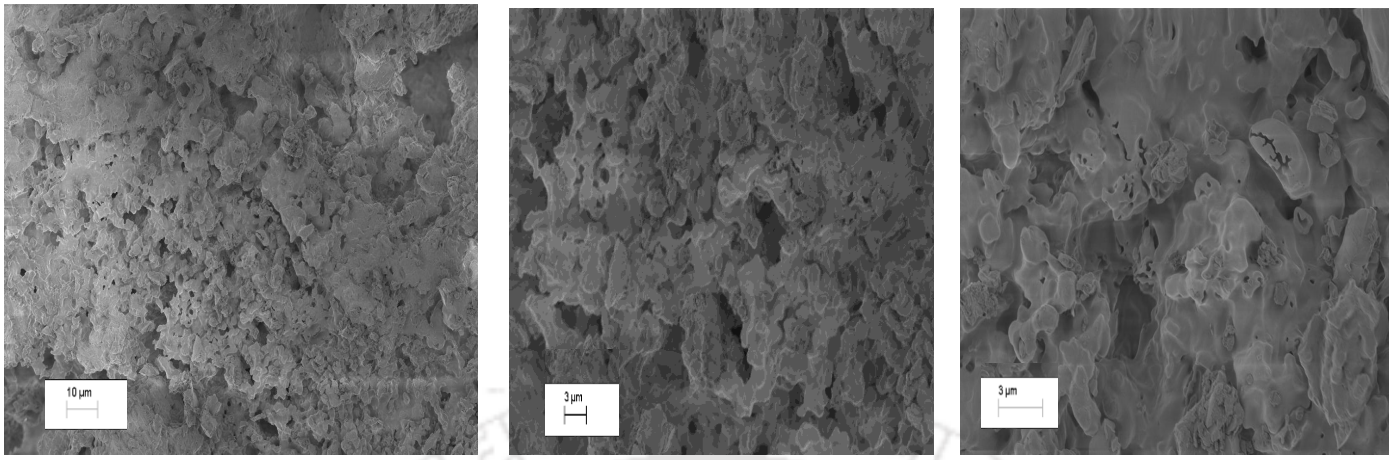

EHT=10.00 kV Mag=1.85 KX WD= 12 mm **EHT=10.00 kV Mag=1.85 KX WD= 12 mm** **EHT=10.00 kV Mag=1.85 KX WD= 12 mm**

(a) **(b)** **(c)**

Figure 3.4. SEM photographs of the prepared ceramic membrane sintered at (a) 900ºC, (b) 950ºC and (c) 1000ºC.

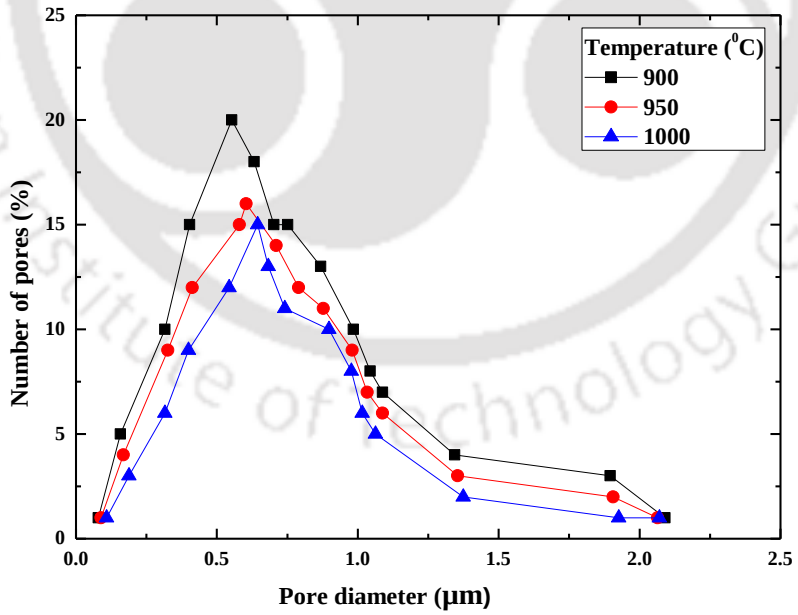

Figure 3.5. Pore size distribution of the prepared membrane sintered at different temperatures.

3.2.1.2 Chemical Stability

Variation of ceramic membrane porosity with pH and NMP solution at different sintered temperature was shown in **Table 3.2**. The membrane porosity was found to decrease with membrane sintering temperatures. It was measured as 0.31 to 0.28 within sintering temperature range of 900 to 1000ºC. The corrosion resistance of the prepared ceramic membranes at different sintering temperatures were analyzed using NaOH (pH=12); HCl (pH=2) and pure NMP solutions. The membranes were subjected at different pH solutions and porosity was measured after seven consecutive days at atmospheric conditions. However, insignificant change (2-6%) in membrane porosity was observed with HCl, NaOH solutions and pure NMP.

Table 3.2. Variation of membrane porosity in HCl, NaOH and NMP at different sintering temperatures

Temperature (°C)	**Porosity (after seven days)**			
	Fresh membrane	**pH: 2**	**pH: 12**	**Pure NMP**
900	0.30	0.33	0.32	0.31
950	0 28	0.29	0.30	0.29
1000	0.26	0.26	0.28	0.28

The ceramic membrane sintered at 1000ºC was dipped in acid, alkali and NMP. Energy-dispersive X-ray spectroscopy (EDX) analysis was performed after seven consecutive days (refer **Table 3.3**).

Table 3.3. Comparison of EDX analysis of fresh membrane, pH=2, pH=12 and pure NMP dip membrane sintered at 1000ºC after seven days

Element Present	Weight (%) (after seven days)			
	Fresh membrane	pH: 2	pH: 12	Pure NMP
Oxygen	45.96	45.80	46.12	45.12
Sodium	7.09	7.18	7.12	7.25
Aluminium	7.73	7.85	7.65	6.89
Silicon	11.04	12.13	11.39	12.13
Thallium	3.56	3.87	3.63	4.63
Calcium	24.62	23.17	24.09	23.89

It was observed that the elemental compositions of the prepared ceramic membrane were found almost invariant with different pH (2 and 12) and pure NMP solution. Similar results were obtained for other membranes prepared at 900 and 950ºC sintering temperatures. Therefore, the ceramic membranes had good corrosion resistance and suitable for different microfiltration applications.

3.2.1.3 Solvent Recovery after Extraction

Extraction experiments were conducted using 5 g of coal and varying solvent volume from 25 mL to 90 mL (w/v ratio varies from 1:5 to 1:18) in order to find out optimum solvent requirement. After extraction process, the non coking parts of coals were recovered through two successive 500 mesh stainless steel screens and coking parts of the coal with organic solvent were collected separately. The percentage of solvent recovery was calculated as the ratio of filtrate volume recovered after extraction to the total volume used for extraction. It was observed from **Figure 3.6** that the solvent

recovery (%) was increased sharply upto coal to solvent ratio in the range of 1:9. and 1:10. The increase in solvent recovery was due to the increase in the amount of solvent. Beyond coal to solvent ratio of 1:10, solvent recovery was found to decrease slightly due to more swelling of coals. In these optimum conditions, the maximum solvent recovery was 98.6 and 97.2%, respectively. Rest amount of solvent remained with non coking parts. Therefore, these ratios were considered for all the extraction experiments. The non coking parts of coal was separated and weighted as 2.32 g and 2.16 g for the coal to solvent ratio of 1:9 and 1:10, respectively (**Figure 3.7**).

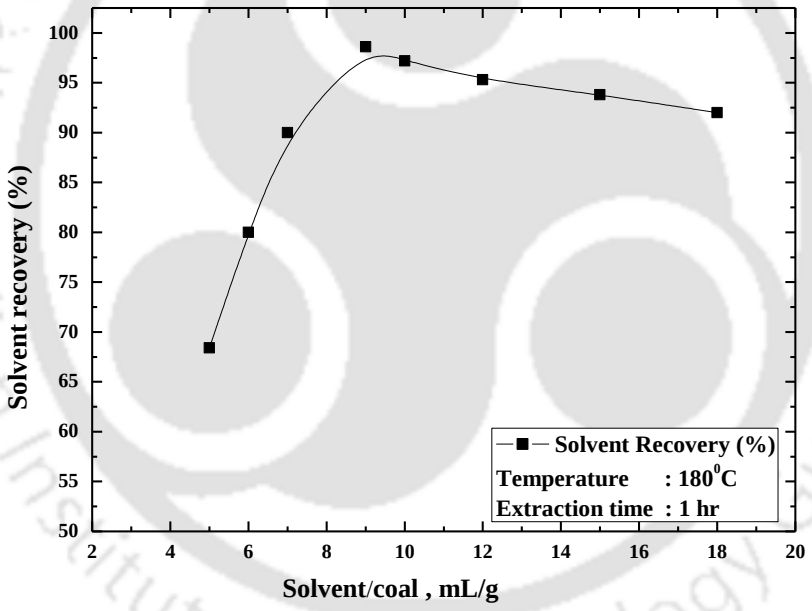

Figure 3.6. Effect on solvent recovery (%) for the variation of solvent/coal ratio.

3.2.1.4 Solvent Recovery at Different Extraction Stages

From the solvent recovery (%) at optimum conditions of coal/solvent (1:9 and 1:10) in three extraction stages, it was observed that 98.2, 72.2 and 70% solvent was recovered in stage one, stage two and stage three, respectively, for the coal to solvent

ratio of 1:9. The decrease in percentage solvent recovery with increase in stage number was due to the increase in impurities in solvent used for each stage. Similar observation was found for the coal to solvent ratio of 1:10, where 97.2, 67.8 and 66.3% of solvents were recovered for successive three stages. This is to be noted here that the extent of solvent recovery (%) was more in case of coal/solvent ratios of 1:9 than that of 1:10 which was corroborated with **Figure. 3.6**.

The coking parts of coal remained in the filtrate and the non-coking fraction was retained by the 500 SS mesh screen. It was found that for the coal to solvent ratio of 1:9, the coking coal fraction remained in the solvent as 2.84, 1.59 and 0.92 g, respectively for successive stages. In first stage, the extraction efficiencies were 56.8 and 53.3%, whereas these were 46 and 45%, respectively, for solvent to coal ratio of 9:1 and 10:1 in the third stage. The decrease in the amount of coking coal with extraction stages was due to the decrease of efficiency of solvent. It might also be found that the amount of coking coal was less in case of coal to solvent ratio of 1:10 than that of 1:9 for all the three stages. Similar trend (as that of coking coal) for non-coking coal retention was observed for three stages.

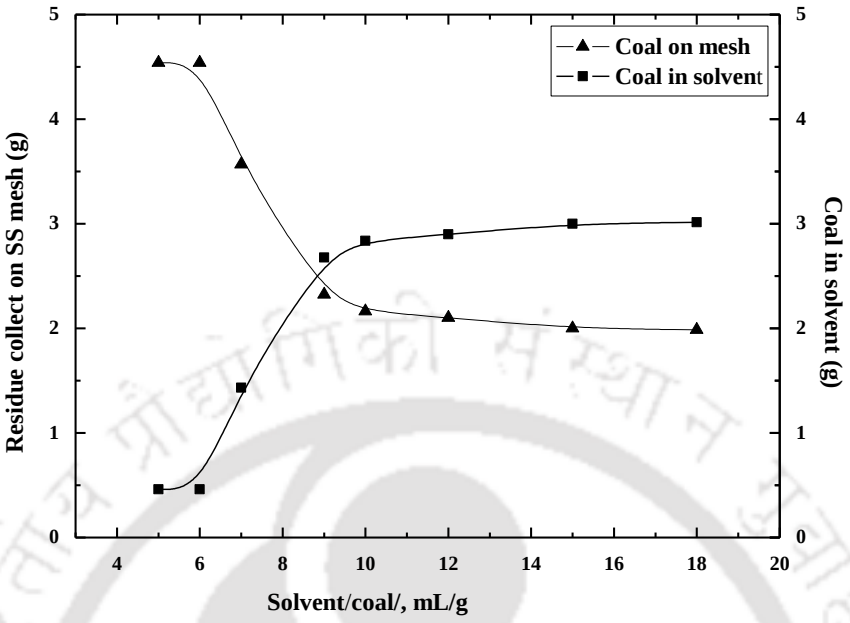

Figure 3.7. Variation of residual coal collected on 500 mesh SS surface and dissolved coal with solvent/coal ratio.

3.2.1.5 Microfiltration Results

In order to recover coking coal from the extract of three stages, microfiltration (MF) experiments were performed at a constant TMP drop of 203 kPa and stirring speed of 500 rpm in batch mode of operation. The variation of permeate flux with time for three stages was shown in **Figure 3.8**. It was observed from the figure that flux declined rapidly with operating time at the beginning of the experiment (within 10 min). After that the decline was gradual. The permeate flux became almost zero after 2 hr.

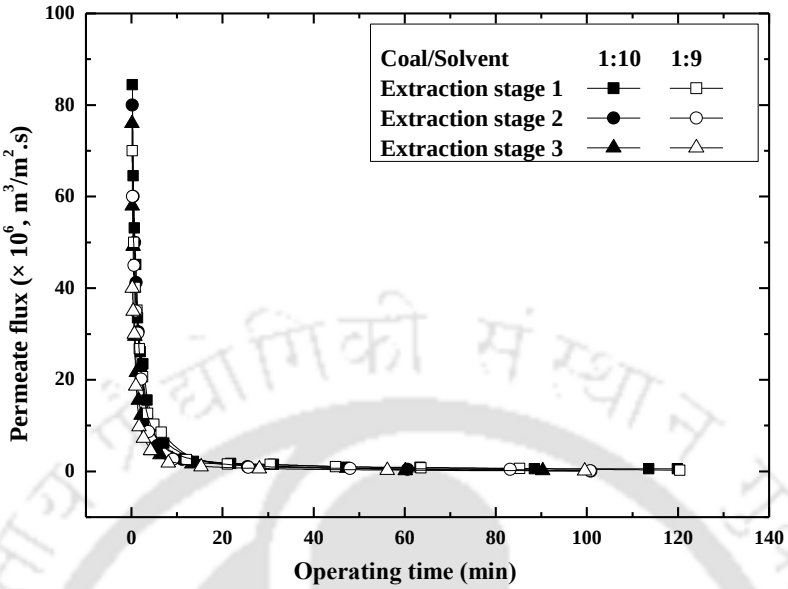

Figure 3.8. Transient flux decline with time for variation of coal/solvent (1:9 and 1:10) for three extraction stages.

The variation of cake and fouling resistance (R_C+R_F) with operating time at coal/solvent (1:9 and 1:10) for three extraction stages was shown in **Figure 3.9**. The combination of these two resistances had increased with operating time for both the cases. The development of the resistances due to cake formation and fouling was more for the filtrate of coal/solvent ratio of 1:9 (w/v) than that of 1:10 (w/v). This was due to higher deposition of coking coal over the membrane surface as extraction was more in coal/solvent ratio of 1:9 (w/v).

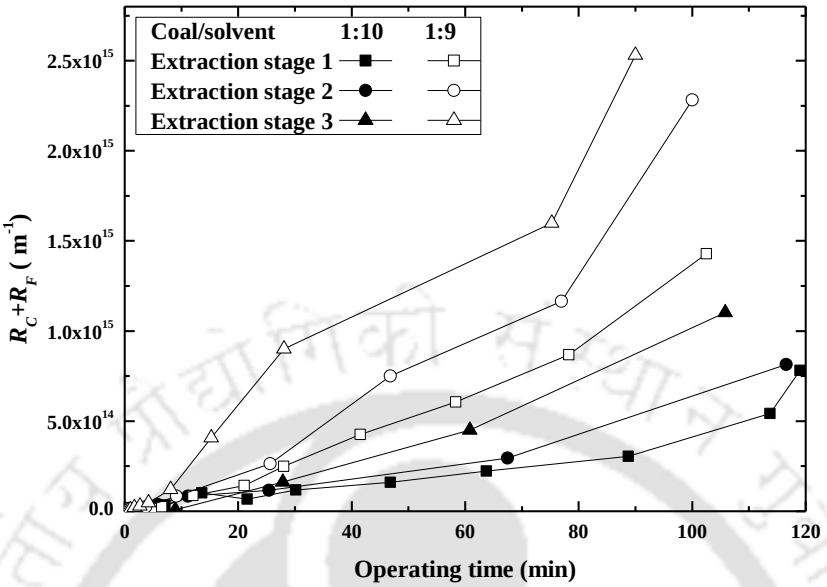

Figure 3.9. Development of cake and fouling resistance with time at coal/solvent (1:9 and 1:10) for three extraction stages.

Furthermore, it was observed that the development of resistance was more in stage two compared to stage one. For example, the sum of cake and fouling resistance (R_C+R_F) was 0.8×10^{15} m^{-1} in stage one (coal/solvent ratio of 1:9) whereas, it was about 1.3×10^{15} m^{-1} in stage two for the same coal/solvent ratio after 80 min of operation. The resistance further increased to 1.9×10^{15} m^{-1} in stage three. The collected permeate was free from coking coal (discussed in subsequent section) and the retentate was thick slurry of mixture of solvent and coking coal. The solvent recovered (%) was calculated from the permeate volume for three stages for optimum conditions of coal to solvent (1:9 and 1:10). It was observed that the organic solvent recovered from microfiltration experiment at optimum conditions of coal to solvent ratio (1:9 and 1:10) after first extraction experiments were around 70 and 71%, respectively. Permeate collected from

extraction stage one was again reused as a feed for solvent in extraction stage two. The solvent recovered at optimum conditions of coal/solvent (1:9 and 1:10) through membrane filtration cell after second extraction stage was 67.3 and 67.9%, respectively. Permeate obtained from second membrane experiment was again reused for extraction stage three and solvent recovered at coal/solvent (1:9 and 1:10) were 65.6 and 66.4%, respectively.

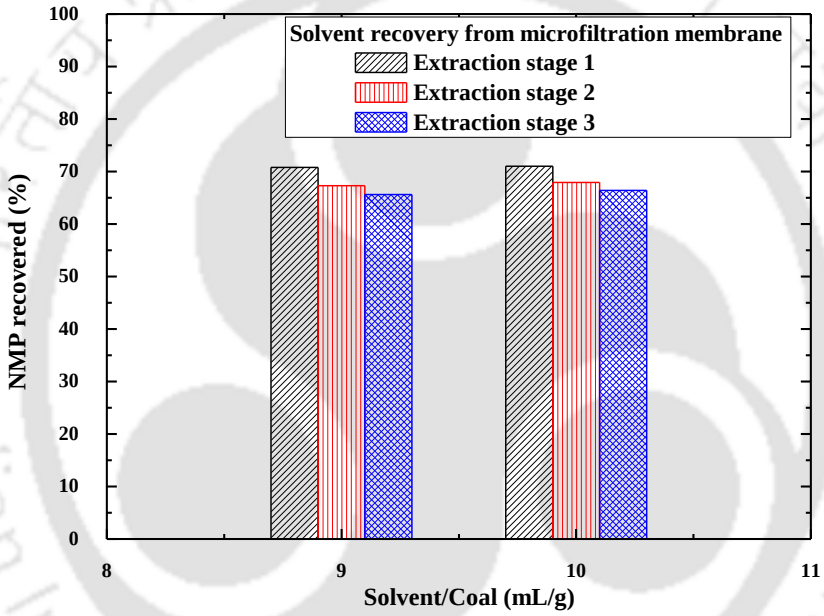

Figure 3.10. Variation of solvent (NMP) recovery with optimum solvent/coal ratios for three extraction stages.

As shown in **Figure 3.10**, solvent recovered from coal/solvent (1:9) was slightly lower (~1%) than solvent recovered from coal/solvent (1:10) at different extraction stages. It might be seen that the increase in percentage recovery from coal/solvent (1:9) to coal/solvent (1:10) was marginal (remains within 67 to 71%) for both the cases. The rest amount of solvent remained with coking coal in the retentate part. Vacuum

filtration technique might be used to get dried coking coal and complete recovery of solvent. From the performance of combined extraction and microfiltration experiments, it might be concluded that the proposed energy intensive method (microfiltration) was the best alternative method for the extraction of coking coal compared to the existing distillation method.

3.2.1.6 Fourier Transforms Infrared Spectroscopy (FTIR) Analysis

Fourier transform infrared spectroscopy (FTIR) analysis was performed to observe the presence of coal in permeate. Diffuse reflectance spectra were recorded with a PerkinElmer spectrum 65 FTIR spectrometer, USA at wave length in the range of 4000 to 400 cm^{-1}. Coal, NMP and permeate sample were mixed separately with KBr in 5:100 (w/w) to make a pellet of less than 20 μm size. The pellet was prepared under an infrared light to prevent possible absorption of water. The spectra of Indian coal, pure NMP and permeate were shown in **Figure 3.11**. The broad absorption band at 3404 cm^{-1} and 1655 cm^{-1} were observed due to N-H stretch [120], 2917 cm^{-1} correspond to C-H group [121], 1030 cm^{-1} correspond to >S=O (sulfoxide group), 535 cm^{-1} correspond to acetates and 468 cm^{-1} was identified as Si-O (silicates) in coal sample. The band at 2136 cm^{-1} and 2143 cm^{-1} were observed in pure NMP and permeate side due to -CN- absorption. The band around 2136 cm^{-1} and 2143 cm^{-1} was absent in coal sample. It confirms the absence of coal in the permeate. Again, the band at 1305 cm^{-1} observed in NMP and permeate due to C-O group was not observed in the coal sample. The distinct peak at 1031 cm^{-1} for the presence of sulphur in pure coal was not found in permeate confirms the complete removal of coal during microfiltration. The peak at 468 cm^{-1} was observed in coal sample due to the kaolinite mineral group

and that peak was not observed in NMP and permeates. This observation indicates that permeate contains only coal free NMP. Further, absence of coal was confirmed by water precipitation test. In this test, water was added in the permeate and coal precipitation was not observed. On the basic of different bands in 2136 cm^{-1}, 2143 cm^{-1}, 1305 cm^{-1}, 1031 cm^{-1}, 468 cm^{-1} and water precipitation test, it may be concluded that coal particles were not passed through the membrane and permeate was totally coal free which can be reused for fresh extraction.

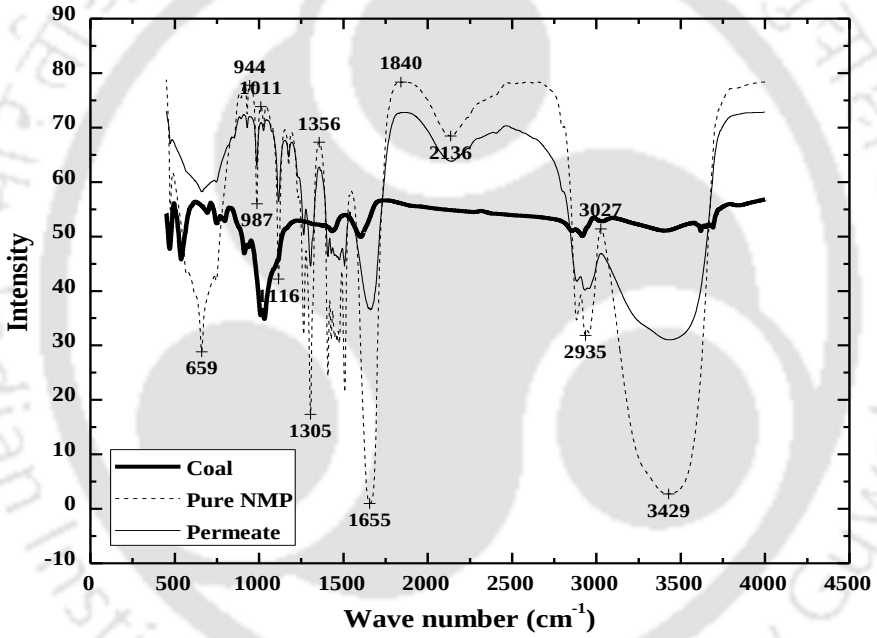

Figure 3.11. FTIR analysis of coal, pure NMP and permeate.

3.2.2 *Summary*

A membrane based technique was proposed to improve the economy of the coke making process from non coking coal. The work summarized fabrication of a defect free ceramic microfiltration membrane with average pore diameter of around

0.80 μm. Membrane characterization was performed and porosity was measured as 0.31 to 0.28 within sintering temperature range of 900 to 1000ºC. The prepared ceramic membrane had good chemical stability in NMP, pH 2 and pH 12 solutions. Coal was extracted at different coal to NMP ratio and the optimum ratio for better extraction was determined as 1:9 and 1:10. Recovered permeate from microfiltration membrane was reused for extraction purpose and process was repeated in three successive stages. In stage one, the filtrate after extraction process was subjected to microfiltration and 71% of pure NMP was recovered as permeate. The permeate obtained from stage one was further utilized for extraction process in stage two and thereafter stage three. Solvent recovered was 68 and 66% for stage two and stage three, respectively. The efficiency for coke recovered in three stages was 98.2, 72.2 and 70%, respectively for the coal to solvent ratio of 1:9 (w/v). The FTIR analysis result showed that the permeate from all three stages was free of coal and might be reused for further extraction process. Therefore, this membrane based technology will definitely reduce the solvent recovery cost using existing distillation technique.

3.3 Fabrication of Cost Effective IOS Ceramic Membrane for the Recovery of Organic Solvent used in Coke Production

In this section, utilization of steel industry waste IOS for the fabrication of cost effective ceramic membrane and its application in coal-solvent separation for the improvement of coke properties, namely, ash and sulphur content reduction and increment of carbon content were discussed.

3.3.1 Results and Discussion

The results and discussions are organized in three sections. Firstly, the membrane synthesis using IOS and their characterizations are provided. The coal extraction test followed by membrane filtration is summarized in the second section. Membrane cleaning and preliminary cost estimation of the fabricated membrane is then outlined.

Membrane Fabrication and Characterization

3.3.1.1 Selection of Membrane Compositions

The inorganic raw materials utilized for the fabrication of IOS ceramic membrane were listed in **Table 3.4**. Four different combinations of the compositions designated as I, II, III and IV were used for membrane synthesis. Both IOS and kaolin were good refractory materials and could withstand high temperature up to 1000°C. It can also bind easily with other inorganic materials due to presence of heavy metals. This was one of the reasons that only the content of IOS and kaolin were changed in membrane fabrication by keeping their total composition unchanged. IOS content was

increased from 5 to 20% for the purpose of the membrane cost reduction. Higher IOS concentration was desirable for low membrane cost. Up to 10% IOS, dissolution of prepared IOS membrane was around 0.5%, whereas, it was about 5.5%, when 15% IOS was used. The membrane was not good corrosion resistant in acid solutions (pH = 3) beyond 10% IOS. By keeping both the parameters in mind, 10% IOS composition (II) was selected for synthesis of membrane used in the subsequent experiments. Three different sintering temperatures, such as, 700, 800 and 900°C were chosen to fabricate IOS ceramic membrane.

Table 3.4. Selection of suitable membrane compositions

Raw materials/Property	**Composition on dry basic (wt %)**			
	I	**II**	**III**	**IV**
IOS	5	10	15	20
Kaolin	45	40	35	30
Calcium carbonate	20	20	20	20
Sodium carbonate	10	10	10	10
Quartz	10	10	10	10
Boric acid	5	5	5	5
Sodium meta silicate	5	5	5	5
Dissolution of IOS membrane in acid solution (pH 3) (%)	**0**	**0.5**	**5.5**	**8.5**

3.3.1.2 Pore Size Distribution, Porosity, Hydraulic Permeability and Corrosion Stability

The average membrane pore diameters (particle number average) were determined to be 0.602, 1.053 and 1.103 µm at sintering temperature of 700, 800 and

900°C respectively, which come in the microfiltration range. It was observed that as sintering temperature increased, the average pore diameter also increased. The small pores as well as void spaces smashed together with big pores and formed uniform packing with increase in temperature. As a result, the average membrane pore numbers sharply decreased with the increase of sintering temperature.

The pore size distribution of the prepared membrane was shown in **Figure 3.12**. It was observed that the variation of percentage pore numbers with pore diameter was characterized by a single sharp peak over a narrow range of pore diameters. This indicated that the selected membrane composition was effective for formation of uniform pore size distribution.

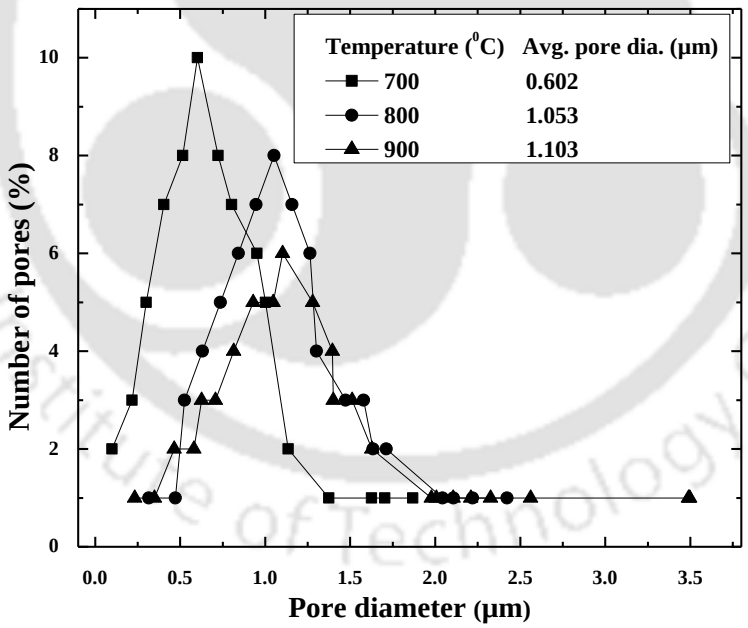

Figure 3.12. Membrane pore size distribution at different sintering temperatures.

The variation of porosity with sintering temperature was represented in **Table 3.5**. It was evident from the result that, the membrane porosity decreased nearly by 9% when the sintering temperature increased from 700 to 900°C. The membrane was densified by decreasing the porosity at higher sintering temperature. With enhancement of sintering temperature porosity decreased and pore size increased due to elimination of small pores and formation of enlarged pores.

The membrane hydraulic permeability (L_p) also followed the same trend as of pore size (**Table 3.5**). The liquid permeability was found to increase from 1.58×10^{-12} to 3.81×10^{-12} (m/Pa.s) because of lager pore size at higher temperature. Due to enhancement of membrane permeability, water molecule convecting towards membrane matrix, permeate faster resulting increase of permeate flux.

Table 3.5. Variation of porosity, pore size and hydraulic permeability with sintering temperature

Sintering Temperature (°C)	**Porosity**			**Pore size (µm)**	**L_p ×10^{12} (m/Pa.s)**
	Fresh Membrane (II)	**pH 2**	**pH 12**		
700	0.33	0.34	0.35	0.601	1.58
800	0.32	0.33	0.34	1.053	2.01
900	0 30	0.32	0.33	1.103	3.81

The porosity increased only by 5 to 9% under chemical corrosion test at pH 2 and pH 12 (**Table 3.5**). This suggested that the membrane synthesized using the

composition II (**Table 3.5**) was refractory in nature and could be used over a wide pH range.

3.3.1.3 SEM and EDX Analysis

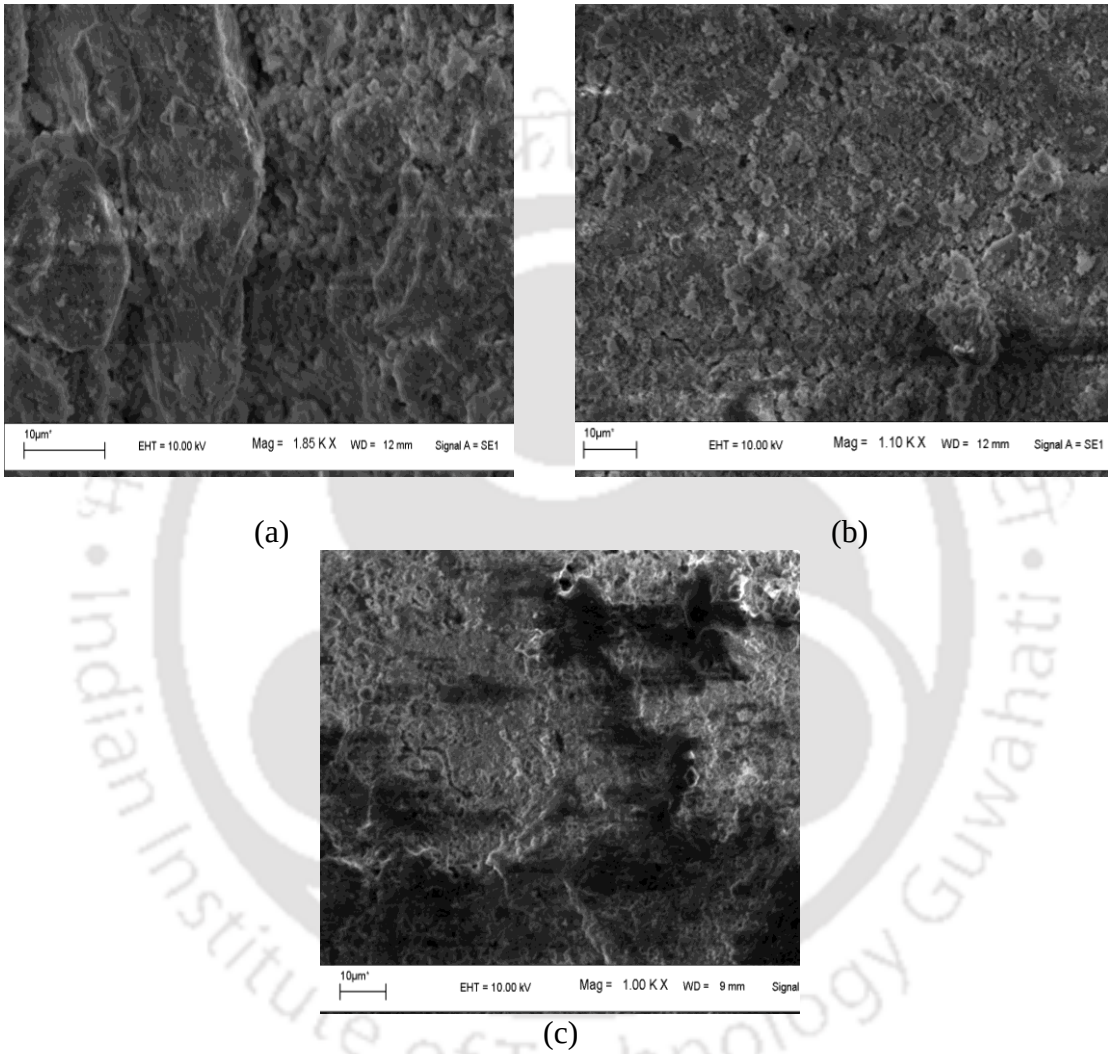

Figure 3.13. SEM images of the synthesized membrane surface at different sintering temperature (°C): (a) 700; (b) 800 and (c) 900.

The SEM images of prepared IOS ceramic membrane at different sintering temperatures ware shown in **Figure 3.13**. It was observed that the small particles

merged with large particle during sintering operation. The ceramic substrates sintered at lower temperature (700°C) showed highly porous structure (**Figure. 3.13a**). The membranes sintered at 800°C and 900°C were more consolidated (**Figures. 3.13b** and **3.13c**).

EDX analysis was performed before (fresh membrane) and after the corrosion test with the membrane sintered at 900°C.The result was shown in **Table 3.6**. It was observed that the elemental composition of the synthesized membrane remained invariant even after the corrosion test. This was in accordance with the results obtained in porosity measurements (**Table 3.6**).

Table 3.6. EDX analysis results of the fabricated membrane (sintered at 900ºC) before and after the corrosion test

Element	**Weight (%)**		
	Fresh membrane	**pH : 2**	**pH : 12**
Oxygen	35.96	35.80	36.12
Sodium	7.09	7.18	7.12
Aluminium	7.73	7.85	7.65
Silicon	11.04	12.13	11.89
Thallium	3.56	3.87	3.63
Iron	34.62	33.17	33.59

Coal Extraction Followed by Membrane Separation

3.3.1.4 Effect of Solvent on Coal Extraction

The lowest possible extracting solvent requirement to achieve the maximum recovery of solvent is always desirable. To determine the optimum solvent to coal ratio, several extraction experiments were performed with both the coal samples under similar test conditions. In extraction experiment, the yields were 62.8 and 61% for coal A and B, respectively, using only NMP as the extracting solvent with the solvent to coal ratio of 10:1 (v/w) (**Table 3.7**).

Table 3.7. Results of solvent extraction and membrane separation of the extract phase

Sample	Expt. No.	Extraction composition			Extract volume (mL)	Residue obtained (g)	Extraction yield (%)	Permeate collected (mL)	NMP recovered (%)
		NMP (mL)	EDA (mL)	Coal (g)					
Coal A	1	50	0	5	42	1.86	62.8	31.5	75
	2	45	0	5	38	1.98	60.4	28.1	74
	3	45	5	5	36	1.75	65.0	26.2	73
Coal B	1	50	0	5	40	1.95	61.0	28.8	72
	2	45	0	5	37	2.01	59.8	25.9	70
	3	45	5	5	35	1.81	63.8	23.8	68

Addition of EDA increases the extraction yield by 2.2% for coal A and 1.8% for coal B at NMP: EDA: coal=9:1:1 (v:v:w). This was explained by synergistic effect of EDA in coal extraction as discussed earlier. The maximum solvent recovery was found to be 75% with the solvent to coal ratio of 10:1 (v/w) for coal sample A. Whereas, the

same was about 72% for coal sample B. A slight decrease in both extraction yield and solvent recovery was observed for coal to solvent ratio of 9:1 (v:w) for both the coals.

3.3.1.5 Proximate and Ultimate Analysis of Raw and Extracted Coal (Coke)

The proximate and ultimate analyses of raw coal and extracted coal (coke) were shown in **Table 3.8**. FC content reduced from 51 to 42.48% in case of coal A. The reduction was around 3% for sample B. The ash content reduction in extracted coal sample (ECS) A was about 32%. It was more than 99% in ECS B. As a result, VM content was found to increase in both the ECS. Mineral matters in ECS A and B was removed by 26 and 95.7%, respectively. The carbon content in ECS increased up to 10 and 24% using coals A and B, respectively. The blended solvents effectively reduced sulphur in the ECS by 76 to 79% in case of both the coal samples. Nitrogen content increased in both ECS due to adsorbed NMP.

Table 3.8 Proximate and ultimate analysis of raw coals and after extracted coals (coke) in Expt. No. 1

Proximate analysis (wt %, daf[1])								Ultimate analysis (wt %, daf)							
Coal sample		MC[2]	Ash	[3]VM	[4]FC	[5]MM	[6]GCV (kcal/kg)	C	N	O	S	Al	Si	Fe	Mo
Raw coal	A	5	25	19	51	28.56	6253	58.8	2	17	2.84	6.09	8.40	2.49	2.4
	B	12	9	35	44	11.81	6376	58.4	13.6	18.4	3.8	2.61	0.8	2.4	-
Extracted coal (coke)	A	3.17	17	37.3	42.5	18.72	6701	64.7	4.15	16.7	0.67	3.12	5.26	3.39	2.01
	B	8.18	0.06	51	40.7	0.499	7433	72.4	15.5	11.3	0.79	-	-	-	-

[1]daf: dry ash free; [2]MC: moisture content; [3]VM: volatile matters; [4]FC: fixed carbon; [5]MM: mineral matters; [6]GCV: gross calorific value

Gross calorific value (GCV) in ECS increased up to 7 (coal A) and 17% (coal B). The results suggest that extracted coal using sample B had better efficiency for iron and steel production.

3.3.1.6 Fourier Transform Infrared Spectroscopy (FTIR) Analysis

FTIR analysis was undertaken to explore the effectiveness of the synthesized membrane for solvent recovery and ECS separation. The FTIR spectra of coal sample A, B, pure NMP and permeate (recovered solvent, mainly NMP) is presented in **Figure 3.14**.

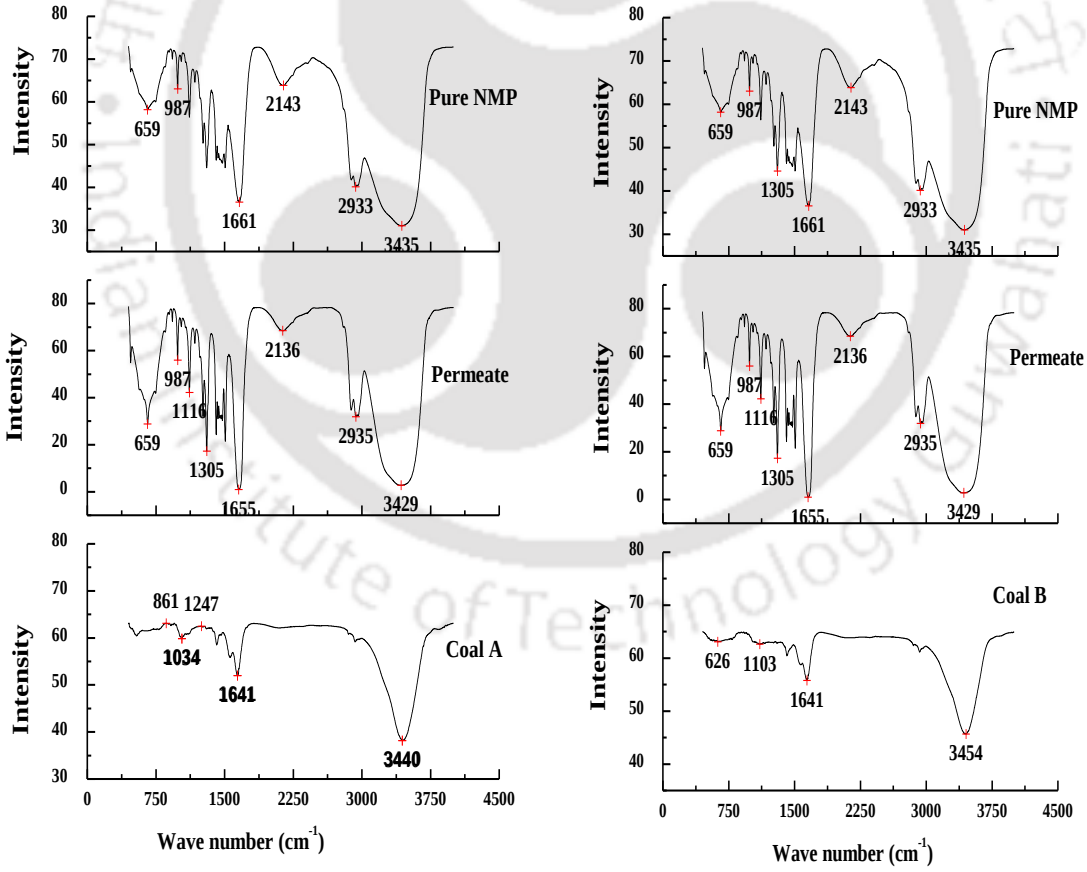

Figure 3.14. FTIR spectra of coal samples, pure and recovered (permeate) NMP.

The broad absorption band at 3440 and 3454 cm^{-1} in case of both coal samples and frequencies at 3429, 3435, 1655 and 1661 cm^{-1} in pure NMP and permeate, were observed due to N-H stretching vibration [121]. Two stronger bands 2933 and 2935 cm^{-1}were observed in pure NMP due to CH_3-CH_2 vibrations. One band at 2917 $cm^{-1}$was attributed to coals (A and B) due to presence of C-H group [122]. The band at 2136 and 2143 cm^{-1} were observed in pure NMP and permeate side due to -CN- absorption band. This was not noted in coal samples. The spectrum at frequency 1641, 1661 and 1655 cm^{-1} were ascribed in coal samples, NMP and pure permeate due to the presence of acyclic C-C groups [123].The spectra at frequency 1305 cm^{-1} was observed in pure NMP and permeates due to the vibration of C-O groups. The same was not observed in coal samples. The bands 659 and 626 cm^{-1}were attributed to Si-O vibrations. The distinct peak at 1034 cm^{-1} was observed in coal samples. The same was absent in NMP and disappeared from permeate because of sulphur removal [123].The peak at 537 cm^{-1}appeared in coal sample due to presence of kaolinite mineral group and disappeared from the permeate collected.

The results indicated that the synthesized membrane was capable to recover almost pure NMP (permeate) free of dissolved/suspended coal particles. Hence, the recovered solvent must be reused efficaciously for further non-coking to coking coal conversion along with the makeup solvent.

3.3.1.7 Membrane Cleaning

Microfiltration IOS ceramic membrane was fouled during solvent recovery from coal organic solvent mixture. Membrane fouling resulted the decline of permeate flux and low solvent recovery on permeate side. Low solvent recovery was due to the pore blocking and settling of non-coking coal on the membrane surface. To reuse the same membrane for solvent recovery purpose, cleaning was necessary. Fresh IOS ceramic membrane permeability (sintered at 900°C) was 3.81×10^{-12} m/Pa.s. After experiment, membrane was fouled and cleaned with three different cleaning agents, such as, deionized water, anionic surfactant (sodium dodecyl sulphate) and organic solvent (NMP). Cleaning efficiency of membrane was measured in terms of recovery of hydraulic permeability and defined as:

$$\text{Cleaning efficiency (\%)} = \left[\frac{Lp_c}{Lp_i}\right]\times100 \qquad (3.8)$$

where Lp_c and Lp_i were membrane hydraulic permeability (m/Pa.s) after cleaning and before fouling experiment. With deionized water, the cleaning efficiency was 48% and recovered membrane permeability was 1.82×10^{-12} m/Pa.s. Hence deionized water was not sufficient to recover the original permeability. It indicated that irreversible fouling was there on membrane surface. SDS was used as another cleaning agent for the removal of irreversible fouling layer. 73% cleaning efficiency was observed with 5 mM SDS (pH = 11) solution and recovered membrane permeability was 2.78×10^{-12} m/Pa.s. With SDS cleaning still some amount of foulant was there. As With NMP was used as a cleaning agent, 90% cleaning efficiency was observed with membrane permeability

of 3.42×10^{-12} m/Pa.s. Hence NMP had maximum ability to remove coking coal foulant from membrane surface.

3.3.1.8 Preliminary Cost Estimation

The main drawback of ceramic membranes was its high fabrication cost compared to polymeric membranes. The fabrication cost of ceramic membrane was one and three orders of magnitude more compared to polymeric membranes [124]. The cost of the synthesized IOS ceramic membrane (Ø 55 mm, thickness 5 mm, membrane II) was calculated on the basis of the analytical grade chemicals (except IOS) used.

Table 3.9. Preliminary cost estimation of the synthesized IOS ceramic membrane

Materials	**Composition II of Table 3.4 (%)**	**Unit price ($/kg)**	**Material used/m^2 (g)**	**Material reqd/m^2(kg)**	**Cost/m^2 ($)**
IOS	10	0	926.46	0.92	0
Kaolin	40	5	3705.84	3.71	18.5
$CaCO_3$	20	5.4	1852.92	1.85	10.0
Na_2CO_3	10	2.56	926.46	0.92	2.37
Quartz powder	10	6.5	926.46	0.92	6.02
Boric acid	5	11.26	463.23	0.46	5.21
Sodium meta silicate	5	11.26	463.23	0.46	5.21
Power consumption @ 0.075$/kWhr					5.95
				Total cost $	53.26

The cost calculated was then linearly extrapolated to per unit square metre of the membrane surface of the same thickness. Total time of running the muffle furnace

(1.8 kW) was 40.42 hr. Total fabrication cost including materials and power consumption was \$53.26/m^2 shown in **Table 3.9**. For bulk manufacturing including the shipment cost added \$26.63/m^2 in total membrane cost, the estimated total cost reached to \$79.89/m^2 [84]. Hence, the utilization of waste IOS could reduce the cost of the ceramic membrane which was comparable with the polymeric membrane.

3.3.2 Summary

This work summarizes the development of an inorganic ceramic membrane for the purpose of membrane cost reduction and as well as utilization of industrial waste iron ore slimes (IOS) to reduce the environmental consequences.

- The average pore diameter of the synthesized IOS ceramic membrane came in the microfiltration range of 0.601 to 1.103 µm. The IOS membranes showed good corrosion stability both at acidic and alkali conditions.
- The synthesized membrane was effective in separation of extraction solvents and dissolved coking coal from the extracted solvent-coal mixture. The efficiency of solvent recovery depends on both type of coals and solvent to coal amount. Maximum 75 and 72% solvent recovery were obtained with coal types A and B, respectively for solvent to coal ratio of 10:1.
- FTIR spectra confirmed that the recovered solvent was almost free from dissolved coal could be used further.
- The fabricated membrane was more effective for reduction of ash and sulfur content and, enhancement of gross calorific value in case of coal B. The proximate and ultimate analysis showed that the purified coal could be used for industrial application such as steel production.

- NMP had maximum cleaning efficiency (%) compared to SDS and deionized water to remove the foulant from membrane surface.
- The cost of prepared IOS ceramic membrane was around \$79.89/m^2.

Chapter 4

FRUIT JUICE CLARIFICATION

Chapter 4

FRUIT JUICE CLARIFICATION

In this chapter, meticulous descriptions are outlined for mosambi juice clarification. Clarification of fruit juice was elucidated by membrane separation. To improve the membrane performance, pretreatment was done. Firstly, packed column based pretreatment process was developed for clarification of juice. Two packing materials i.e., glass beads and molecular sieves were utilized to clarify juice. Packed bed pretreated juice qualities were compared with other pretreatment methods, namely, centrifugation, fining agent addition and combined centrifugation followed by fining agent addition. Spiral wound ultrafiltration membrane was employed with and without permeate recycle. Experiments were carried out both in laminar and turbulent flow regimes to evaluate the performance. Fouled spiral wound ultrafiltration membrane was cleaned with three different cleaning agents, such as, deionized water, SDS and EDTA solution.

The work described in this chapter is published at ***Desalination*** 322 (2013), 94-103 and ***International Journal of Chemical Science and Engineering,*** 7 (1) (2013), 945-949 and ***Desalination*** 337 (2014) 43–51.

4.1 Materials and Methods

4.1.1 Materials

Fresh mosambi fruits and screw type extractor were purchased from local market of Guwahati, India. Packed materials, namely glass beads (0.0035 m) and molecular sieves (0.013×0.0015 m) were procured from Loba Chemie Pvt. Ltd, Mumbai, India. Fining agents, namely, gelatin and bentonite were procured from Merck Ltd, Mumbai, India.

Sucrose (MW 342.3), pectin (degree of esterification 63-66% with MW 20000-100000); cleaning agents, namely, sodium dodecyl sulphate (SDS) and ethylenediaminetetraacetic acid (EDTA) were purchased from Loba Chemie Pvt. Ltd, Mumbai, India. All the analytical grade chemicals were used without further treatment.

4.1.2 Systematic Scheme of Pretreatment

Good quality fresh mosambi fruits (quantity 4 kg) were washed with deionized water and scrubbed with dry cotton cloth. After that, it was cut in two halves and peeled (manually) properly. The halves were passed through screw type extractor and extracted juice was collected in a beaker (capacity 2 L). Extracted juice was filtered by low density polyethylene mesh (100 µm) to remove heavy pulp from raw juice. Heavy pulps of juice were retained on mesh surface and discarded, fine juice was collected separately in another beaker (capacity 2 L). Physiochemical properties of fine filtered mosambi juice were shown in **Table 4.1**.

Table 4.1. Physiochemical properties of raw mosambi juice

Browning index (A_{420})	Clarity (%T_{660})	TSS (°Brix)	pH	Density (g/cm^3)	Viscosity ×10^{-3} (Pa.s)	AIS (wt %)
2.25	0.6	9.3	4.5	1.10	3.30	0.30

Fine filtered juice was clarified by different pretreatment methods. The detailed schemes of different processes applied before pretreatment were shown in **Figure 4.1**.

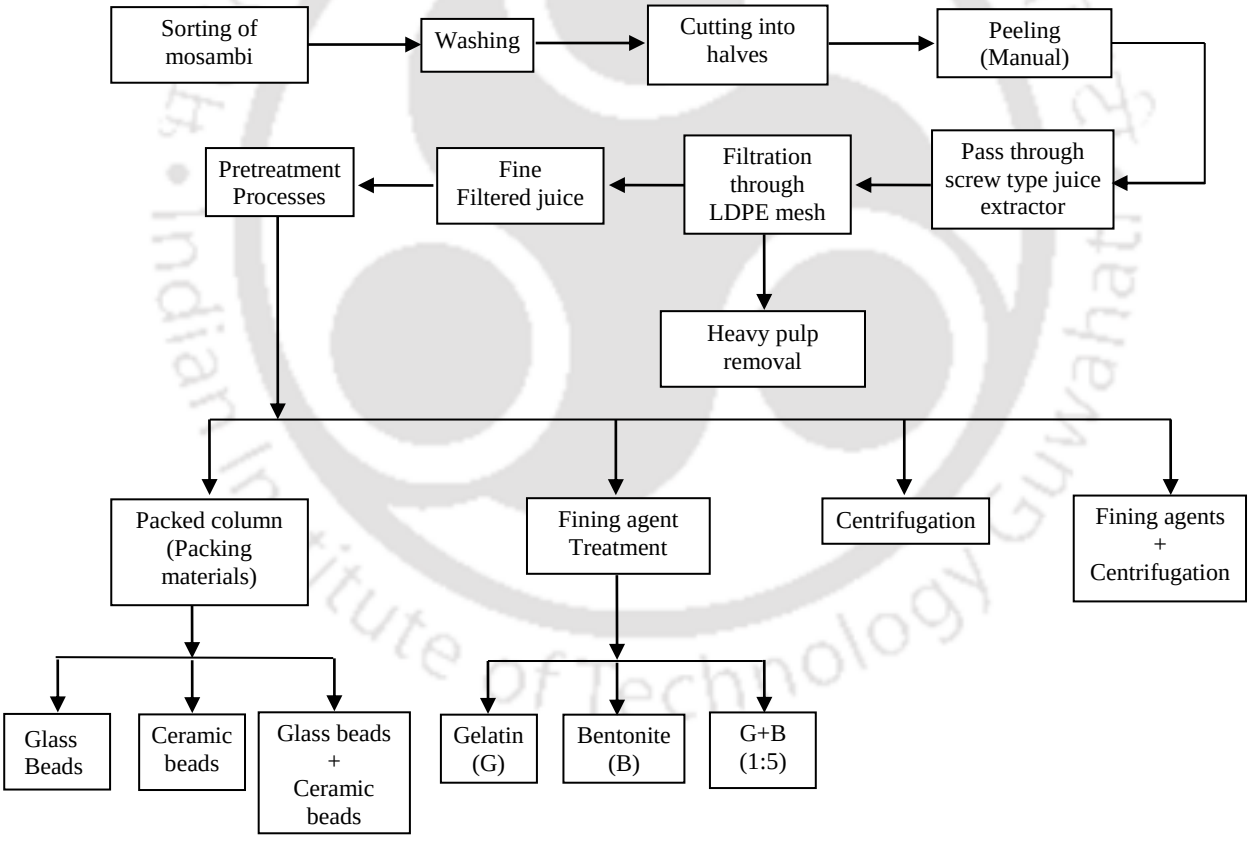

Figure 4.1. Flowchart for extraction of mosambi juice by different pretreatment methods.

4.1.3 Experimental Set up

Packed Bed Column

Experimental set up pretreatment of raw mosambi juice through packed column was performed by a laboratory scale pilot plant fabricated at IIT Guwahati. Packed column made up with perspex, consisted with the specifications as: internal diameter (*d*) 0.03 m, length (*L*) 0.32 m and volume 227×10^{-6} m^3. Two tapered neoprene rubber corks with same dimensions (0.0002 m length, upper surface diameter 0.031 m and lower surface diameter 0.029 m) were placed at top and bottom of the column. Two different packing support materials such as, glass beads (0.0035 m, void fraction 0.68) and molecular sieves (0.013×0.0015 m, void fraction 0.57, BET surface area 574 m^2/g and total pore volume 0.374 mL/g) were used for clarification of juice. Two tubes (diameter 0.0063 m) were fitted in two rubber corks and fixed at both ends of the column; to circulate the juice inside the column was shown in **Figure.4.2.** Empty space of column was filled with supports materials. Packed materials, molecular sieve strongly adsorbed the suspended material on its surface. Other packed material, glass bead had been limited to only charge dependent cells. The perspex column was tightened at clamp support and fixed with clamp stand. The bottom tube of the column was connected with peristaltic pump outlet and inlet tube was connected with feed beaker (fine filtered mosambi juice). Feed beaker was kept in the water bath at temperature of 28±2ºC to prevent the degradation. Peristaltic pump was started in forward direction and flow rate was adjusted by controllable point. Clarified juice samples were collected at different time intervals.

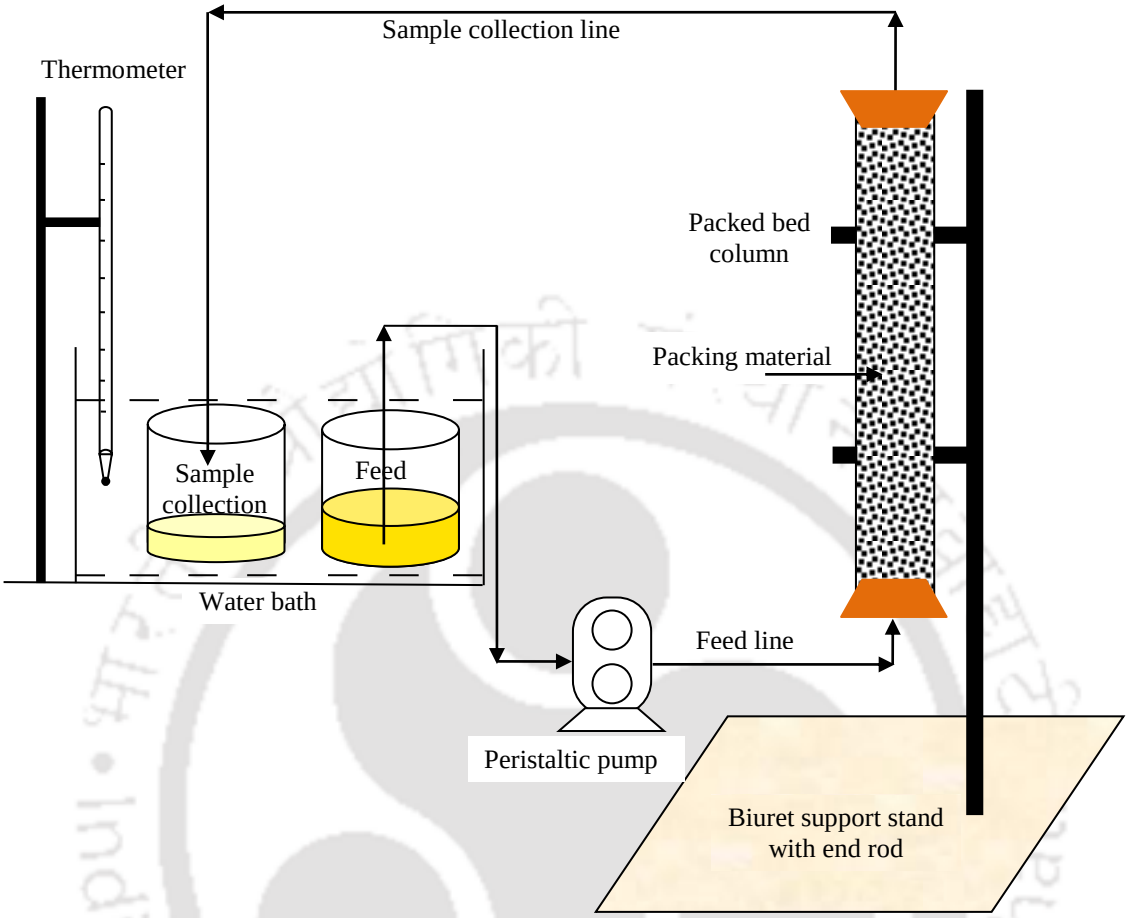

Figure 4.2. Schematic flow diagram of packed bed column filled with packing materials.

Pilot Plant of Spiral Wound Ultrafiltration Membrane

The membrane experiments were conducted in a spiral wound membrane set up. The schematic flow diagram of the Perma Pilot Plant (a spiral wound configuration with ultrafiltration membrane module for research purpose) was shown in **Figure 4.3**. The experimental setup was supplied by M/s Permionics Membranes Pvt. Ltd., Gujarat, India. Spiral wound membrane module was connected with a feed tank (20 L). A cooling tank (20 L) was provided to control the temperature of retentate. Two

rotameters were connected with retentate and permeate line to measure flow rates of retentate and permeate, respectively. To manipulate feed flow rate and TMP drops in membrane module, a part of feed was recycled through a by-pass line. High TMP drops (up to 6904 kPa) triplex plunger pump was attached with the pilot plant to circulate the feed in UF membrane module.

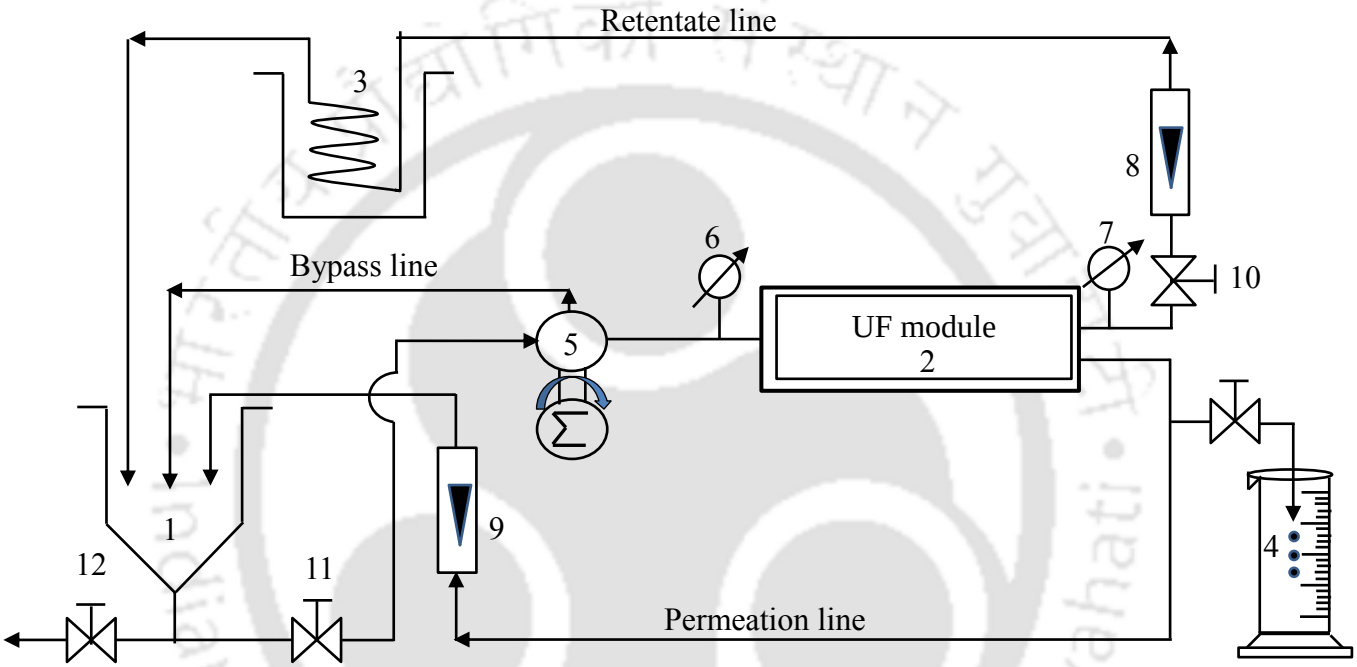

Figure 4.3. Schematic diagram of spiral wound ultrafiltration membrane: (1) feed tank, (2) UF spiral wound membrane module, (3) cooling tank, (4) measuring cylinder, (5) plunger pump, (6) inlet pressure gauge, (7) outlet pressure gauge, (8) retentate flow rate, (9) permeate flow rate, (10) retentate control valve, (11) feed control valve, (12) drainage valve.

Spiral wound UF polyamide membrane module having molecular weight cut off (MWCO) of 30 kDa was procured from M/s Permionics Membranes Pvt. Ltd., Gujarat, India. The detailed specifications of UF membrane were as follows: hydraulic permeability: 3.1×10^{-11} m/Pa.s, pore size: 0.001µm, typical operating pressure range:

414-690 kPa, maximum operating pressure: 1034 kPa, allowable pH range: 4-11, operating temperature: 120ºC.

Polyamide UF membrane module with effective cross sectional area of 1 m^2, length of 510 mm and diameter of 73 mm was housed in stainless steel (SS 316) cylindrical shell. Flow rate (up to 10 lpm) of the feed was controlled with the help of rotameter and control valve. One control valve was attached at the outlet of the retentate line to maintain the desired TMP drops inside the membrane module. To measure the ionic conductivity of permeate; one conductivity metre was attached with the module. Temperature had influence in the permeate flux. Therefore, a cooling tank was provided to maintain the temperature of feed tank. Before experiment, UF membrane module was compacted with deionised water at 758 kPa for 1 hr.

4.1.4 Experimental Methods

Pretreatment of Mosambi Juice

Overall systematic scheme for pretreatment of mosambi juice was shown in **Table 4.2.** During packed column pretreatment, two different packing materials such as, glass beads and molecular sieves were used separately and clarified juice qualities were compared each other. To improve the efficiency of clarified juice during packed bed pretreatment, two columns of same dimension were attached in a series mode operation. First column was filled with glass beads and other column was packed by molecular sieves respectively. Reynolds number calculation for various flow rates were shown in Appendix. Operating time for pretreatment of juice by column was 60 min. All the experiments were conducted at room temperature (28±2ºC).

Table 4.2 Operating conditions for clarification of mosambi juice by different pretreatment methods

Sl. No.	Pretreatment	Feed flow rate (cm^3/hr)	Dose (mg/L)	Rotor speed, rpm *(RCF), *g*
1	Packed column supported with glass beads	50, 100, 200, 300, 400 and 500	--	--
2	Packed column supported with molecular sieves	50, 100, 200, 300, 400 and 500	--	--
3	One glass bead and other molecular sieve supported column, attached in series in packed operation	50	--	--
4	Gelatin	--	500 to 4000	--
5	Bentonite	--	500 to 4000	--
6	Gelatin+Bentonite (1:5)	--	400+2000 and 500+2500	--
7	Centrifugation	--	--	6000 (4684)
8	Centrifugation+Gelatin	--	2500	4500 (2635)
9	Centrifugation+Bentonite	--	2500	4500 (2635)
10	Centrifugation + Gelatin + Bentonite	--	4500+400+2000 and 4000+500+2500	4500 (2635) and 4000 (2081)

***RCF = Relative centrifugal force**

With fining agent pretreatment, fining agents such as, gelatin (G), bentonite (B) and combined (G+B) were used for clarification of raw juice. Physicochemical properties of clarified juice were studies in detail with variations of fining agent dose. Gelatin was usually used up to 3000 mg/L. Bentonite and combined fining agents

(G+B; 1:5) were used up to 4000 mg/L [125-127]. Various fining agents were mixed with juice and kept in ultrasonic bath for 15 min to break the bigger suspended materials and stored for 2 hr at temperature of 28±2ºC. After that, juice was filtered through Whatman filter paper grade 598 (25 µm) and clarified juice was collected separately for analysis purpose. Centrifugation (C) was another pretreatment method for clarification of juice. During centrifugation, suspended materials were separated due to centrifugal force. In centrifugation operation, the juice was centrifuged (Remi Instruments Ltd., Mumbai, India) up to 6000 rpm to remove the maximum suspended solids from raw juice. Efficiency of the clarified juice was found to increase by combined (fining agent with centrifugation) pretreatment methods. Here, the raw juice was mixed with fining agents afterward it was centrifuged at optimum condition.

Juice Clarification through Spiral Wound Ultrafiltration Membrane

Main constituents of citrus fruit were pectin, sucrose and water. Generally pectin content in citrus juice was from 2 to 3 g/L and where sucrose content varied from 7 to 12 °Bx. In the present study, 2 g/L pectin and 9°Bx sucrose were added in per litre solution deionized water and stirred at 2000 rpm for 30 min duration for preparation of synthetic juice. Prepared synthetic juice was laid in feed tank and experiments were conducted at laminar flow regime (flow rate 4 lpm, Reynolds number 1455). Reynolds number calculation for various flow rates were shown in Appendix. Constant feed flow rate (4 lpm) was maintained by adjusting of control valves. Experiments were conducted at two different operating conditions, such as, with and without permeate recycle at three different TMP drops (414, 552 and 690 kPa). With permeate recycle, samples were collected at a definite time intervals for analysis of

purpose and remaining amounts of permeate were recycled to feed tank. Total time to run this experiment was 180 min. For without permeate recycle, samples were collected continuously without recycling permeate to the feed tank till the finish of feed. To maintain the TMP drops inside the membrane module, feed and retentate outlet control valves were adjusted. The temperature of the feed tank was measured periodically and maintained at 28±2ºC with the help of cooling tank by circulating coolant. As shown in **Table 4.3**, the experiments were conducted at various operating conditions.

Table 4.3 Operating conditions for clarification of juice through spiral wound UF membrane

Permeate streams	**Retentate streams**	**TMP drops (kPa)**	**Feed flow Rate (lpm)**	**Reynolds No**
With and without recycle	Recycle	414, 552 and 690	4	1455
			11	4001

4.1.5 Sample Analysis

Different physiochemical properties, such as, browning index, clarity, soluble solid contents in terms of ºBrix, pH, acidity, viscosity, density, pectin content (wt %) and were measured for raw and clarified juice. All the properties were measured three times.

LPSA (Laser Particle Size Analyser, Mastersizer 2000 of M/s Malvern Instruments Ltd., UK) was used to measure the pectin particle distribution in feed

solution. On the basis of particle size distribution date, the average particle size was calculated using the following formula: $d_s = \left[\frac{\sum_{i=1}^{n} n_i d_i^2}{\sum_{i=1}^{n} n_i} \right]^{0.5}$

where d_s is the average particle diameter, d_i is the particle diameter of i^{th} and n_i is the number of particle dispersed for particular diameter.

During citrus juice clarification, loss of nutrient and formation of undesirable compound like hydroxymethylfurfural was measured in terms of browning index. It was determined by absorbance value at 420 nm, using UV spectrophotometer. Clarity was measured as percentage transmittance at 660 nm by using an UV spectrophotometer (Perkin-Elmer Precisel, Lamda-35, Canada) [128]. A total soluble solid (TSS) in terms of ºBrix was determined by using an ABBE -3L Benchtop Refractometer (Thermospectonic, USA) [129]. The pH values of all samples were determined by using a digital pH meter (VSI. Electronics Pvt. Ltd., Punjab, India). Viscosity of the sample was determined by using a HAAKE rheostress (Thermo Scientific, Germany) at a constant water bath at temperature of 28±1ºC. Relative viscosity(η_r) is defined as the ratio of $\eta(t)/\eta(0)$; where $\eta(t)$ is the viscosity of solution after time *t* min of pretreatment and $\eta(0)$ is the viscosity of raw juice [130]. Density of the juice was measured by accurately weighing 25 mL of sample into a pycnometer bottle with a capacity of 25 mL. Pectin content was measured in terms of alcohol insoluble solids (AIS). AIS was determined by boiling 20 mL of juice mixed with 300 mL of methanol solution for 30 min. After simmering, the filtered residue was again washed with methanol solution. The residue was dried at 100ºC for two hr and was expressed in terms of wt (%) [131].

4.1.6 Pretreatment Methods

4.1.6.1 Pretreatment through Packed Beds

The fresh mosambi juice was passed through packed bed column. Three different experiments, such as, column supported with glass beads (0.0035 m), column supported with molecular sieves (0.013×0.0015 m) and combined column treatment were performed. In combined column treatment, two columns of same dimensions were arranged in series; first column supported with molecular sieve and second column was packed with glass beads. Individual experiments were conducted at different flow rates and clarified juice qualities were compared. During column pretreatment, heavy pulps or suspended materials of juice were trapped in packing support passive. Hence the improvements of physicochemical properties were observed. After each experiment, glass beads and molecular sieves were cleaned with distilled water thoroughly and dried for 2 hr in oven at 80ºC.

4.1.6.2 Pretreatment with Fining Agents

Different fining agents, such as, gelatin (G), bentonite (B) and combined gelatin and bentonite (G+B) were used for pretreatment of raw mosambi juice. Fining agents were found to decrease the potential of haze formation by removing high molecular weight compound such as pectin; resulting enhanced clarity and reduced viscosity of clarified juice.

Gelatin

Gelatin was a protein substance, extract from collagen and widely used for the clarification of fruit juice. Positively charged gelatin reacts with negatively charged pectin in the juice, resulting precipitate formation. That precipitate settles down in 30 min and clarified mosambi juice was obtained. Significant amount of colloid particles still remain in the clarified mosambi juice, because of their fibre like structures. Physicochemical properties, such as, clarity, viscosity and alcohol insoluble solids were improved clarified juice. Gelatin concentration was varied in raw mosambi juice under acidic condition and the optimum quantity of gelatin was measured [132].

Bentonite

Bentonite was used as a traditional fining agent in juice industry, due to its highest clarification ability. Negatively charged bentonite reacts with positively charged protein to form a complex pulp. Complex mixture was settled down within 30 min and clarified juice was obtained. Ionic species, hydroxymethylfurfural, sucrose and pectin were absorbed with bentonite molecules. Hence the improvement of physicochemical properties was observed. Under acidic condition, bentonite was added with varying of dose in raw juice to estimate the optimum concentration [132].

Gelatin and Bentonite Combination

Combined fining agents (gelatin and bentonite) have enhanced the clarification efficiency of juice quality compared to single fining treatment. Gelatin and bentonite mixture were added (G:B = 1:5, w/w) in raw mosambi juice under acidic conditions. Combined fining agents act on pectin and protein, respectively, resulting complex

precipitate formation and settle down within 30 min. Hence the improvement of different physicochemical properties such as, clarity, alcohol insoluble solids and viscosity are observed [87].

4.1.6.3 Pretreatment by Centrifugation

If an average particle size in the dispersion was around 5 µm or less then it undergoes Brownian motion, hence it does not sediment under gravity. Therefore, a stronger centrifugal force was applied in order to separate the molecules. A centrifuge tube (capacity 15 mL) with a conical bottom was used for centrifuge purpose with effective time of 20 min. The sample was centrifuged with variation of machine rpm from 1500 to 6000 (Relative centrifugal force, RCF, *g* varies from 293 to 4684) to estimate the optimum rpm at 28±2ºC. The suspended materials in juice were settled due to centrifugal force acting on these materials, resulting improvement of physicochemical properties were observed in clarified juice [133].

4.1.6.4 Pretreatment by Combination of Centrifugation and Fining Agent Addition

To increase the efficiency of clarified juice in terms of removal of maximum suspended solids, pectin and polysaccharide from raw juice, combined operation (fining agent addition followed by centrifugation) were applied under acidic condition. Gelatin and bentonite (1:5; w/w) was added in raw juice after that it was centrifuged. After centrifugation complexes pulps were settled down in centrifuge tube and clarified juice was collected separately. Operational time of centrifugation was 20 min. Hence the improvement of browning index, clarity, alcohol insoluble solids and viscosity

property were observed. The physicochemical properties were enhanced compared to single centrifugation or fining agent treatment.

4.1.7 Process Evaluation

Spiral wound UF membrane module performance during clarification of synthetic juice, at two operating conditions, such as, with and without permeate recycle were analysed in terms of volume reduction factor (VRF), permeate flux and total resistance. The VRF was calculated using the Eq. (4.1).

$$VRF = \frac{V_0}{V_R(t)} = \frac{V_0}{V_0 - V_P(t)} \tag{4.1}$$

Where V_0 was the initial volume (mL) of feed, $V_R(t)$ was the final volume (mL) of retentate at particular time (t) and $V_P(t)$ was the volume collected on permeate side at particular time for both experiment conditions. Generally the *VRF* values vary from one and infinity. At the start of any UF process, VRF was one, since all the volumes was in the retentate and $V_R(t) = V_0$. On the other hand, when the entire feed was passed through permeate streams $(V_R(t) = 0)$, VRF was infinity [134]. Permeate flux (J_w, $m^3/m^2 \cdot s$) and membrane permeability L_p for UF membrane module with time were analysed by using the Darcy's law [86].

$$J_w = \frac{V_p}{A_m\, dt} = \frac{\Delta P}{\mu\, R_T} \tag{4.2}$$

where A_m was the membrane cross sectional area (m^2), V_p was filtrate volume (mL) collected on permeate side at particular time interval dt (sec), ΔP is TMP drops (kPa), μ was the viscosity (Pa.s) of permeate sample and R_T was the total resistance (m^{-1}). Total resistance, R_T, was the combination of three resistances (R_C, R_F and R_M) as:

$$R_T = R_C + R_F + R_M \tag{4.3}$$

R_C was the cake layer resistance (m^{-1}) formed on membrane surface, R_F was the fouling layer resistance (m^{-1}) on membrane surface and R_M was the clean membrane resistance which was calculated from pure water flux as $R_M = \frac{\Delta P}{\mu_w J_w}$; μ_w was the pure water viscosity [135, 136]. After each experimental run, membrane module was cleaned by applying three different cleaning agents, such as, deionised water, SDS and EDTA solution, separately. At a time, single cleaning agent was used and measured its fouling recovery performance in terms of recovery of membrane permeability (L_p) and membrane flux. Fouled membrane resistance was calculated by using the equation

$$R_F = \frac{\Delta P}{\mu_w J_F} - R_M \tag{4.4}$$

The resistance caused by the cake layer formation can be estimated by the equation:

$$R_C = [R_T - (R_F + R_M)] \tag{4.5}$$

All the resistances were calculated for with and without permeate recycle after each experiment.

4.1.7.1 Theory for Membrane Transport Equation at Laminar Flow Regime

The volumetric flux is defined as:

$$J_w = Lp\ [\Delta P - \Delta\pi] \tag{4.6}$$

According to Van't Hoff equation, the osmatic pressure difference ($\Delta\pi$) is defined as [137].

$$\Delta\pi = RT(C_m - C_p) \tag{4.7}$$

where C_m is the molar solute concentration on membrane surface, C_p is the molar solute concentration on permeate side, R is gas constant (8.314 J/mol.K), T is absolute temperature, Substituting all value of $\Delta\pi$ in Eq. (4.6) we have:

$$J_w = L_p\left[\Delta P - RT(C_m - C_p)\right] \tag{4.8}$$

It is assumed that the entire solute particle retains on membrane surface and there is no pectin molecule on permeate side (C_p=0). Accumulation of the impermeable solute on the membrane surface leads to the development of a concentration polarization layer which may be determined by the concentration polarization model, i.e.,

$$\frac{C_m - C_p}{C_0 - C_p} = \exp\left(\frac{J_w}{k}\right) \tag{4.9}$$

k is the mass transfer coefficient and is expressed as D/δ, where D is the solution diffusivity and δ is the film thickness. Then Eq. (4.9) is represented as:

$$\frac{C_m}{C_0} = \exp\left(\frac{J_w}{k}\right) = \left(1 + \frac{J_w}{k}\right) \tag{4.10}$$

Rearranging the Eq. (4.8):

$$J_w = L_p\left[\Delta P - \frac{C_0 C_m RT}{C_0}\right] \tag{4.11}$$

Putting the value of C_m/C_0 in Eq. (4.11), and then the volumetric flux is expressed as;

$$J_w = L_p\left[\Delta P - \left(1 + \frac{J_w}{k}\right) C_0 RT\right] \tag{4.12}$$

or

$$J_w = \frac{1}{\mu R_M}\left[\Delta P - \left(1 + \frac{J_w}{k}\right) C_0 RT\right] \tag{4.13}$$

where R_M is the membrane resistance (1.79×10^{13} m^{-1}) and μ is the viscosity of permeate. Then volumetric flux is represented by

$$J_w = \frac{\Delta P - C_0 RT}{\mu R_m + \frac{C_0 RT}{k}} \tag{4.14}$$

According to De et al., the mass transfer coefficient (k) can be expressed for Newtonian fluids at laminar flow for spiral wound module [138, 139].

$$k = 0.777\left[\frac{uD^2}{hd_e}\right]^{1/3} \tag{4.15}$$

where u is the feed velocity (0.203 m/s); d_e is equivalent diameter (5.83×10^{-2} m); h is the spacer thickness (4×10^{-3} m) and D is the diffusivity (m^2/s).

Brownian Diffusion Model

Brownian diffusion model explains the diffusional limitation originated by soluble molecule accumulation near membrane. For appreciable small particles, Brownian diffusion becomes a significant transport mechanism for subsequent particles. According to Brownian diffusion model, the Brownian diffusivity (D_B) is expressed by Stokes Einstein relationship as:

$$D_B = \frac{KT}{6\pi\mu a} \tag{4.16}$$

where K is the Boltzmann constant (1.38×10^{-23} J/K), T is absolute temperature (301 K), μ is the viscosity of particle free solution (1×10^{-3} kg/m.s) and a is particle size, applicable for particle size less than 0.1 µm [107]. Substituting the constant values (K, T and μ) in Eqs. (4.15 and 4.16), the final expression of Brownian diffusivity is

$$D_B = \frac{2.204\times10^{-19}}{a} \tag{4.17}$$

Mass transfer coefficient k is expressed as:

$$k = \frac{2.682 \times 10^{-12}}{a^{2/3}} \tag{4.18}$$

Substituting the k value in Eq. (4.14), the final expression of volumetric flux is represented as:

$$J_w = \frac{\Delta P - 2502 C_0}{1.79 \times 10^{13} \mu + 9.327 \times 10^{14} a^{2/3} C_0} \tag{4.19}$$

Shear Induced Diffusion Model

Shear induced diffusion model corresponds to random contact between two particles which aggravate random displacement of the particle within feed stream as well as on the membrane surface. Shear induced diffusivity is defined as:

$$D_s = 3.63 \frac{u a^2}{d_e} \tag{4.20}$$

where 'u', 'd_e' and 'a' are the feed velocity, equivalent diameter and particle radius, respectively. Shear induced diffusion model is an important for particle size between 0.5 and 30 μm [108]. Substituting the value of u and d_e in Eq. (4.20), the final expression of shear induced diffusivity is obtained as:

$$D_s = 12.639 a^2 \tag{4.21}$$

Putting the Shear induced diffusivity (D_s) in Eq. (4.15) and the mass transfer coefficient is obtained as:

$$k = 39.89 a^{4/3} \tag{4.22}$$

Substituting the mass transfer coefficient in Eq. (4.14) and the final expression of volumetric flux (J_w) is represented by:

$$J_w = \frac{\Delta P - 2502 C_0}{1.79\times10^{13}\mu + 62.73\frac{C_0}{a^{4/3}}} \tag{4.23}$$

Combined Diffusion Model

The particle size distribution of solute in permeate may vary from a wide range (less than 0.1 to 30 μm). As a result, diffusivity will vary in a wide range. So, a combination of Brownian diffusion and shear induced diffusion model is developed. The combined diffusivity (D_c) is defined as [140]:

$$D_c = D_B + D_s \tag{4.24}$$

Substituting the values of D_B and D_s in Eq. (4.24), then

$$D_c = \frac{2.204\times10^{-19}}{a} + 12.639\,a^2 \tag{4.25}$$

Putting the combined diffusivity (D_c) in Eq. (4.15) and the mass transfer coefficient is communicated as

$$k = 7.3458\left[\frac{2.204\times10^{-19}}{a} + 12.639\,a^2\right]^2 \tag{4.26}$$

After substituting the mass transfer coefficient in Eq. (4.14), the final expression of volumetric flux (J_w) is denoted by

$$Jw = \frac{\Delta P - 2502\,C_0}{1.79\times10^{13}\mu + \dfrac{340 C_0}{\left[12.639\,a^2 + \dfrac{2.204\times10^{-19}}{a}\right]^2}} \tag{4.27}$$

The flux values were calculated for these diffusion models and compared with experimental flux values.

4.1.7.2 Theory for Membrane Transport Equation at Turbulent Flow Regime

According to De et al., the mass transfer coefficient (k) can be expressed for Newtonian fluids at turbulent flow regime for spiral wound module as [138]:

$$k = 0.182D\left[\frac{\mathrm{Re}^{1.75}\,Sc}{wd_e^{\,2}}\right]^{\frac{1}{3}} \tag{4.28}$$

where Re is Reynolds number (4001), Sc is the Schmidt number defines as ($\mu/\rho D$), w is module width (29×10^{-2} m) d_e is equivalent diameter (5.83×10^{-2} m) and D is the diffusivity (m^2/s), depends on solute particle size [86]. Substituting all the properties in Eq. (4.28), the final expression of mass transfer coefficient was defined as:

$$k = 51.69D^{2/3}\mu^{1/3} \tag{4.29}$$

According to previous work, volumetric flux was defined as [141]

$$J_w = \frac{\Delta P - C_0 RT}{\mu R_M + \dfrac{C_0 RT}{k}} \tag{4.30}$$

Brownian Diffusion Model

The Brownian diffusivity (D_B) is inversely proportional to solute particle size [141]. Substituting the Brownian diffusivity value in Eq. (4.29), and the final expression of mass transfer coefficient (k) and volumetric flux (J_w) are represented as:

$$k = \frac{2.51\times10^{-13}\mu^{1/3}}{a^{2/3}} \tag{4.31}$$

$$J_w = \frac{\Delta P - 2502.5C_0}{1.79\times10^{13}\mu + \dfrac{9.96\times10^{13}C_0\,a^{2/3}}{\mu^{1/3}}} \tag{4.32}$$

Shear Induced Diffusion Model

The Shear induced diffusivity is proportional to square off solute particle size [141]. Putting the Shear induced diffusivity (D_s) in Eq. (4.28) and the mass transfer coefficient is communicated as $k = 276 a^{4/3} \mu^{1/3}$ (4.33)

Substituting the mass transfer coefficient in Eq. (4.33) and the final expression of volumetric flux (J_w) is represented by:

$$J_w = \frac{\Delta P - 2502.5 C_0}{1.79 \times 10^{13} \mu + \dfrac{9.07 C_0}{a^{4/3} \mu^{1/3}}} \tag{4.34}$$

Combined Diffusion Model

The combined diffusivity is defined as the summation of Brownian and shear induced diffusivity [138]. The mass transfer coefficient is communicated as

$$k = 51.69 \mu^{0.33} \left\{ \frac{2.204 \times 10^{-19}}{a} + 12.639 a^2 \right\}^{2/3} \tag{4.35}$$

The expression of mass transfer coefficient is substituted in Eq. (4.30), and the final expression of volumetric flux (J_w) is represented by Eq. (4.29) as:

$$J_w = \frac{\Delta P - 2502.5 C_0}{1.79 \times 10^{13} \mu + \dfrac{48.41 C_0}{\mu^{1/3} \left\{ \dfrac{2.204 \times 10^{-19}}{a} + 12.639 a^2 \right\}^{2/3}}} \tag{4.36}$$

For turbulent flow, theoretical flux values for different diffusion models were estimated and compare with experimental flux values.

4.2 Pretreatment of Mosambi Juice

Clarification of mosambi juice was discussed in this section. The variations of clarified juice qualities with the flow rate in packed column, fining agents dose and rpm in centrifugation were analysed. Preliminary cost estimation for one litre juice clarification was done among all pretreatment methods.

4.2.1 Results and Discussions

4.2.1.1 Effect on Relative Viscosity and Clarity of Clarified Juice with Variation of Feed Flow Rate through Packed Column, Supported with Glass Beads (0.0035 m)

Variation of relative viscosity and clarity of clarified juice with operating time at different feed flow rates were shown in **Figures 4.4(a)** and **4.4(b)**, respectively. It was observed from **Figure 4.4(a)** that relative viscosity of clarified juice decreased gradually with time upto 45 min. Beyond 45 min, variation in relative viscosity was not significant and steady state was achieved.

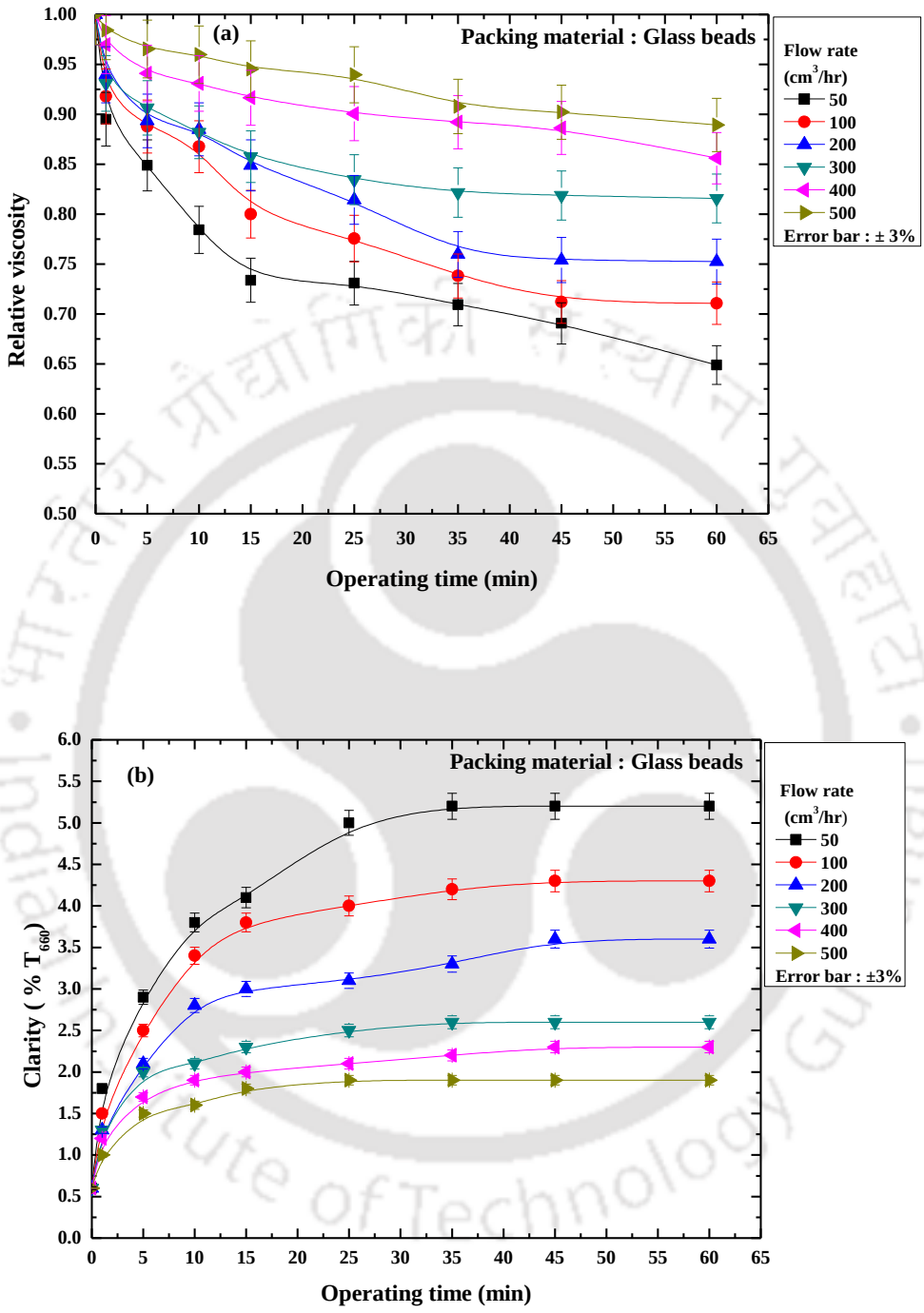

Figure 4.4. Variation of relative viscosity (a) and clarity (b) with operating time for different flow rates in a glass bead loaded column.

With increase of feed flow rate from 50 to 500 cm^3/hr, viscosity increased and clarity decreased in clarified juice due to passage of suspended molecule. At 50 cm^3/hr, maximum suspended materials were trapped in column leading to the improvement of juice qualities. Relative viscosity of clarified juice was decreased up to 25.13% and clarity was found to increase from 0.6 to 5.2%. When feed flow rate was increased from 50 to 500 cm^3/hr, clarity was found to decrease by 36.5% whereas relative viscosity increased from 0.65 to 0.9 due to presence of higher molecular weight compound such as pectin and phenol, shown in **Figure 4.4(b)**.

4.2.1.2 Effect on Relative Viscosity and Clarity of Clarified Juice with Variation of Feed Flow Rate in Packed Column, Supported With Molecular Sieve (0.013×0.0015 m)

In this column study, glass beads were replaced by molecular sieve. Suspended solids were adsorbed in molecular sieve, resulting juice viscosity decrease and clarity increase. The void fraction of glass beads and molecular sieves were 0.68 and 0.57, respectively. The void fraction was decreased due to compact packing. It was favourable for trapping more suspended solids in column. Variation of relative viscosity and clarity with operating time at feed flow rates were shown in **Figures 4.5(a)** and **4.5(b)**. Initially relative viscosity declined sharply within 15 min, after that decline was gradual and continued upto 45 min. as shown in **Figure 4.5(a)**.

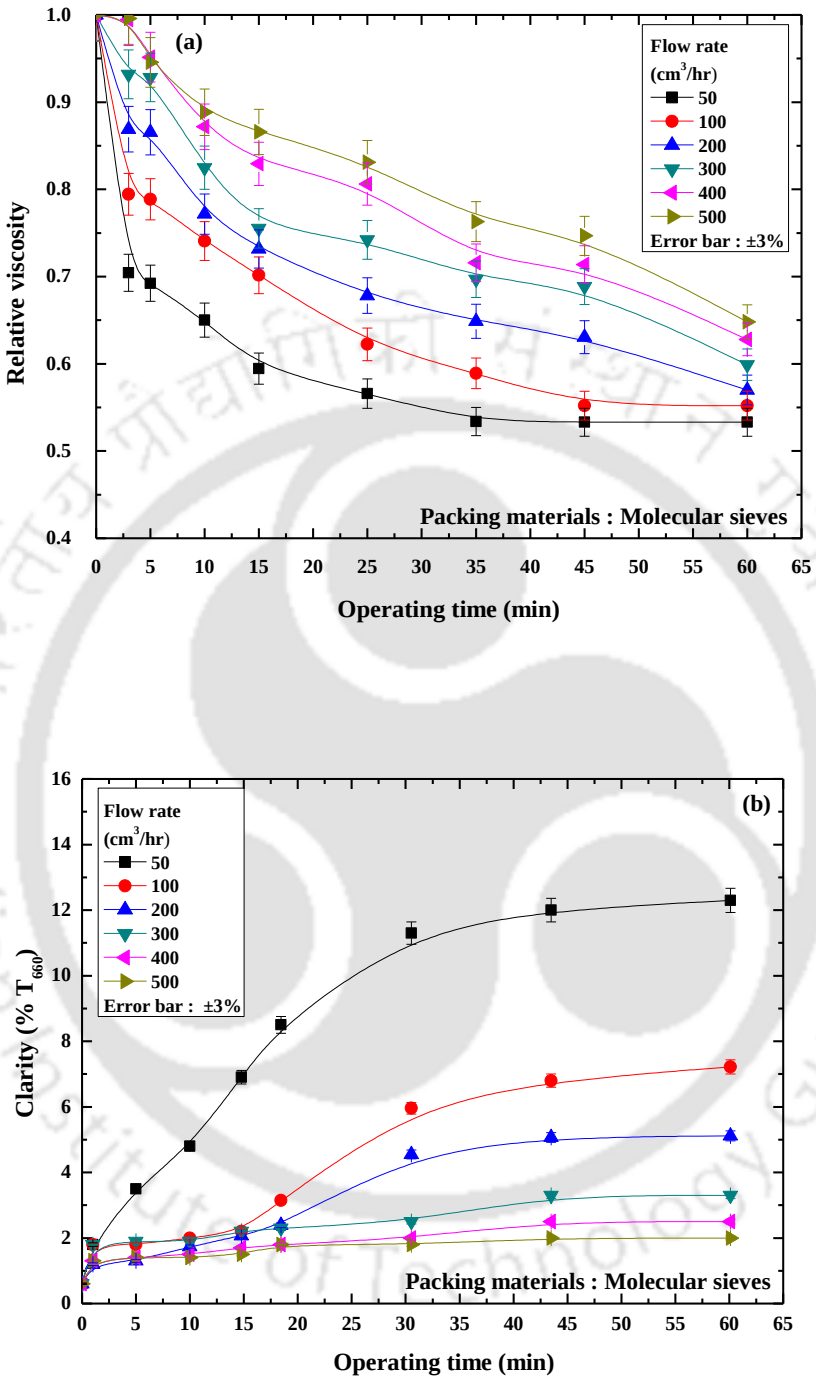

Figure 4.5. Variation of relative viscosity (a) and clarity (b) with operating time at different flow rates in a packed bed column supported with molecular sieve.

At feed flow rate of 50 cm^3/hr, the relative viscosity was decreased up to 35% and clarity was increased from 0.6 to 12.3% in clarified juice. With increase of the feed flow rate more suspended materials were passed through packed column, resulting decrease in juice qualities. For example, at feed flow rate of 500 cm^3/hr, relative viscosity decreased up to 35.2% and clarity increased from 0.6 to 2% in clarified sample, shown in **Figure 4.5(b)**.

In column studies, clarified juice qualities were immensely dependent on support materials, such as, glass beads and molecular sieves. Molecular sieves had more compact packing compared to glass beads due to smaller size, resulting maximum reduction of suspended materials from raw juice. Maximum improvements of physical properties were observed at low flow rate of 50 cm^3/hr. At a feed flow rate of 50 cm^3/hr maximum reduction of relative viscosity was 25.13 and 35.1% respectively, with packing support of glass beads and molecular sieves. Clarity was improved from 0.6 to 5.2% with glass beads support and 0.6 to 12.3% with molecular sieves. Another arrangement, combined packed column was used to improve the efficiency of clarified juice. With combined column arrangement, 42.3% viscosity was reduced, clarity was increased by 16.3% and alcohol insoluble solid was reduced by 48.5%.

4.2.1.3 Effect on Viscosity and Clarity of Clarified Juice Passing through Two Packed Columns in Series

Two columns were arranged in continuous series operation. First column was filled with glass beads and other column was filled with molecular sieves. Firstly, the raw juice was passed through glass beads column and after that clarified juice was passed through other column supported with molecular sieves. Variation of clarity and

viscosity with operating time at low feed flow rate of 50 cm^3/hr, was shown in **Figure 4.6**. During series column arrangement, lower particle size such as, pectin and pulp were passed through first column. These were trapped in second column resulting enhancement of clarified juice qualities. With combined operations, clarity of clarified juice was increased from 0.7 to 16.3% and viscosity reduced by 42.3% at optimum time of 45 min. Hence, pretreated juice qualities such as, clarity and viscosity had improved compared to single column pretreatment method.

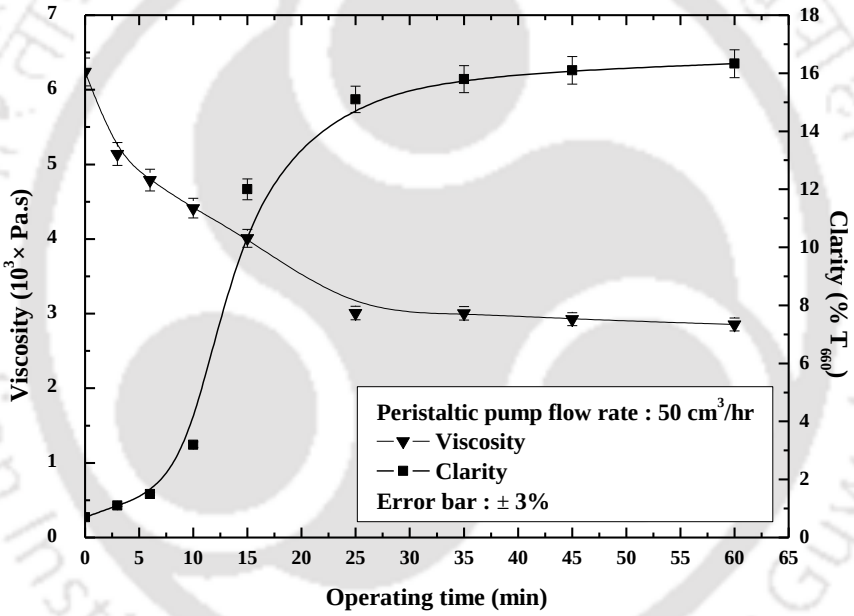

Figure 4.6. Effect on viscosity and clarity with time in series of glass and molecular sieve packed beds at 50 cm^3/hr.

During combined packed bed treatment, particle size distribution (PSD) of raw and clarified juice were measured by laser particle size analyser (Malvern instruments, Mastersizer 2000).

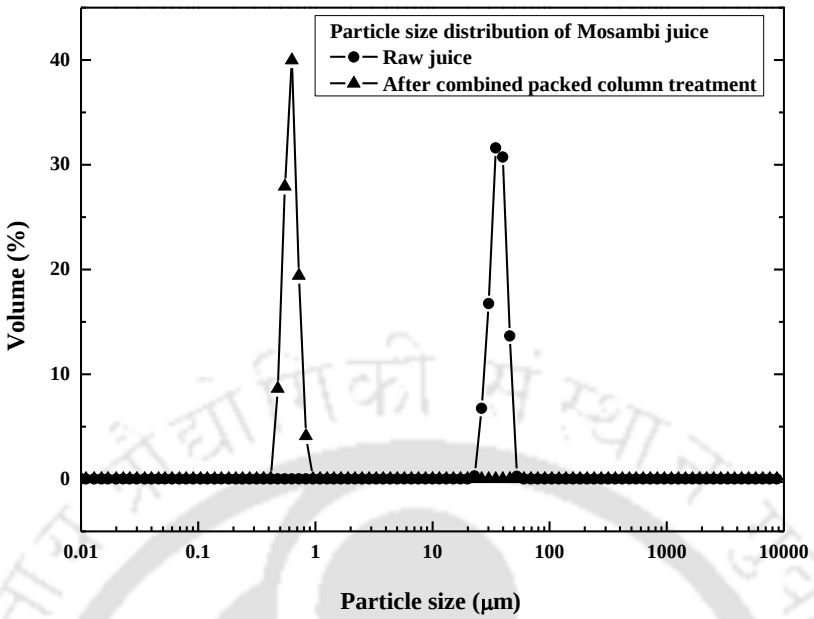

Figure 4.7. Particle size distribution of fresh mosambi juice and pretreated juice with packed column.

The average particle size of fresh mosambi juice was 40 μm. After prereatment through combined packed column operation, average particle size of mosambi juice was reduced to less than 1 μm, which was in the microfiltration range. Particle size distributions of raw and treated juice were shown in **Figure 4.7.** Average particle size was calculated using standard formula [141]. It indicated that maximum bigger particles in raw mosambi juice were retained in column after pretreatment.

4.2.1.4 Variation of Relative Viscosity and Clarity on Fining Agent Addition

Other method for pretreatment was fining agent addition, such as, gelatin, bentonite and gelatin-bentonite (G:B = 1:5, w/w) combination. In this process, the

effects of relative viscosity and clarity with variation of dose (ppm) were studied in detail.

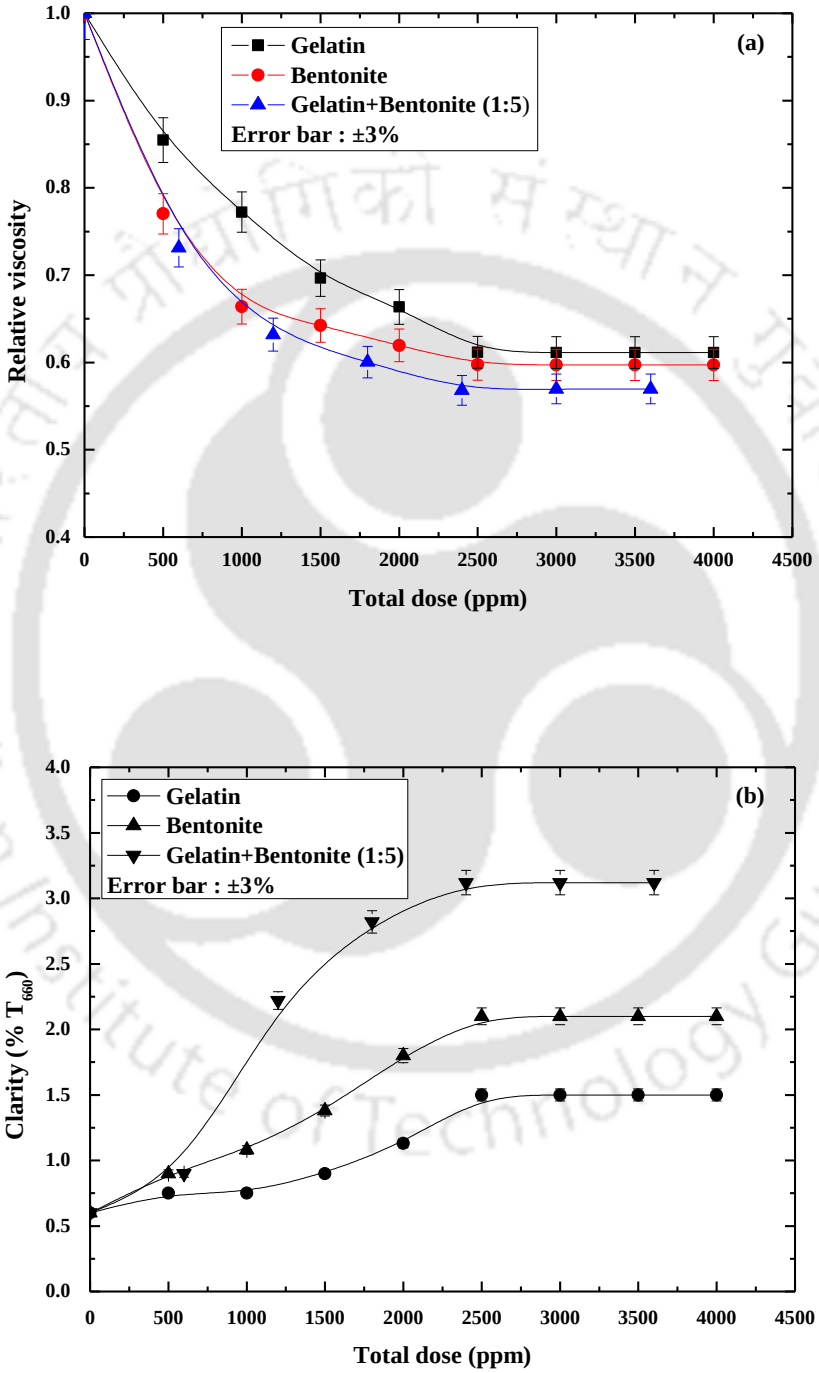

Figure 4.8. Variation of (a) relative viscosity and (b) clarity with fining agents dose.

Initially gelatin, bentonite reacted with raw juice; complex precipitate was formed and settled down within 30 min. Then juice was passed through Whatman filter paper, grade 598 (25 µm) and filtered juice was collected separately. It was observed that initial relative viscosity decreased drastically up to 3000 ppm with different fining agents, after that, there was no significant change in relative viscosity. As shown in **Figure 4.8(a)**, relative viscosity reduced upto 38.8% with gelatin, 40.2% with bentonite and 43.1% with (G:B = 1:5). The optimum dose of different fining agent was 3000 ppm.

For removal of suspended solid from raw juice, clarity of clarify juice was increased (refer **Figure 4.8(b**)). Clarity increased with gelatin from 0.6 to 1.4%, bentonite from 0.6 to 2.1% and combined (G:B = 1:5, w/w) from 0.6 to 3.1. Clarified mosambi juice had good clarity and low viscosity. It was observed, that combined (G:B =1:5, w/w) had best quality compare to single fining such as, gelatin and bentonite. The reason behind this is already discussed in section 4.1.6.2.

4.2.1.5 Effects of Centrifugation

Next pretreatment method was centrifugation. The important parameter was determining the usefulness of the centrifuge machine rpm (revolution per minute) at which the physical properties of juice such as, clarity and viscosity was achieved at an acceptable level. This was determined by increasing the rpm of the centrifuge machine until the clarity and viscosity exceeded the acceptable level or there was breakthrough of physical properties of mosambi juice stream. Juice clarity was increased sharply with the increase of machine rpm from 1500 to 4500 or *g* values from 293 to 4684. Beyond 4500 rpm, the increase in clarity was marginal. Initially, the clarity was increased from

0.6 to 85.6% and viscosity was decreased from 2.56 to 1.42×10^3 Pa.s with enhancement of rpm from 0 to 6000 or *g* values from 0 to 4684. Clarified juice viscosity was decreased due to removal of suspended particles and the treated juice was clear and visible. Optimum rpm of machine was 4500 rpm, shown in **Figure 4.9.**

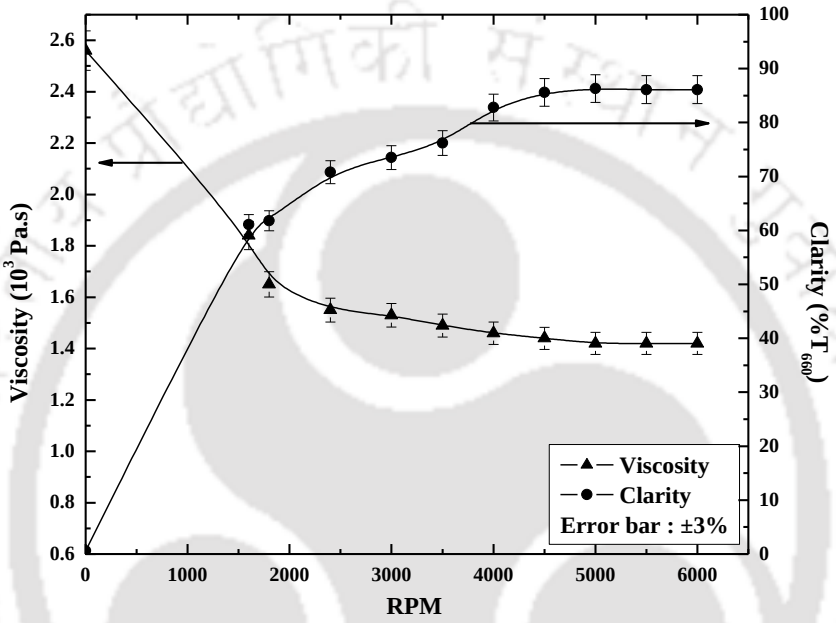

Figure 4.9. Variation of steady state viscosity and clarity with rpm.

4.2.1.6 Effects on Physicochemical Properties of Treated Raw Juice for Combined Pretreatment Operation (Fining Agent Addition and Centrifugation)

In this method, mosambi juice was pretreated with fining agent and centrifugation combination. The optimum dose of fining agent was 3000 ppm and optimum rpm of centrifugation was 4500 rpm (discussed in previous sections, 4.2.1.4 and 4.2.1.5). Pretreated juice quality after combined operation had good clarity and low viscosity due to maximum removal of suspended solid compared to single pretreatment

operation. Clarity was found to increase from 0.6 to 86.6% with (C+G), up to 87% with (C+B) and 88.9% with (C+G+B) operations. The viscosity decrease was 41% with (C+G), 42% with (C+B) and 46.2% with (C+G+B) operations.

4.2.1.7 Quality Analysis and Cost Estimation of Juice Pretreated With Different Methods

Initial total soluble solid of raw juice was 9.3°Brix and after pretreatment, it was 8.5°Brix, whereas, clarified juice density was reduced from 1.10 to 1.05 g/cm^3. Clarified juice qualities after various pretreatment methods were shown in **Table 4.4**. Maximum reductions of viscosity and clarity were 42.32 and 16.3% respectively, with combined column operation. There was no significant difference in pH of raw juice and clarified juice obtained after different pretreatment methods. Cost estimation for pretreatment of mosambi juice (one litre) by applying different pretreatment methods was also shown in **Table 4.4**. During packed bed, maximum pectin content was removed (48.5%) by combined column operation. Minimum cost among all pretreatment processes was packed column run by peristalatic pump. Single centrifugation power cost was lowered compared to combined operation of centrifugation. For fining agent addition minimum cost was found out with bentonite. Centrifugation combined with fining agents addition pretreated cost was higher compared to single centrifugation and fining agent operation. Centrifugation combined with gelation pretreatment cost was extreme in all methods.

Table 4.4 Variation in physicochemical properties of mosambi juice and cost estimation after applied different pretreatment methods

Sl. No	Pretreatment methods	AIS Reduction (%)	Clarity (% T_{660})	Viscosity Reduction (%)	Consumption	Cost of raw materials (₹)	Operating Cost (₹)	Operating Cost ($)[#]
1	Packed Column (glass beads)	40.0	5.2	25.1	40 W	4.54/kWh	0.1816	0.00293
2	Packed Column (molecular sieve)	45.0	12.3	35.1	40 W	4.54/kWh	0.1816	0.00293
3	Packed Column in series	48.5	16.3	42.3	40 W	4.54/kWh	0.1816	0.00293
4	Centrifugation	73.0	85.6	40.6	200 W	4.54/kWh	0.908	0.0146
5	Gelatin	78.2	1.4	38.8	1 kg	1138	2.845	0.0458
6	Bentonite	69.0	2.1	40.2	1 kg	628	1.570	0.0253
7	Gelatin+ Bentonite (1:5)	78.0	3.1	43.1	1kg+5kg	4278	2.139	0.0345
8	Centrifugation+ Gelatin	81.0	86.6	41.0	200W+1kg	4.54/kWh+1138	3.753	0.0605
9	Centrifugation+ Bentonite	81.5	87.0	42.0	200W+1kg	4.54/kWh+628	2.478	0.0406
10	Centrifugation+ Gelatin+Bentonite	82.5	88.9	46.2	200W+1kg +5kg	4.54/kWh+1138 +3140	3.047	0.0491

[#]1 US $ = ₹ 62.00

4.2.2 Summary

The physicochemical properties of the clarified mosambi juice after different pretreatment methods such as, packed column, fining agent addition, centrifugation and combination of fining agent addition and centrifugation were studied in detail.

- In packed column, treated mosambi juice qualities were superior in molecular sieve supported column compared to glass bead supported column.
- Clarified mosambi juice quality was found to degrade with increase of feed flow rate from 50 to 500 cm^3/hr.
- With increase of relative centrifugal force, *g* values from 293 to 4684 during centrifugation, clarified juice clarity increased by 85.6% and the optimum *g* value was 2634.
- With fining agent, such as, gelatin, bentonite and combination of gelatin and bentonite (G:B = 1:5, w/w) addition, clarified juice qualities in terms of clarity and viscosity were also improved but still pectin remained in the clarified juice.
- Combined gelatin and bentonite operations had maximum ability to improve clarity by 43.1% and 78% pectin removal. Combined fining agent addition and centrifuged juice quality were improved compared to single pretreatment, but it was not cost effective.
- Maximum improvements of 88.9% clarity, 46.2% viscosity reduction and 82.5% pectin removal with centrifugation and combined fining agent addition of gelatin and bentonite (G:B = 1:5, w/w) were observed.
- Among all pretreatment process, packed column operation cost was lowest (0.00293$/1 L raw juice).

4.3 Performance of Spiral Wound UF Membrane Module in Laminar Flow Regime

In this section, clarification of synthetic juice through spiral wound ultrafiltration at laminar flow regime was discussed. Experiments were conducted at two operating conditions; namely, with and without permeate recycle at different TMP drops. Membrane performance was analysed in both conditions. Different diffusion models were considered to estimate the theoretical flux.

4.3.1 Results and Discussions

4.3.1.1 Variation of Permeate Flux with Time for with and without Permeate Recycle

Transient flux decline profiles for with and without permeate recycle were shown in **Figures 4.10(a)** and **(b)**, respectively. As shown in **Figure 4.10(a)** for with permeate recycle, the permeate flux declined sharply with time for first 20 min. After that, permeate flux decline was marginal and continued up to 120 min. Beyond 120 min, variation in permeate flux was negligible and steady state was achieved. The steady state permeate flux values at different TMP drops (414, 552 and 690 kPa) were 8.50×10^{-6}, 12.34×10^{-6} and 14.87×10^{-6} $m^3/m^2.s$ respectively after 180 min run of the experiment. Due to enhancement of TMP drops (driving force), permeate flux was found to increase. Permeate flux decline was dependent on several factors, such as, concentration polarization, gel layer formation and pore blocking. Initial flux decline was due to the concentration polarization after that flux decline was due to the cake filtration [142, 143].

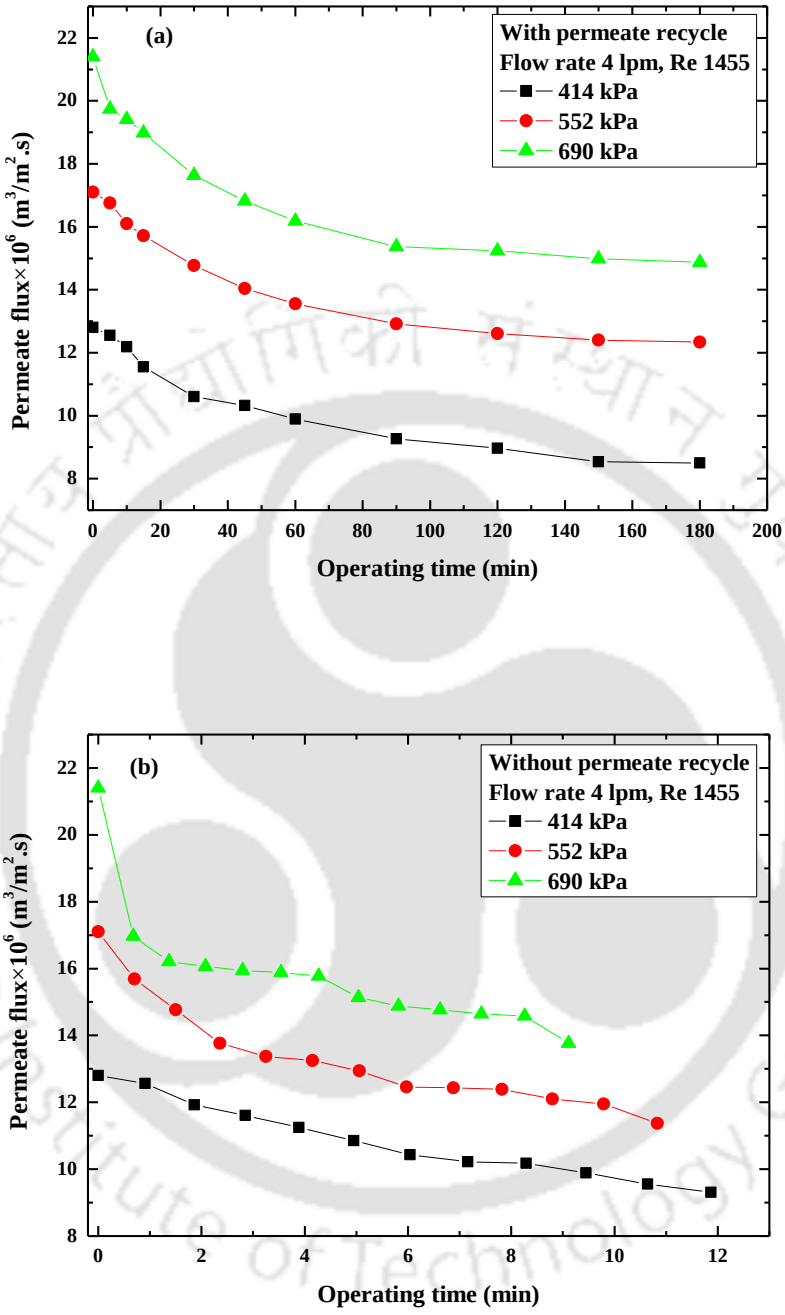

Figure 4.10. Transient flux decline (a) with and (b) without permeate recycle.

Concentration polarization was caused by the accumulation of pectin molecules on the membrane surface in a short period of time, which turned into a gel layer and

acted as an additional resistance on membrane surface. Around 52 to 53% permeates were collected (for 414, 552 and 690 kPa) in 180 min. As a result, 48 to 47% permeates were recycled to achieve the product quality as desired. Hence, recycle scheme can be translated into industrial operation for getting improved quality of the products.

For without permeate recycle, the permeate flux declined continuous due to the increase of pectin concentration on membrane surface and transient flux decline followed a batch cell profile. As shown in **Figure 4.10(b)**, the final permeate flux at different TMP drops were 9.31×10^{-6}, 11.37×10^{-6} and 13.77×10^{-6} $m^3/m^2.s$, respectively. Maximum operating time was 11.9 min at 414 kPa, whereas it was only 9.1 min at 690 kPa for clarifying 10 L of feed solution.

As permeate was collected continuously without recycling, concentration polarization was profound in without permeate recycle case and it behaved like a batch filtration cell. As a result, the decline in permeate flux was more compared to permeate recycle.

4.3.1.2 Variation of VRF with Time for with and without Permeate Recycle

Variation of *VRF* with operating time at different TMP drops (414, 552 and 690 kPa) for with and without permeate recycle was shown in **Figures 4.11(a)** and **(b)**. Increase of *VRF* had a significant impact of permeate quality and membrane performance. With driving force (ΔP), permeation rate was enhanced resulting *VRF* to increase. In both the cases, retentate was recycled. For with permeate recycle, the increase of *VRF* was gradual as permeate was also added with the retentate. This was shown in **Figure 4.11(a)**. In case of without permeate recycle, as the permeate sample was continuously taken out; a sharp change in *VRF* was observed.

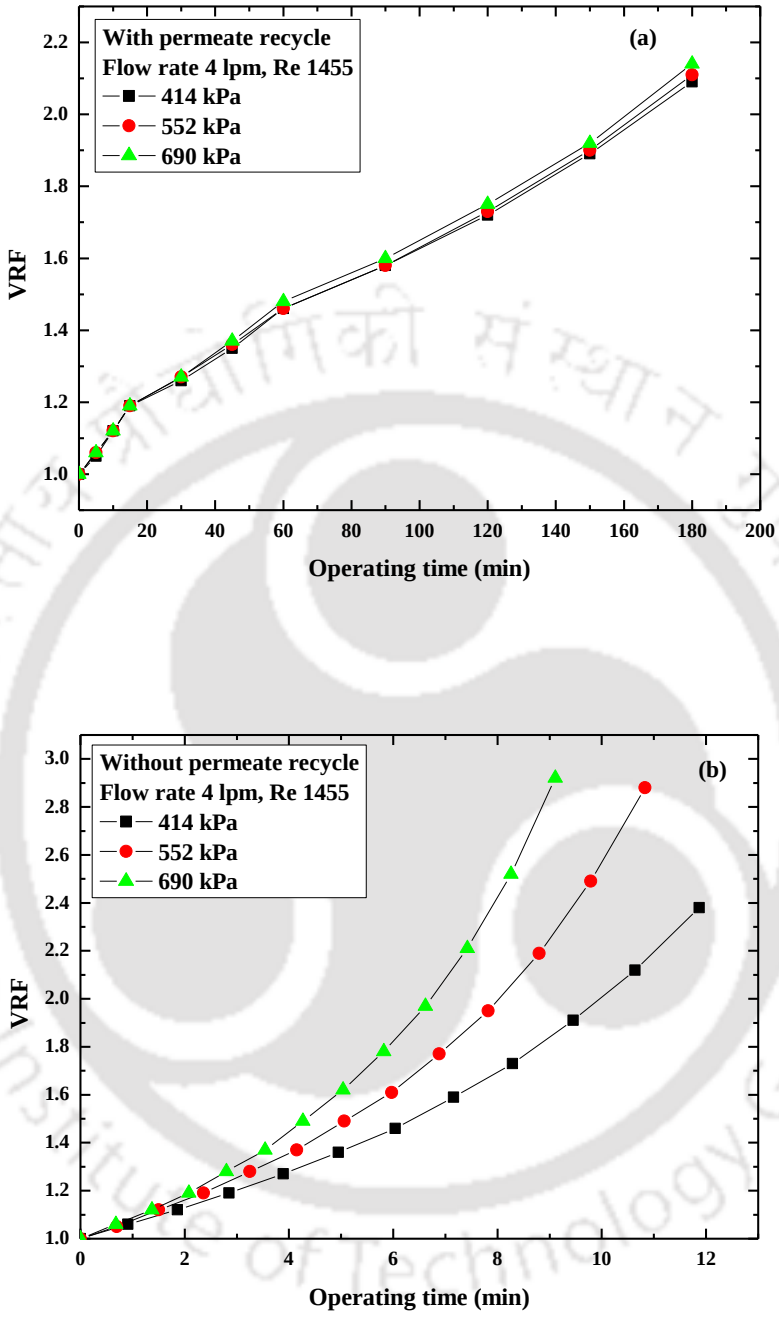

Figure 4.11. Variation of VRF with operating time (a) with and (b) without permeate recycle.

Figure 4.11(b) showed the variation of *VRF* with operating time for without permeates recycle. After 180 min, the *VRF* was 2.09 at TMP drops of 414 kPa for with permeate recycle. It increased to 2.14 when TMP drop was raised upto 690 kPa. In case of without permeate recycle, the *VRF* was increased from 2.38 to 2.88 as TMP drops increased from 414 to 552 kPa. Further increase in *VRF* to 2.92 was observed when TMP drops increased from 552 to 690 kPa, within operating time 9.1 min.

For without permeate recycle, the *VRF* value was higher compared to with permeate recycle due to higher fouling of membrane surface. For without permeate recycle maximum *VRF* value of 2.92 achieved within 9.1 min, but for with permeate recycle, the maximum *VRF* was achieved as 2.14 after 180 min. On the basis of gradual increase of *VRF*, with permeate recycle process is considered as the best process for long operating time, less membrane fouling and increase of membrane life [144, 145].

4.3.1.3 Resistance Variation during Membrane Filtration for with and without Permeate Recycle

Study on permeate flux decline during membrane filtration with operating time at different TMP drops for with and without permeate recycle is also very important in filtration efficiency study. Permeate flux decline profile with operating time was analysed by resistance in series model. During filtration, pectin molecules accumulated on membrane surface, turning into a gel layer to act another membrane surface [146].

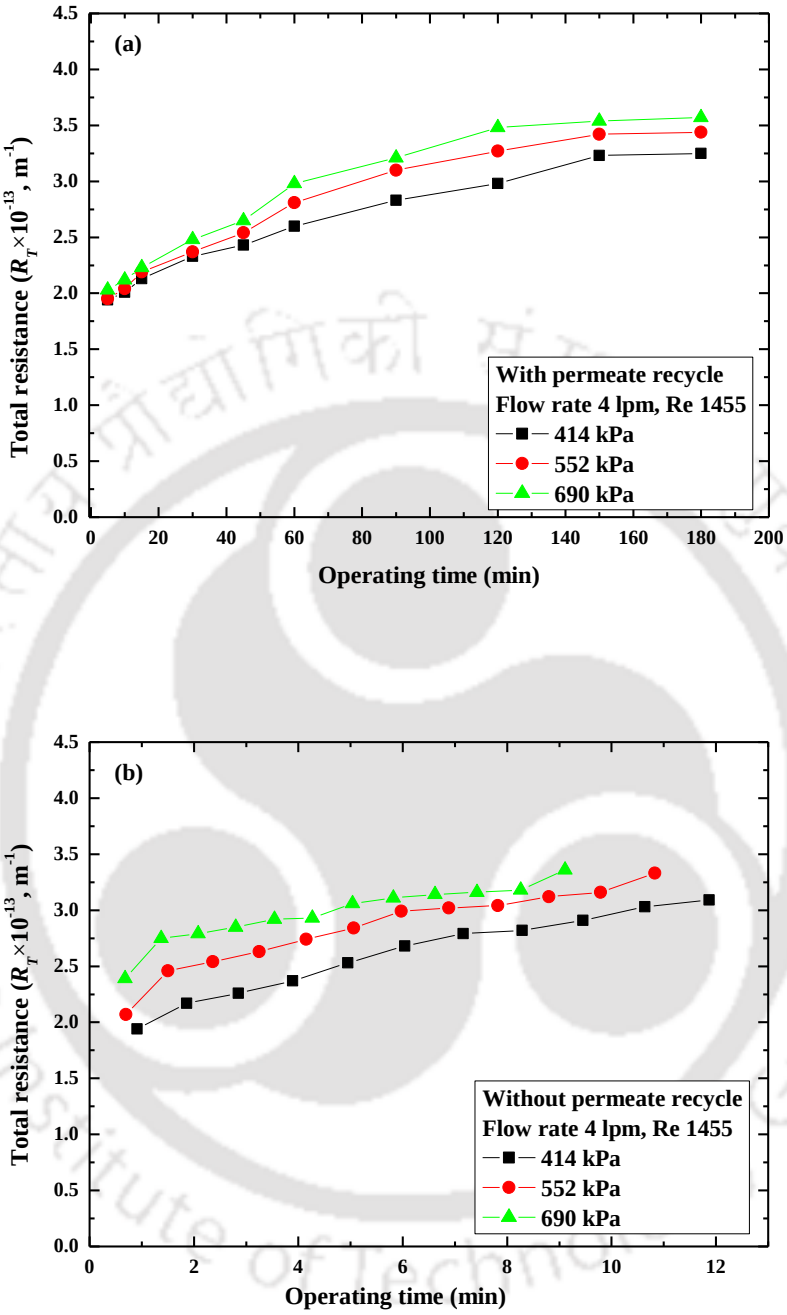

Figure 4.12. Variation of total resistance with operating time for (a) with and (b) without permeate recycle.

Both the cases, with and without permeate recycle, pectin molecules adsorbed on membrane surface, resulting in enhanced total resistance of membrane (R_T) with operating time. The variation of total resistance with operating time was shown in **Figures 4.12(a)** and **(b)**. As shown in **Figure 4.12(a)** for with permeate recycle, with the increase of TMP drops from 414 to 690 kPa, total resistance of membrane were increased from 3.25×10^{13} to 3.59×10^{13} m^{-1} after a 180 min run. As TMP drops increased, pectin molecules moved rapidly towards membrane surface resulting in enhancement of total resistance [147]. Total membrane resistance for without permeate recycle was continuously increased to 3.09×10^{13} m^{-1} due to rapid deposition of pectin particles on membrane surface within a short operating time of 11.9 min at 414 kPa. Similarly, at 690 kPa TMP drops, total resistance reached to 3.36×10^{13} m^{-1} after 9.1 min. These were shown in **Figure 4.12(b)**. So, without permeate recycle, total membrane resistance was increased within a short duration (9.1 to 11.9 min), but for with permeate recycle, total resistance increased slowly in 180 min run. Hence, the development of total resistance due to deposition of pectin molecules were less for with permeate recycle compared to without permeate recycle for a particular operating time of operation.

4.3.1.4 Variation of J_{exp} with J_{cal} using Different Diffusion Models for with and without Permeate Recycle

Three diffusion models, namely, Brownian, shear induced and combined diffusion model were used on the basis of particle size of the solute in the permeate to calculate permeate flux values (J_{cal}) and compared with experimental flux values (J_{exp}).

Particle size distribution of pectin in the feed was shown in **Figure 4.13**. The calculated average particle size of pectin in feed was 93.4 µm.

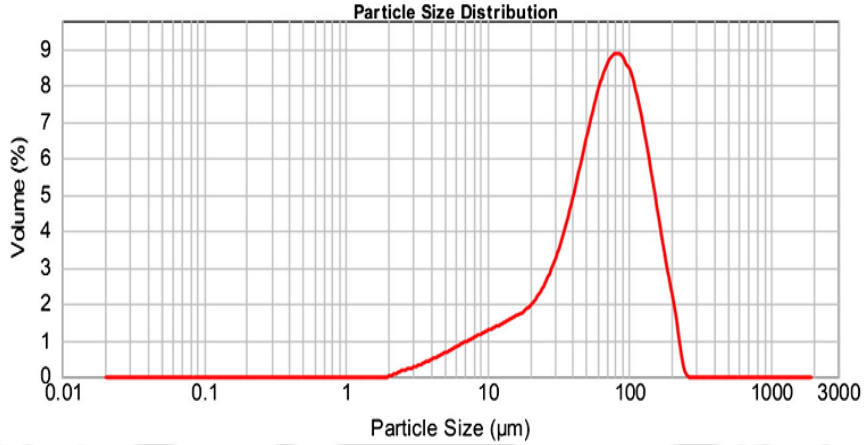

Figure 4.13. Particle size distribution of pectin in feed.

The variation of J_{exp} with J_{cal} for with and without permeate recycle was shown in **Figures 4.14(a)** and **(b)**, respectively. It was observed from **Figure 4.14(a)** that the J_{exp}/J_{cal} for Brownian diffusion model was in the range of 0.94 to 1.03. For example, at 552 kPa TMP drops, the experimental permeate flux was 12.3×10^{-6} $m^3/m^2\cdot s$, whereas model calculated value was 11.9×10^{-6} $m^3/m^2\cdot s$. Hence, the experimental permeate flux values varied within ±6% of the calculated permeate flux values for with permeate recycle. The calculated permeate flux values using combined diffusion model were within ±14% of experimental permeate flux values. Whereas, J_{exp}/J_{cal} varied from 1.45 to 1.59 for shear induced diffusion model. It was clear from these observations that the permeate did not contain appreciable amount of pectin molecules and the particle sizes in the permeate were less than 0.1 µm. Moreover, shear induced diffusivity is proportional to the square of particle size multiplied by the rate of shear. Whereas,

Brownian diffusion coefficient is inversely proportional to the particle size and independent of shear rate [107].

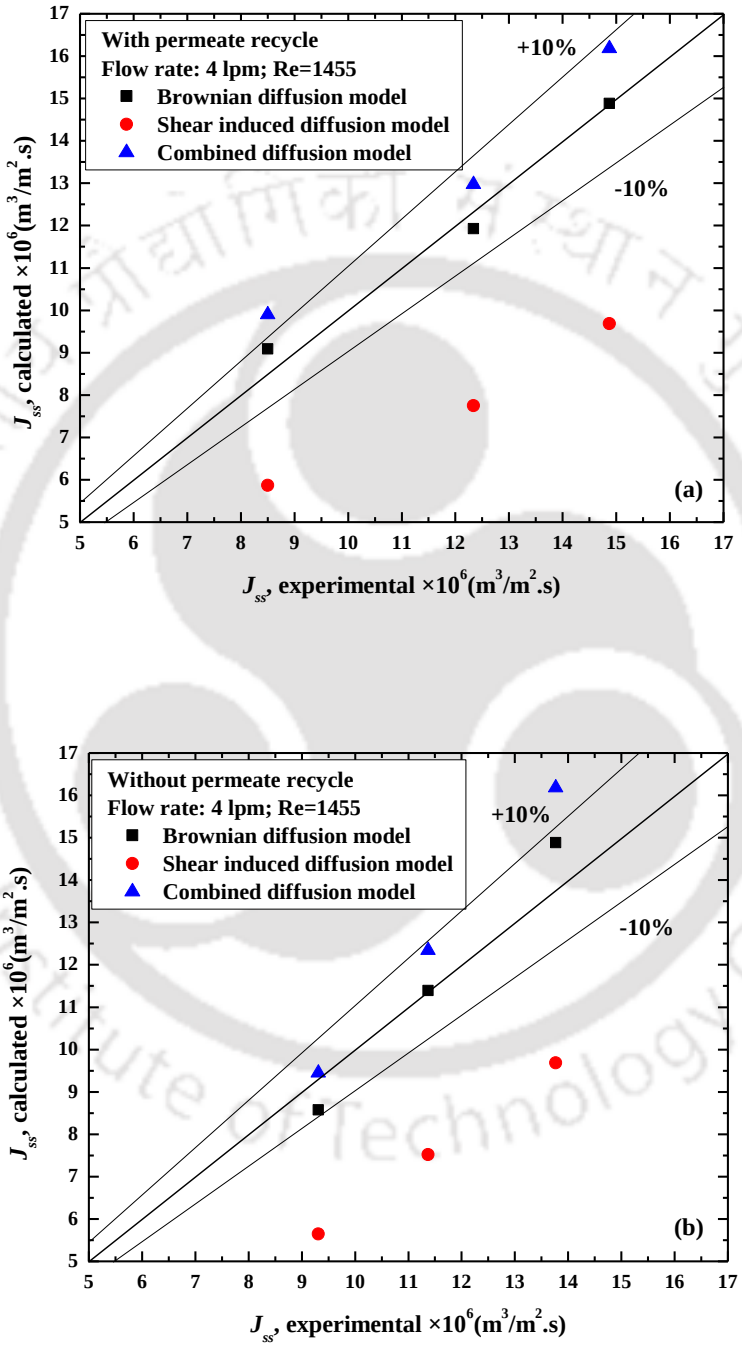

Figure 4.14. Variation of J_{exp} with J_{cal} using Brownian, shear induced and combined diffusion models for (a) with and (b) without permeate recycle.

As a result, predicted permeate flux using shear induced model in laminar regime deviated more from the experimental permeate flux values. Similar trends were observed for without permeate recycle and were presented in **Figure 4.14(b)**. For Brownian diffusion model, J_{exp}/J_{cal} values were obtained in the range of 0.93 to 1.09. These values varied from 1.42 to 1.65 for shear induced diffusion model. For combined diffusion model, the experimental permeate flux was 13.8×10^{-6} $m^3/m^2\cdot s$ and the model calculated value was 16.2×10^{-6} $m^3/m^2\cdot s$. at 690 kPa TMP drops. So, the experimental flux values were within ±15% of the calculated permeate flux values. Both for with and without permeate recycle, Brownian diffusion model predicted flux values were best fitted with experimental flux values. Though the prediction of permeate flux values using Brownian diffusion model for with recycle is better than without recycle. This is due to slight lower solute concentration in the permeate than the ones assumed in the model.

4.3.1.5 Permeate Quality

Permeate qualities in terms of TDS, turbidity, clarity, viscosity, AIS, density and ionic conductivity in the treated synthetic juice before and after clarification through spiral wound UF membrane module for with and without permeate recycle were shown in **Table 4.5**. It was observed from **Table 4.5,** that TDS reductions were 43 and 28.5%, respectively, from raw synthetic juice for with and without permeate recycle. Due to more passage of pectin molecule through membrane pores, TDS values in the permeate were increased when TMP drops were increased. With permeate recycle, TDS values were less due to skimming effects. Maximum TDS removal was observed at lowest TMP drops of 414 kPa for both cases. Clarity of the permeate

samples were directly related to TDS removal. With and without permeates recycle, increment of clarity were 9.5 and 3.7% respectively from raw synthetic juice.

Table 4.5 Comparison of physiochemical properties of permeates at steady state with and without permeate recycle (laminar)

Physicochemical Property	**Feed**	**Retentate**	**With permeate recycle**			**Without permeate recycle**		
			TMP drops (kPa)			**TMP drops (kPa)**		
			414	**552**	**690**	**414**	**552**	**690**
TDS (mg/L)	140	210	80	85	90	100	105	115
Turbidity (NTU)	45	60	13.5	15	17	20	22	24
Clarity (% T_{660})	89	65	97.5	96.1	94.2	95.4	93.6	92.3
Viscosity (mPa.s)	2.12	2.56	1.29	1.34	1.36	1.44	1.46	1.49
AIS (g/L)	2	5	0.020	0.052	0.030	0.040	0.052	0.055
Density (g/cm^3)	1.10	1.18	1.01	1.01	1.01	1.04	1.04	1.04
Ionic conductivity (µS)	0.21	0.25	0.12	0.13	0.14	0.16	0.17	0.20
Sucrose (g/L)	90	95	75	70	68	74	72	70

Presence of sucrose and pectin molecules in stream made it haze resulting turbidity increase and decrease in clarity. Turbidity and clarity of raw synthetic juice were 45 NTU and 89%, respectively. With and without permeate recycle, the turbidity values at different TMP drops of 414, 552 and 690 kPa were 13.5, 15, 17 NTU and 20, 22, 24 NTU, respectively. With permeate recycle, turbidity had lower values compared to without permeate recycle due to low concentration of pectin and sucrose in permeate solution. Increase of TMP drops for with and without permeates recycle, increase in

turbidity due to enrichment of the pectin and sucrose concentration in permeate. Viscosity and AIS followed the same trend as that of TDS. Density slightly decreased from 1.10 to 1.01g/cm^3 and 1.04 g/cm^3 for with and without permeates recycle due to removal of pectin particle. Ionic conductivity decreased from 0.21 to 0.13 µS for without permeate recycle whereas the change was marginal for without permeate recycle. The pH of the feed was measured as 3.86. pH was found to be almost invariant in the permeate samples for both the operating conditions.

4.3.2 Summary

Synthetic juice was clarified through spiral wound UF membrane module at two different operating conditions, such as, with and without permeate recycle. Membrane performance was analysed in terms of *VRF*, and transient flux decline. The following conclusions were drawn from the present investigations:

- At low operating time, transient flux decline was higher in without permeate recycle compared to with permeate recycle, due to continuous deposition of solute particle on membrane surface.
- Rate of *VRF* was rapid in without permeate recycle due to higher fouling of membrane surface.
- Total membrane resistance was higher in without permeate recycle at a low operating time and enhanced with TMP drops, which affected the membrane performance for continuous operation.
- On the basis of particle size distribution of pectin molecule, different diffusion models were assumed; Brownian diffusion model estimated flux values were best fitted within ±9% with the experimental flux data.

- Maximum improvements of physical properties were observed for with permeate recycle at 414 kPa. Clarified juice qualities were degraded with the increase of TMP drops.

4.4 Performance of Spiral Wound UF Membrane Module in Turbulent Flow Regime

In this section, clarification of synthetic juice through spiral wound ultrafiltration at turbulent flow regime for with and without permeates recycle. Membrane performance were analysed in both conditions, with variations of TMP drops. On the basis of pectin particle size in permeate sample different diffusion was assumed to estimate the theoretical flux value.

4.4.1 Results and Discussion

4.4.1.1 Variation of Permeate Flux with Time for with and without Permeate Recycle

At turbulent flow regime, variation of permeate flux with operating time at different TMP drops (414, 552 and 690 kPa) for with and without permeate recycle was represented in **Figures 4.15(a)** and **(b)**. With permeate recycle, permeate flux declined sharply with operating time for first 20 min at different TMP drops, shown in **Figure 4.15(a)**. Decline of permeate flux was due to concentration polarization, accumulation of pectin particles on membrane surface at short operating time [141]. For operating time between 20 to 60 min, decline in permeate flux was marginal. After 20 min, concentration polarization turned into a gel layer formation due to continuous deposition of pectin particles on membrane surface and continued upto 90 min. Gel layer provided an extra resistance on membrane surface resulting block of membrane pores and decreased the permeation rate. Steady state permeate flux value was achieved at 90 min. Steady state permeate flux at different TMP drops were 12.46×10^{-6},

15.25×10^{-6} and 18.28×10^{-6} $m^3/m^2.s$. With enhancement of TMP drops, steady state permeate flux was increased due to enhanced driving force. Around 52 to 53% clarified permeate volume were collected within 180 min operating time at different TMP drops.

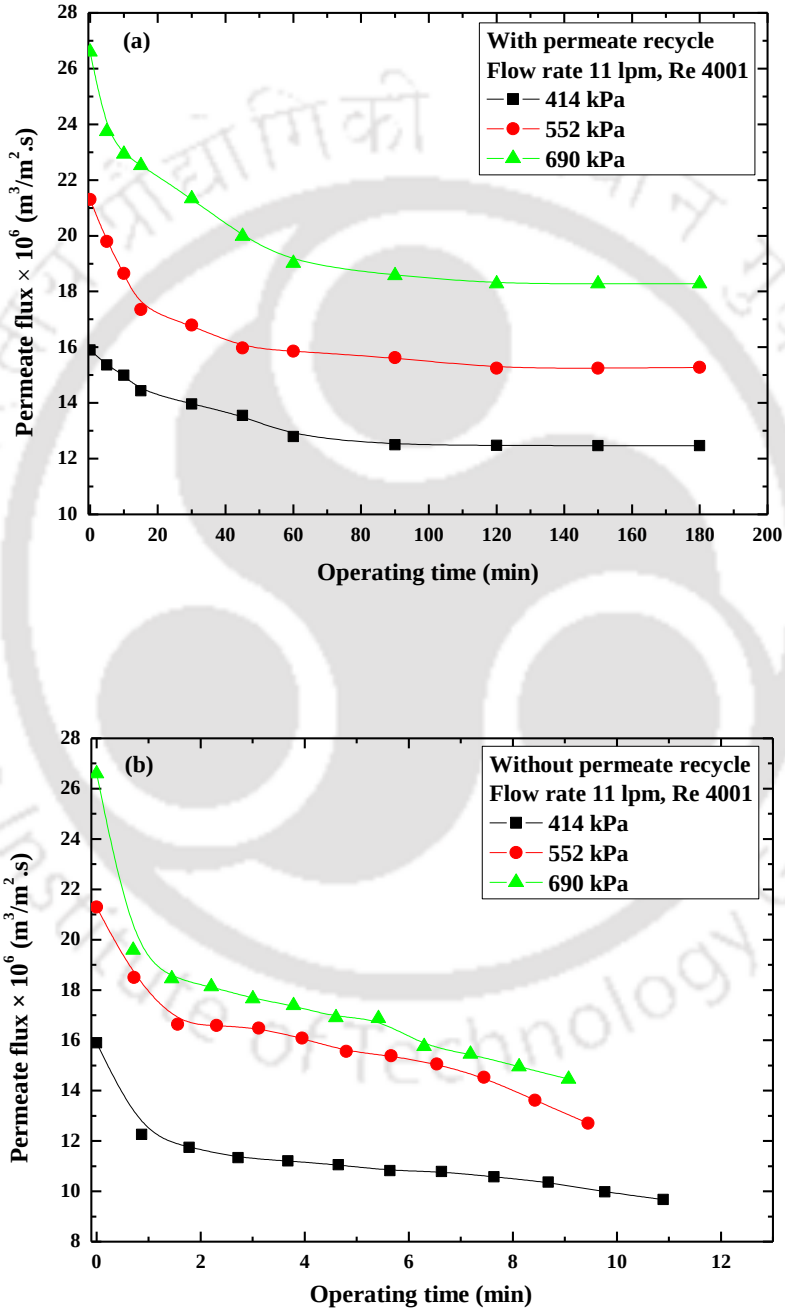

Figure 4.15. Transient flux decline (a) with and (b) without permeate recycle.

Continuous permeate samples were collected without recycling permeate in feed tank resulting transient flux decline continuously within short operating time and was shown in **Figure 4.15(b)**. Without permeate recycle, rate of pectin particle deposition on membrane surface was increased and transient flux decline followed a batch cell profile. At different TMP drops (414, 552 and 690 kPa), the final permeate flux values were 9.67×10^{-6}, 12.7×10^{-6} and 14.45×10^{-6} $m^3/m^2.s$, respectively. The operating times to clarify 10 L feed were 10.89 min at 414 kPa and 9.1 min at 690 kPa.

At turbulent flow regime, with permeate recycle, steady state permeate flux value was decreased and for without permeate recycle, operating time to reach the final flux value was lesser compared to laminar flow regime. With increase of flow rate (11 lpm, Re 4001) growth of pectin layer formation over membrane surface was decreased, resulting lower permeate flux decline with short operating time and more permeate samples were collected compared to laminar flow regime for with and without permeate recycle. For with permeate recycle; at laminar flow regime steady state permeate flux was achieved at operating time 120 min, but with enhancement of turbulence, operating time to reach the steady state was reduced upto 30 min at different TMP drops (414, 552 and 690 kPa).

4.4.1.2 Variation of VRF with Time for with and without Permeate Recycle

VRF played an important role to study the membrane performance. For both with and without permeate recycle, the variation of VRF with operating time was shown in **Figures 4.16(a)** and **(b**). For with and without permeate recycle, VRF raised continuously.

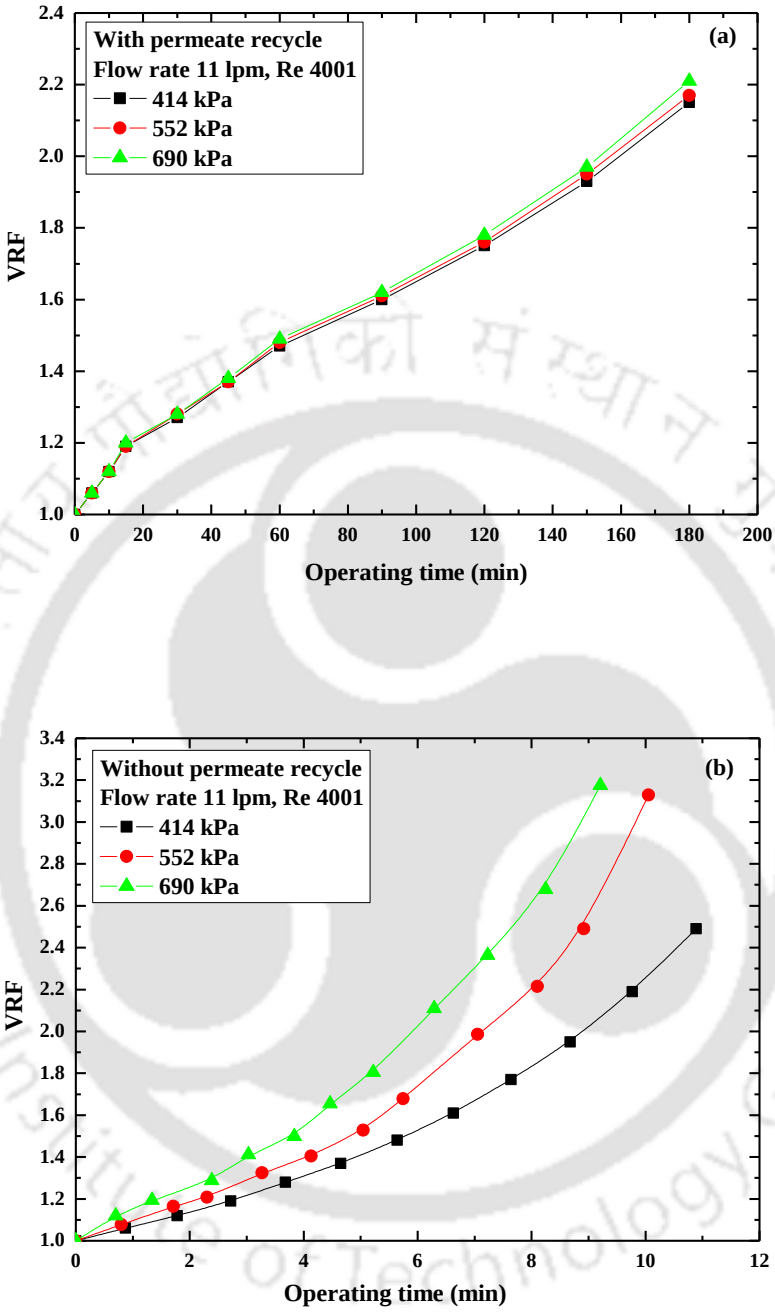

Figure 4.16. Variation of VRF with operating time (a) with (b) without permeate recycle.

As shown in **Figure 4.16(a)**, for with permeate recycle, VRF raised linearly with operating time. At different TMP drops (414, 552 and 690 kPa) final VRF values were 2.15, 2.17 and 2.21 within operating time of 180 min. For without permeate recycle, VRF rose linearly up to 6 min after that it raised gradually (shown in **Figure 4.16(b)**). With increase of TMP drops from 414 to 690 kPa, operating time decreased from 10.89 to 9.1 min, and VRF rose from 2.49 to 3.17. VRF rise gradually affected the membrane performance due to enhancement of pectin molecule attraction on membrane surface. Molecule attraction turned membrane live pores into partially blocked pores. After that these turned into dead pores for continuous application. For with permeate recycle, at 690 kPa, a maximum VRF of 2.21 was achieved with in operating time of 180 min, but in case of without permeate recycle, this value was achieved with in operating time of 6.89 min. On the basis of results, membrane performance was improved in with permeate recycle for long operating time.

With enhancement of Reynolds number from 1455 to 4001, deposition of solute layer over membrane surface was decreased resulting improvement of permeation rate for with and without permeates recycle. Enhancement of permeate rates resulted VRF increase as compared to laminar flow regime for with and without permeate recycle. As TMP drop was increased from 414 to 690 kPa, permeation rate increased resulting VRF rise. For example, laminar flow regime, with increase of TMP drops from 414 to 690 kPa, VRF was varied from 2.09 to 2.13 and 2.38 to 2.92 with and without permeate recycle. With increase of flow rate from 4 to 11 lpm at TMP drops (414, 552 and 690 kPa), solute deposition layer was decreased and resultant VRF upgraded from 2.15 to 2.21 and 2.49 to 3.17 for with and without permeate recycle.

4.4.1.3 Resistance Variation during Membrane Filtration for with and without Permeate Recycle

For both cases with and without permeate recycle, pectin particles deposited on membrane surface and turned into gel layer. As shown in **Figures 4.17(a)** and **(b)**, total resistance was increased with of operating time. With permeate recycle, total resistance raised sharply within 60 min, after that deviation was small, shown in **Figure 4.17(a)**. After 60 min, variation of total resistance with operating time was small due to permeate recycle in feed tank and dilution of feed sample. With increase of TMP drops from 414 to 690 kPa, total resistance was found to increase from 2.52×10^{13} to 2.87×10^{13} m^{-1}, due to enhancement of pectin molecule attraction on membrane surface, after 180 min run of instrument.

For without permeate recycle, total resistance continuously increased with operating time (shown in **Figure 4.17(b)**) due to continuously deposition of pectin molecules on membrane surface. Without permeate recycle, pectin composition in retentate sample was increased with operating time and total resistance increase followed a batch cell profile. At TMP drops 414 kPa, total resistance of 2.98×10^{13} m^{-1} was reached within operating time of 10.89 min. With increase of TMP drops from 552 to 690 kPa, total resistance was increased from 3.02×10^{13} to 3.2×10^{13} $m^{-1}$and operating times were decreased from 9.45 to 9.1 min. At a particular operating time, total resistance increment for with permeate recycle was less compared to without permeate recycle due to dilution of feed sample for recycling of permeate sample.

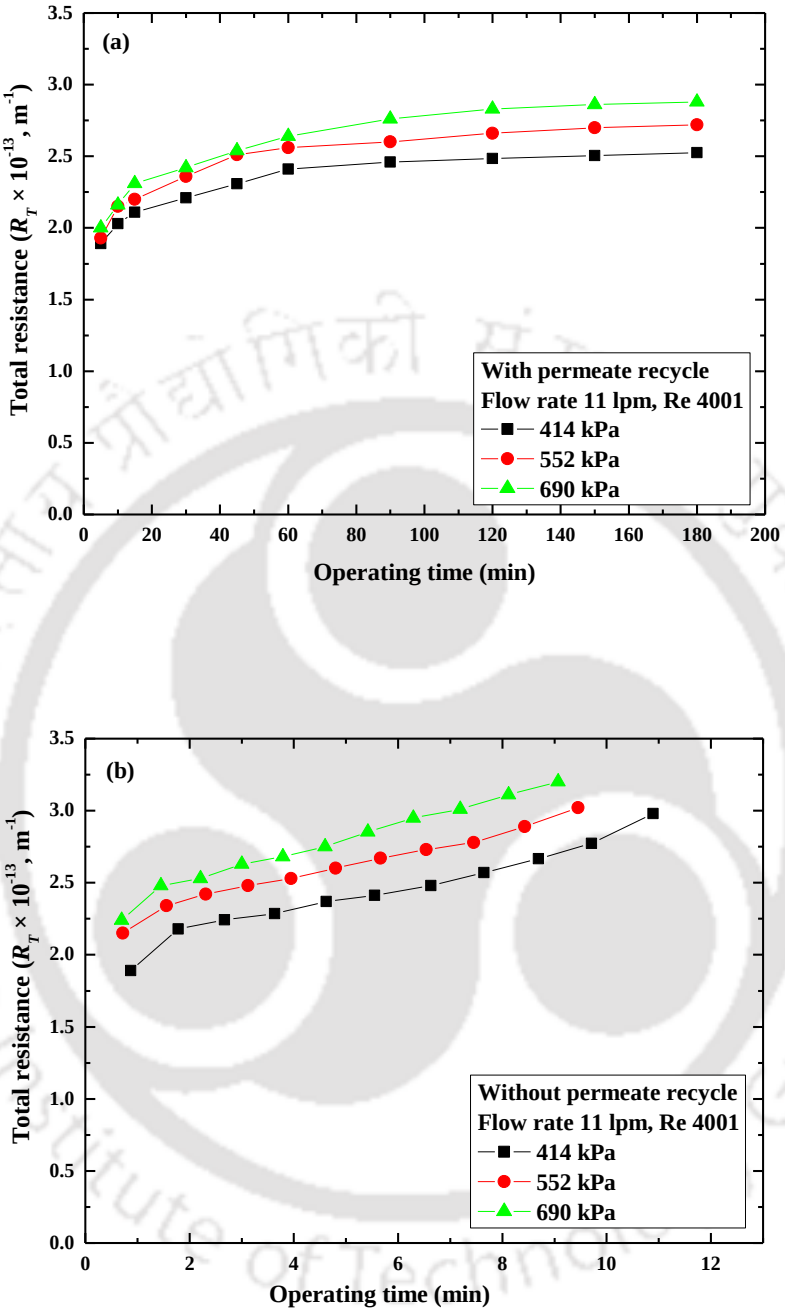

Figure 4.17. Variation of total resistance with operating time for (a) with and (b) without permeate recycle.

With increase of flow rate (11 lpm, Re 4001), of solute (pectin) particle deposition on membrane surface decreased and total resistance developed on membrane surface was decreased compared to laminar flow regime for with and without permeate recycle. With increase of TMP drops from 414 to 690 kPa, 23 to 19% total resistances was decreased for with permeate recycle and 4 to 5% decreased for without permeate recycle compared to laminar flow regime. Less membrane fouling had improved the membrane performance. In both the conditions (laminar and turbulent flow), total resistance of membrane was increased without permeate recycle with increase of driving force (TMP drops) due to more solute attraction.

4.4.1.4 Variation of J_{exp} with J_{cal} using Different Diffusion Models For with and without Permeate Recycle

In turbulent flow regime, bigger pectin molecules were broken into finer particles due to high shear stress. Permeate contained pectin in the form of floc during breakage. Pectin particle agglomerated after settling of permeate sample. Particle size distribution of pectin in permeate sample was in range of 0.1 to 3.5 µm. Average particle size of pectin in permeate sample was observed less than 2.5 µm. On the basis of particle size distribution in permeate, different diffusion models such as, Brownian, shear induced and combined diffusion model were used to estimate the theoretical flux. For with and without permeate recycle, variation of J_{exp} vs J_{cal} at different TMP drops (414, 552 and 690 kPa) was shown in **Figures 4.18(a)** and **(b)**.

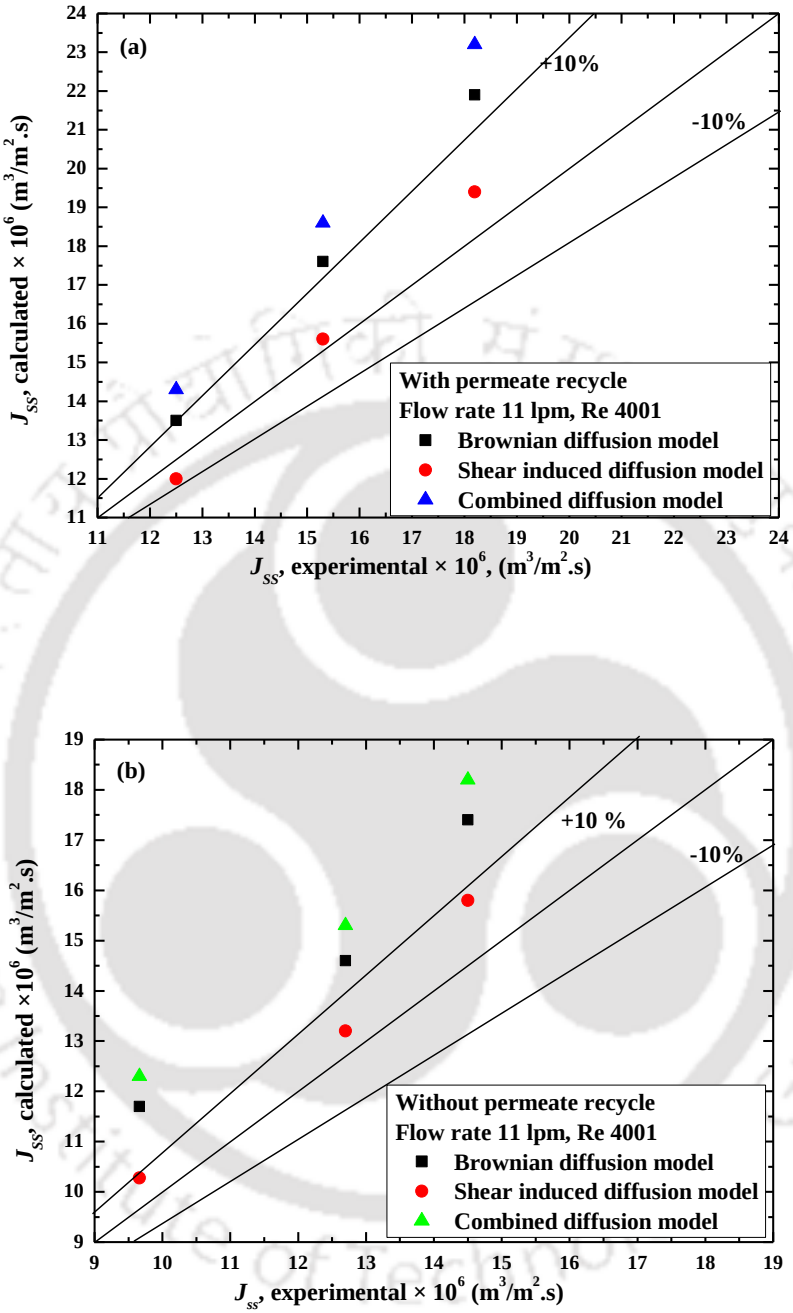

Figure 4.18. Variation of J_{exp} with J_{cal} using Brownian, shear induced and combined diffusion models for (a) with and (b) without permeate recycle.

The average particle of pectin in permeate was 1.8 µm and corresponding diffusivity was 1.12×10^{-10} m^2/s. Ratio of J_{exp} vs J_{cal} was in the range of 0.94 to 1.05 with increase of TMP drops from 414 to 690 kPa, as shown in **Figure 4.18(a)** With permeate recycle, experimental flux at 414 and 690 kPa were 12.6×10^{-6} and 18.2×10^{-6} $m^3/m^2.s$ respectively. The corresponding theoretical flux for shear induced diffusion model was 12×10^{-6} and 19.4×10^{-6} $m^3/m^2.s$. The variations of J_{exp}/J_{cal} were within range of ±6%. Brownian and combined diffusion model estimated permeate flux values were in the range of ±17% and ±20% respectively.

For without permeate recycle, trends were observed and was represented in **Figure 4.18(b)**. For shear induced diffusion model, J_{exp}/J_{cal} was obtained in the range of 0.92 to 0.96, (within ±8%). For Brownian and combined diffusion model, J_{exp} vs J_{cal} came within the range of 18 and 22%. In both cases for with and without permeate recycle shear induced diffusion model estimated flux data was best fitted with experimental data and came in the range of ±10%.

Operating conditions laminar and turbulent flow regime were directly dependent of feed flow rate and feed flow rate was dependent on cross flow velocity. Diffusivity was important factor to calculate the theoretical flux at different diffusion models such as, Brownian and shear induced.

Brownian diffusivity was inversely proportional of particle size (submicron) and independent of shear rate [141]. At low velocity (laminar flow), mostly solute particles were retained through membrane surface only lower (submicron) molecules were passed through membrane pores. Due to independent of shear rate or at low velocity Brownian diffusion model estimate flux value was best fitted with experimental flux results for laminar flow regime compared to turbulent flow regime [142]. With increase

of shear rate Brownian diffusion predicted data was deviated with experimental flux results. According to Eq. (4.31), Brownian diffusion predicted mass transfer coefficient decreases with increase of particle size, resulting estimated flux value decrease and not fitted for turbulent flow regime.

Shear induced diffusion coefficient was dependent on shear rate and applicable of particle size in micron. The shear rate directly depends on cross flow velocity. With increase of shear rate, pectin submicron size particle was passed through membrane pores and pectin particles clustering. Due to clustering, pectin particle size increased, resultant shear induced diffusivity estimated flux data was best fit with experimental flux value at turbulent flow regime.

4.4.1.5 Permeate Quality

Different physicochemical properties such as, TDS, turbidity, clarity, viscosity, AIS, density, ionic conductivity of feed, retentate and permeate sample at different TMP drops (414, 552 and 690 kPa) for with and without permeate recycle were shown in **Table 4.6.**

Removal of pectin molecules through UF membrane surface, resultant permeate qualities were improved and retentate sample physicochemical properties were increased due to rejection of solute molecules. Feed TDS was 140 mg/L due to presence of pectin and sucrose. After membrane separation, maximum reduction of TDS was 39.2 and 23.5% for with and without permeates recycle. With enhanced TMP drops and turbulence, more pectin and sucrose molecules passed through membrane pores, resulting permeate TDS increase. With permeate recycle, retentate streams were diluted, so TDS value was decreased compared to without permeate recycle.

Table 4.6 Comparison of physiochemical properties of permeates at steady state with and without permeate recycle (turbulent)

Physicochemical property	Feed	Retentate	With permeate recycle			Without permeate recycle		
			TMP drops (kPa)			TMP drops (kPa)		
			414	552	690	414	552	690
TDS (mg/L)	140	218	85	89	94	107	109	117
Turbidity (NTU)	45	75	15.2	17.8	18.4	23.5	24.8	26
Clarity (% T_{660})	89	50.7	96.3	95.5	94	94.5	93.1	92.2
Viscosity (mPa.s)	2.12	2.56	1.29	1.34	1.35	1.40	1.44	1.48
AIS (g/L)	2	6.5	0.025	0.038	0.042	0.051	0.056	0.06
Density (g/cm^3)	1.10	1.18	1.01	1.01	1.01	1.05	1.05	1.05
Ionic conductivity (µS)	0.22	0.30	0.11	0.13	0.14	0.17	0.20	0.21
Sucrose (g/L)	90	96	77	72	70	74	72	70

Maximum TDS removal was observed at TMP drops of 414 kPa for both the cases. After clarification, turbidity was found to decrease. With increase of TMP drops, permeate sample turbidity increased due to passage of pectin molecules. With increase of TMP drops from 414 to 690 kPa, turbidity was increased from 15.2 to 18.4 NTU for with permeate recycle and 23.5 to 26 NTU for without permeate recycle. Permeate sample clarity was enhanced with removal of pectin from feed solution. For with and without permeate recycle improvements of clarity 9 and 7% were observed. Feed become haze in presence of pectin and sucrose, resulting turbidity increase. Maximum reduction of viscosity was observed at low TMP drops 414 kPa. 39.1 and 27% reduction of viscosity was observed for with and without permeate recycle. At 690 kPa, reductions of viscosity were 33.3 and 30.2% for with and without permeate recycle.

AIS followed the same trend as. Density was slightly decreased from 1.10 to 1.01 g/cm^3 and 1.05 g/cm^3 for with and without permeates recycle due to removal of pectin molecule. Ionic conductivity was decreased from 0.22 to 0.11 µS for with permeate recycle and for without permeate recycle change was marginal. Sucrose concentration in permeate sample was decreased from 90 to 77 g/L for with permeate recycle and 90 to 74 g/L for without permeate recycle.

With enhancement of turbulence permeate quality was decreased compared to laminar flow due to increase of pectin concentration in permeate sample from 0.020 to 0.025 g/L with permeate recycle and from 0.040 to 0.051 g/L for without permeate recycle at TMP drops of 414 kPa. Whereas, at 690 kPa, it increased from 0.030 to 0.042 g/L for with permeate recycle and from 0.055 to 0.060 mg/L for without permeate recycle. With enhancement of TMP drops from 414 to 690 kPa, TDS concentration in permeate sample was increased from 85 to 94 mg/L for with permeate recycle and from 107 to 117 mg/L for without permeate recycle at turbulent flow regime.

4.4.2 Summary

At turbulent flow, for with and without permeate recycle, synthetic juice were clarified through spiral wound ultrafiltration membrane module. Membrane performances such as, transient flux decline, VRF and total resistance were compared with laminar flow regime. The following conclusions were drawn from the present investigations:

- At turbulent flow, for without permeate recycle; transient flux was higher with short operating time compared to with permeate recycle. At turbulent flow, decline of permeates flux was lower compared to laminar flow profile.
- Total resistance was increased sharply in short operating time for without permeate recycle. In turbulent flow, resistance developed over membrane surface was lesser compared to laminar flow operating conditions.
- Due to increase of turbulence, shear induced diffusion model estimated flux values were best fitted within ±10% with the experimental flux data.
- At low TMP drops (414 kPa) studied herein, maximum improvements of physical properties were observed. Permeate qualities were degraded with the increase of TMP drops and turbulence due to increase of pectin concentration in permeate.

4.5 Comparison of Spiral Wound UF Membrane Performance at Laminar and Turbulent Flow Regime

In this section, spiral wound ultrafiltration membrane performance, such as, transient flux decline, volume reduction factor and total resistance for different operating conditions, for with and without permeate recycle at laminar flow results were compared with turbulent flow regime. The results were summarized in ***Table 4.7.***

Table 4.7 Comparison of results for with and without permeate recycle at laminar and turbulent flow regime

TMP drops (kPa)	Transient flux decline (%)				VRF				Total Resistance×10^{-13} (m^{-1})			
	With recycle		Without recycle		With recycle		Without recycle		With recycle		Without recycle	
	Laminar	Turbulent	Laminar	Turbulent	Laminar	Turbulent	Laminar	Turbulent	Laminar	Turbulent	Laminar	Turbulent
414	27.3	21.4	33.6	31.0	2.09	2.15	2.38	2.49	2.98	2.24	3.29	2.90
552	28.1	28.2	36.0	33.7	2.11	2.17	2.88	3.12	3.03	2.44	3.33	2.94
690	33.6	31.6	39.2	35.8	2.13	2.21	2.92	3.17	3.15	2.56	3.38	3.22

Laminar (Re: 1455); Turbulent (Re: 4001)

Transient Flux Decline

In laminar flow region, transient flux decline was 27.3 and 33.6%, respectively, for with and without permeate recycle at 414 kPa. Whereas, the decline in turbulent

flow regime was lower and was 21.4 and 31.6%, respectively. As Reynolds number was increased from 1455 to 4001, concentration polarization was reduced resulting higher decline in permeate flux values. With enhancement of TMP drops from 414 to 690 kPa, transient flux decline was found to increase from 21.4 to 31.6% at turbulent flow regime and similar type of observation was observed at laminar flow regime. With the increase of driving force, i.e., TMP drops, more solvents were passed through the membrane and thereby, increased the percentage flux decline.

Volume Reduction Factor (VRF)

Final VRF value was 2.09 and 2.38 for with and without permeate recycle at 414 kPa in laminar flow region. For turbulent flow regime, it was 2.15 to 2.49 for with and without permeate recycle, slightly higher than in laminar case. With increase of TMP drops from 414 to 690 kPa, for laminar flow region, VRF was raised from 2.09 to 2.13 and 2.38 to 2.92, for turbulent flow regime for with and without permeate recycle due to enhancement of driving force. With enhanced turbulence, mostly pectin particles were rejected by membrane surface. Due to rejection of pectin particles more solvents were passed through membrane pores resulting permeate rate and VRF rise. At 690 kPa TMP drops, for with permeate recycle VRF was raised from 2.13 to 2.21 and 2.928 to 3.17 for with and without permeate recycle. Similar observations were observed for other TMP drops (414 and 552 kPa).

Total Resistance

At 414 kPa in laminar flow region, total resistance at the end of experiment was 2.98×10^{13} and 3.29×10^{13} m^{-1} for with and without permeate recycle. It varied from

2.24×10^{13} and 2.9×10^{13} m^{-1} for with and without permeate recycle at turbulent flow regime. With TMP drops, more solute particles were convected towards membrane surface, resulting rise of total resistance. For example, at laminar flow regime, total resistance was raised from 2.98×10^{13} to 3.15×10^{13} m^{-1} (47 to 65%) and 3.29×10^{13} to 3.38×10^{13} m^{-1} (59.3 to 65.5%) for with and without permeate recycle. At turbulent flow regime, total resistance was raised from 2.24×10^{13} to 2.56×10^{13} m^{-1} (33.3 to 43.5%) and 2.90×10^{13} to 3.22×10^{13} m^{-1} (53.4 to 61%) for with and without permeate. With turbulence, solute deposition on membrane surface was reduced resulting decrease in total resistance from 2.98×10^{13} and 2.24×10^{13} m^{-1} (47 to 33.3%) for with permeate recycle at 414 kPa. Similar trends were observed for other TMP drops (552 and 690 kPa).

Estimation of Theoretical Flux

Based on diffusion of solute particles through membrane, various models such as, Brownian, shear induced and combined diffusion model were assumed to estimate the theoretical flux. At laminar flow regime, Brownian diffusion model estimated flux data were best fitted within ±10% of experimental flux data due to lower pectin particle size (< 0.1 µm) in permeate. With enhancement of turbulence, submicron size pectin particles were passed through membrane pores and appeared in permeate sample. Pectin particles were clustering in permeate sample. Due to clustering, pectin particle size was enhanced upto 2.5 µm and shear induced diffusion model predicted permeate flux values were best fitted with experimental flux (±10%).

4.6 Cleaning of Fouled Membranes

In this section, fouled spiral wound ultrafiltration during fruit juice clarification was cleaned with different cleaning agents. Cleaning performance was measured in terms of recovery of membrane permeability. Optimum cleaning agent dosages were also evaluated.

4.6.1 Effects of Cleaning Agent Type on Membrane Permeability Recovery

Fouling of membrane is generally defined as the deposition of solute particles on membrane surface, resulting decline in permeate flux and enhancement of membrane resistance. Removal of solute particles (pectin) on membrane surface was done either by physical or chemical methods. Fouled UF spiral wound membrane module was cleaned with three different techniques, such as, by circulating deionised water through the module; by using anionic surfactant, such as, SDS and by using a chelating agent, namely, EDTA. Pectins, also known as pectic polysaccharides, are rich in galacturonic acid. Several distinct polysaccharides have been identified and characterised within the pectic group. In low methoxyl pectins (<50% esterified), calcium ions are present in the gels at low pH (3-4.5). During cleaning, EDTA breaks the ionic bridges formed between calcium ions and the ionised carboxyl groups of the galacturonic acid of pectin resulting in enhanced efficiency. SDS cannot break the ionic bridge. Maximum operating time to perform the cleaning experiment was 20 min. A low TMP of 69 kPa was maintained during cleaning operation of fouled membrane modules using 9 lpm flow rate at 28±2°C temperature. Initial hydraulic permeability of compacted UF membrane was 3.1×10^{-11} m/Pa.s. Firstly, fouled spiral wound UF membrane module was cleaned with deionised water. The cleaning efficiency (%) was

measured in terms of recovery of permeability and was shown in **Figure 4.19.** Cleaning efficiency with deionised water was 61% and recovered membrane permeability was 1.89×10^{-11} m/Pa.s. Hence, deionised water was not enough to recover the initial membrane permeability. It indicated that some of the irreversible fouling layers were largely available on membrane surface. SDS, an anionic surfactant, was used as another cleaning agent for recovering membrane permeability after fouling. 75% cleaning efficiency was observed when 1 mM SDS (pH=11) was used as recovered membrane permeability was 2.33×10^{-11} m/Pa.s in a separate experiment. Here, some amounts of foulant were there after cleaning with SDS. When fouled was cleaned with with 4 mM EDTA (pH=11) solution, membrane permeability was recovered as 2.82×10^{-11} m/Pa.s with 91% cleaning efficiency. So EDTA was more favourable cleaning agent compared to SDS and deionised water to increase the cleaning efficiency and membrane permeability. During cleaning experiments, SDS and EDTA solution reacted with pectin molecules to reduce the intermolecular adhesion force and pectin molecules ultimately dissolved in SDS and EDTA solutions [36].

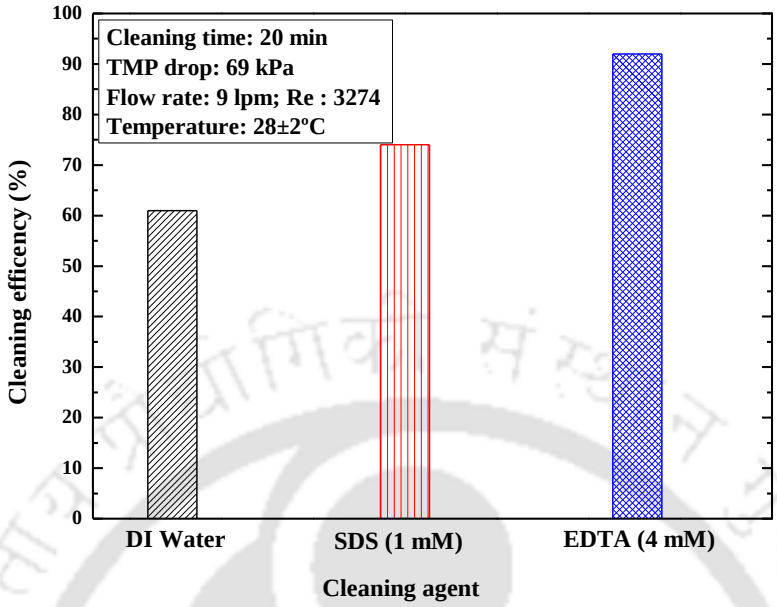

Figure 4.19. Variation of cleaning efficiency with cleaning agent type.

4.6.2 Optimization Study of Cleaning Dose

To optimize the dose of SDS (pH=11) and EDTA (pH=11) in terms of original flux recovery SDS concentration was varied from 0.1 to 1 mM whereas, EDTA concentration was varied from 1 to 4 mM. Pure water flux at 69 kPa was 21.39×10^{-6} $m^3/m^2.s$ and after clarification of synthetic juice membrane flux was reduced to 5.2×10^{-6} $m^3/m^2.s$. The variation of permeate flux values with SDS concentration was shown in **Figure 4.20(a)**. It was observed from the figure that with the increase of SDS dose, permeate flux was found to increase. When SDS concentration was increased from 0.1 to 0.2 mM, permeate flux recovery was increased from 46 to 55%. 74% flux recovery was observed when SDS concentration was further increased to 0.5 mM. Beyond this concentration, recovery of permeate flux was marginal. Hence, 0.5 mM SDS concentration was taken as optimum surfactant dose.

With EDTA, the recovery of permeate flux was increased from 5.2×10^{-6} $m^3/m^2.s$ to 16.54×10^{-6} $m^3/m^2.s$ when dose was 1 mM. The results were shown in **Figure 4.20(b)**. Like SDS dose, further increase in permeate flux was observed with increase in EDTA dose. When EDTA dose was 3 mM, the recovery of flux was 92%. Further increase in EDTA dose to 4 mM could not increase the permeate flux recovery. So, 3 mM EDTA was considered as the optimum dose. All the experiments were performed two times.

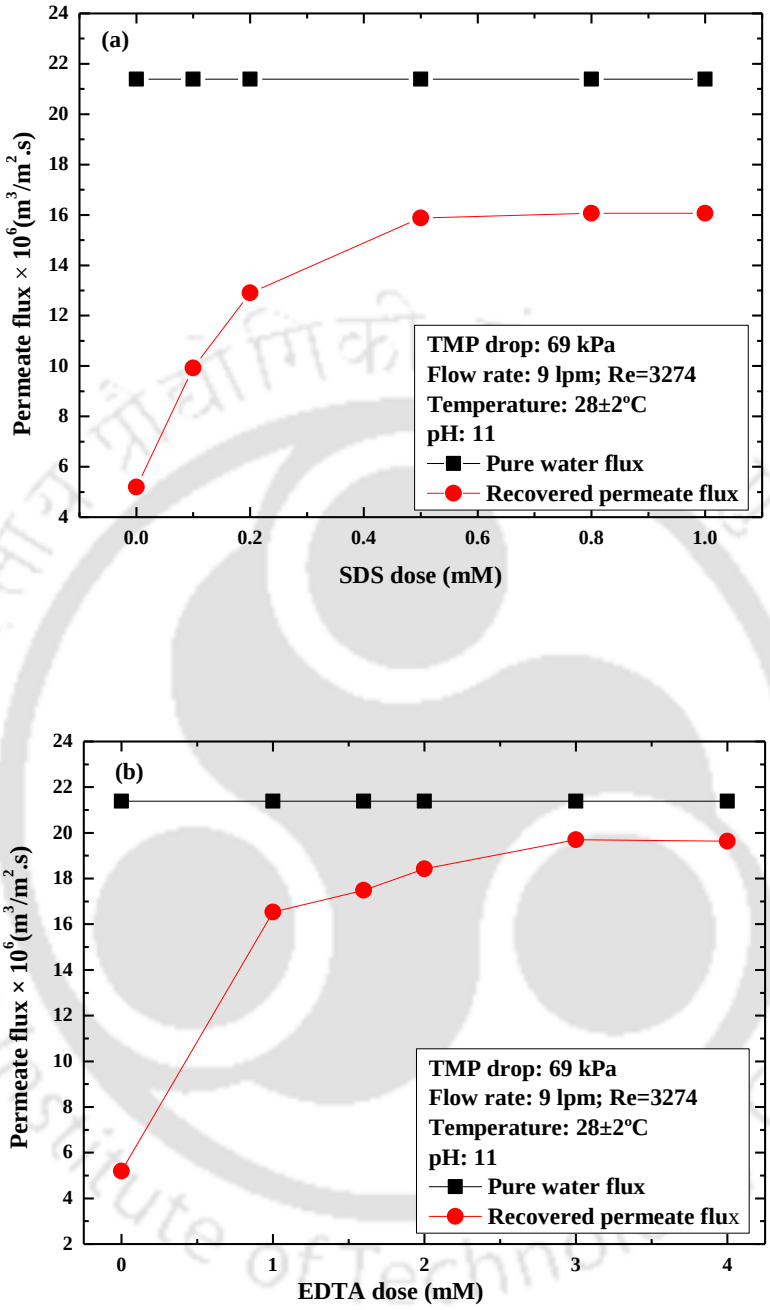

Figure 4.20. Optimization of SDS and EDTA concentrations to recover the original permeate flux.

4.6.3 Summary

- Circulating deionized water and cleaning agent SDS were not enough to remove the entire solute particles from membrane surface. Maximum cleaning efficiency of 91% was observed with 3 mM EDTA Solution.
- Considering quality of the permeate, permeate flow rate, fouling resistance and production rate, with permeate recycle operation is selected as the efficient mode of operation for the clarification of synthetic juice.

Chapter 5

FINAL CONCLUSIONS

Chapter 5

FINAL CONCLUSIONS

Applicability of various membrane based separation processes is attempted in this thesis in context of oily wastewater treatment, separation of coal-solvent mixture and fruit juice clarification. Polymer and ceramic membranes are used to remove the impurities.

- During cross flow microfiltration of oily wastewater, permeate quality was degraded with TMP drops due to passage of oil particles in permeate side and improved with increase of cross flow velocity due to high shear stress. Oil concentration in the permeate sample was reduced from 192 to 4.5 mg/L and COD from 2000 to 225 mg/L. Recovered water from oil-water emulsion was within the permissible limit and can be reused for domestic and industrial purpose. Various diffusion models, namely, concentration polarization, Brownian diffusion, shear induced diffusion models were used to calculate theoretical flux values. A combined model based on Brownian and shear induced diffusion was developed. Proposed combined diffusion model estimated flux values were more closer (±10%) within experimental flux values for both laminar and turbulent flow regimes.

Chapter 5

- For separating coal-solvent mixture, a defect free ceramic membrane with pore size of 0.8 µm was successfully fabricated from inorganic constituents to recover organic solvent and coke from coal-solvent mixture. Membrane sintered at 1000°C had good chemical stability both in acidic (pH: 2) and alkaline (pH: 12) solution, verified by EDX analysis. After extraction, extract was passed through membrane filtration cell and organic solvent was recovered from permeate side whereas coke parts were deposited on membrane surface. Maximum solvent recovery (%) was found at optimum dose of coal/solvent ratio (w/v) of 1:9 and 1:10, respectively. During membrane experiment, permeate rate decreased and total resistance was found to rise with operating time due to the deposition of coke on membrane surface. Recovered organic solvent from permeate side was again utilized for next stage extraction experiment as it was free from coal particles, confirmed by FTIR analysis.
- To reduce fabrication cost of ceramic membrane, steel industry waste IOS was utilized with inorganic materials. The low cost IOS membrane was used to recover organic solvent from coal-solvent mixture. Mixed organic solvents had ability to improve the extraction yield during coal extraction. Recovered coke after membrane experiment had high carbon, low sulfur and high calorific value. NMP had maximum cleaning efficiency (%) to remove the foulant from membrane surface. Preliminary cost of IOS ceramic membrane was around $\$79.89/m^2$.

- During clarification of fruit juice, operating cost of juice pretreatment through packed bed was lowest compared to other pretreatment methods, namely,

centrifugation, fining agent addition and centrifugation combined with fining agents addition. Maximum improvement of physicochemical properties was observed with centrifugation combined with fining agents addition, but its pretreatment cost was highest. During synthetic juice clarification through spiral wound UF membrane, permeate quality of with permeate recycle had better compared to without permeate recycle. With TMP drops, permeate quality were degraded in both operating conditions, with and without permeate recycle. At laminar flow regime, Brownian diffusion model estimated flux data were best fitted with experimental flux data due to lower pectin particle size in permeate. In turbulent flow regime, due to clustering, pectin particle size was enhanced and shear induced diffusion model predicted permeate flux values were best fitted with experimental flux. Fouled spiral wound UF membrane was cleaned with different cleaning agents, such as deionized water, SDS and EDTA. 3 mM EDTA had maximum ability to recover 91% original permeability after fouling.

Perspectives of Future Work

Study on low cost cleaning for different fouled membranes, color removal from recovered organic solvent during coal extraction, efficacy of IOS membrane in other applications and removal of bitterness from clarified juice during storage are the perspectives of future work.

REFERENCES

REFERENCES

[1] C.C. Striemer, T.R. Gaborski, J.L. McGrath, P.M. Fauchet, Charge- and size-based separation of macromolecules using ultrathin silicon membranes, Nature, 445 (2007), 749-753.

[2] S. Kara, E. Gurbulak, M. Eyvaz, E. Yuksel, Treatment of winery wastewater by electrocoagulation process, Desalination and Water Treatment, 51 (2013), 5421-5429.

[3] M. Kotti, N. Dammak, I. Ksentini, L. B. Mansour, Effects of impurities on oxygen transfer rate in the electroflotation process, Indian Journal of Chemical Technology, 16 (2009), 513-518.

[4] Z. Berk, Food Process Engineering and Technology, Elsevier, First Edition 2009.

[5] O.E. Fayemi, A.S. Ogunlaja, P.F.M. Kempgens, E. Antunes, N. Torto, T. Nyokong, Z.R. Tshentu, Adsorption and separation of platinum and palladium by polyamine functionalized polystyrene-based beads and nanofibers, Minerals Engineering, 53 (2013), 256-265.

[6] S. Ramaswamy, H. Huang, B. Ramarao, Separation and Purification Technologies in Biorefineries, John wiley publication, First Edition 2013.

[7] Y.A.N.Q. Xuan, L.X. Hai, W.Z. Xing, W.J. Xi, G.H. Jun, H.Q. Yang, P.W. Jie, W.X. Fei, Extraction of lithium from lepidolite using chlorination roasting water leaching process, Transactions of Nonferrous Metals Society of China, 22 (2012), 1753-1759.

[8] A. Behnamfard, M.M. Salarirad, F. Veglio, Process development for recovery of copper and precious metals from waste printed circuit boards with emphasize on palladium and gold leaching and precipitation, Waste Management, 33 (2013), 2354-2363.

[9] E. Temmel, S. Wloch, U. Muller, D. Grawe, R. Eilers, H. Lorenz, A.S. Morgenstern, Separation of systems forming solid solutions using counter-current crystallization, Chemical Engineering Science, 104 (2013), 662-673.

References

[10] L. Nilsson, E.U. Schlunder, Contact drying combined with membrane separation: Dewatering rates of porous spheres wetted with four different liquid mixtures, Chemical Engineering and Processing, 37 (1998), 317-330.

[11] L. Deng, Y. Li, Z. Chen, G. Liu, H. Yang, Separation of swine slurry into different concentration fractions and its influence on biogas fermentation, Applied Energy, 114 (2014), 504-511.

[12] A. Malovanyy, H. Sakalova, Y. Yatchyshyn, E. Plaza, M. Malovanyy, Concentration of ammonium from municipal wastewater using ion exchange process, Desalination, 329 (2013), 93-102.

[13] J. Sun, D. Cui, X. Chen, L. Zhang, H. Cai, H. Li, Fabrication and characterization of microelectromechanical systems-based gas chromatography column with embedded micro-posts for separation of environmental carcinogens, Journal of Chromatography, 1291 (2013), 122-128.

[14] S. Khan, T.G. Kazi, N.F. Kolachi, J.A. Baig, H.I. Afridi, F. Shah, A simple separation/preconcentration method for the determination of aluminum in drinking water and biological sample, Desalination, 281 (2011), 215-220.

[15] Market Report: Global Membrane Technology Market, Acmite Market Intelligence, 2013, pp.21.

[16] M. Mulder, Basic principles of membrane technology, Springer, Second Edition, 2007.

[17] B.K. Dutta, Principles of Mass Transfer and Separation Processes, PHI Learning Private Limited, Second Edition, 2009.

[18] M. Cheryan, Ultrafiltration and Microfiltration Handbook, CRC Press, Second Edition, 2000.

[19] H. Bruschke, Industrial application of membrane separation processes, Pure and Applied Chemistry, 67 (1995), 993-1002.

[20] F. Macedonio, L. Katzir, N. Geisma, S. Simone, E. Drioli, J. Gilron, Wind-Aided Intensified eVaporation (WAIV) and Membrane Crystallizer (MCr) integrated brackish water desalination process: Advantages and drawbacks, Desalination, 273 (2011), 127-135.

[21] J.L. Acero, F.J. Benitez, F.J. Real, C. Garcia, Removal of phenyl-urea herbicides in natural waters by UF membranes: Permeate flux, analysis of resistances and rejection coefficients, Separation and Purification Technology, 65 (2009), 322-330.

[22] R.W. Field, D. Wu, J.A. Howell, B.B. Gupta, Critical flux concept for microfiltration fouling, Journal of Membrane Science, 100 (1995), 259-272.

[23] A. Bottino, C. Capannelli, A.D. Borghi, M. Colombino, O. Conio, Water treatment for drinking purpose: ceramic microfiltration application, Desalination, 141 (2001), 75-79.

[24] B.V. Bruggen, G. Cornelis, C. Vandecasteele, I. Devreese, Fouling of nanofiltration and ultrafiltration membranes applied for wastewater regeneration in the textile industry, Desalination, 175 (2005), 111-119.

[25] M.R. Garud, V.S. Kore, S.G. Kulkarni, A Short Review on Process and Applications of Reverse Osmosis, Universal Journal of Environmental Research and Technology, 3 (2011), 233-238.

[26] L.K. Wang, J.P. Chen, Y.T. Hung, N.K. Shammas, Membrane and Desalination Technologies, Humana Press, First Edition, 2011.

[27] Z.F Cui, H.S Muralidhara, Membrane Technology: A Practical Guide to Membrane Technology and Application in Food and Bioprocessing, Elsevier, First Edition, 2010.

[28] B.S. Lalia, V. Kochkodan, R. Hashaikeh, N. Hilal, A review on membrane fabrication: Structure, properties and performance relationship, Desalination, 326 (2013), 77-95.

[29] O. San, C. Ozgur, Fabrication of glassy ceramic membrane filters for filtration of spring water with clogging phenomena, Journal of Membrane Science, 305 (2007), 169-175.

[30] Z.Y. Jun, W.K. Fen, W.Z. Jun, Z. Liang, L.S. Shen, Fouling and cleaning of membrane-a literature review, Journal of Environmental Sciences, 12 (2000), 241-251.

[31] A. Broeckmann, J. Busch, T. Wintgens, W. Marquardt, Modeling of pore blocking and cake layer formation in membrane filtration for wastewater treatment, Desalination, 189 (2006), 97-109.

References

[32] Y.S. Polyakova, A.L. Zydney, Ultrafiltration membrane performance: Effects of pore blockage/constriction, Journal of Membrane Science, 434 (2013), 106-120.

[33] P. Bacchin, P. Aimar, V. Sanchez, Model for Colloidal Fouling of Membranes, American Institute of Chemical Engineers Journal, 41(1995), 368-376.

[34] G. Crozes, C. Anselme, J. Mallevialle, Effect of Adsorption of Organic Matter on Fouling of Ultrafiltration Membranes, Journal of Membrane Science, 84 (1993), 61-77.

[35] L. Dudley, Membrane Autopsies for Reversing Fouling in Reverse Osmosis, Membrane Technology, 95 (1998), 9-12.

[36] W.S. Ang, A. Tiraferri, K.L. Chen, M. Elimelech, Fouling and cleaning of RO membranes fouled by mixtures of organic foulants simulating wastewater effluent, Journal of Membrane Science, 376 (2011), 196-206.

[37] P. Lipp, C.H. Lee, A.G. Fane, C.J.D. Fell, A fundamental study of the ultrafiltration of oil-water emulsions, Journal of Membrane Science, 36 (1998), 161-177.

[38] U. Daiminger, W. Nitsch, P. Plucinski, S. Hoffmann, Novel techniques for oil water separation, Journal of Membrane Science, 99 (1995), 197-203.

[39] Y. Zhao, Y. Tan, F.S. Wong, A.G. Fane, N. Xu, Formation of dynamic membranes for oily water separation by crossflow filtration, Separation and Purification Technology, 44 (2005), 212-220.

[40] M. Gryta, K. Karakulski, The application of membrane distillation for the concentration of oil-water emulsions, Desalination, 121 (1999), 23-29.

[41] S. Elmaleh, N. Ghaffor, Cross-flow ultrafiltration of hydrocarbon and biological solid mixed suspensions, Journal of Membrane Science, 118 (1996), 111-120.

[42] D. Sun, X. Duan, W.L. Zhou, D. Zhou, Demulsification of water-in-oil emulsion by using porous glass membrane, Journal of Membrane Science, 146 (1998), 65-72.

[43] J.A. Zeevalkink, J.J. Brunsmann, Oil removal from water in parallel plate gravity-type separators, Water Research, 17 (1983), 365-373.

[44] A. Cambiella, J.M. Benito, C. Pazos, J. Coca, Centrifugal separation efficiency in the treatment of waste emulsified oils, Chemical Engineering Research and Design, 84 (2006), 69-76.

[45] A. Cambiella, E. Ortea, G. Rios, J.M. Benito, C. Pazos, J. Coca, Treatment of oil-in-water emulsions: Performance of a sawdust bed filter, Journal of Hazardous Materials, 131 (2006), 195-199.

[46] T.S. Kristiansen, A. Lewis, P.S. Daling, A.B. Nordvik, Heat and chemical treatment of mechanically recovered w/o emulsions, Spill Science and Technology Bulletin, 2 (1995), 133-141.

[47] R.M. Bande, B. Prasad, I.M. Mishra, K.L. Wasewar, Oil field effluent water treatment for safe disposal by electroflotation, Chemical Engineering Journal, 137 (2008), 503-509.

[48] J. Cui, X. Zhang, H. Liu, K.L. Yeung, Preparation and application of zeolite/ceramic microfiltration membranes for treatment of oil contaminated water, Journal of Membrane Science, 325 (2008), 420-426.

[49] S. Deng, S. Sourirajan, K. Chan, B. Farnand, T. Okada, T. Matsuura, Dehydration of oil-water emulsion by pervaporation using porous hydrophilic membranes, Journal of Colloid and Interface Science, 141 (1991), 218-225.

[50] T. Mohammadi, M. Kazemimoghadam, M. Saadabadi, Modeling of membrane fouling and flux decline in reverse osmosis during separation of oil in water emulsions, Desalination, 157 (2003), 369-375.

[51] J. Mueller, Y. Cen, R.H. Davis, Crossflow microfiltration of oily water, Journal of Membrane Science, 129 (1997), 221-235.

[52] H. Ohya, J.J. Kim, A. Chinen, M. Aihara, S.I. Semenova, Y. Negishi, O. Mori, M. Yasuda, Effects of pore size on separation mechanisms of microfiltration of oily water using porous glass tubular membrane, Journal of Membrane Science, 145 (1998), 1-14.

[53] M. Bodzek, K. Konieczny, The use of ultrafiltration membranes made of various polymers in the treatment of oil-emulsion wastewater, Waste Management and Research, 12 (1992), 75-84.

[54] K. Karakulski, A. Kozlowski, A.W. Morawski, Purification of oily wastewater by Ultrafiltration, Separation Technology, 5 (1995), 197-205.

[55] M. Heran, S. Elmaleh, Prediction of cross-flow microfiltration through an inorganic tubular membrane with high frequency retofiltration, Chemical Engineering Science, 56 (2001), 3075-3082.

References

[56] K. Scott, I.F. Convey, A. Adhamy, Application of crossflow microfiltration to emulsion sepration in extraction process, Journal of Membrane Science, 72 (1992), 245-257.

[57] M. Cheryan, Food and beverage industry applications, in R.D. Noble, S.A. Stern (Eds.), Membrane Separation Technology Principles and Applications, Elsevier, The Netherlands, (1995).

[58] J. Hermia, Constant pressure blocking filtration laws application to power-law non-newtonian fluids, Chemical Engineering Research and Design, 60 (1982), 183-187.

[59] A.S. Jonsson, B. Jonsson, H. Byhlin, A concentration polarization model for the ultrafiltration of nonionic surfactants, Journal of Colloid and Interface Science, 304 (2006), 191-199.

[60] W.S.W. Ho, K.K. Sirkar, Membrane Handbook, Kluwer Academic Publisher, First Edition, 2001.

[61] P. Pospisil, R. Wakeman, I. Hodgson, Shear stress-based modelling of steady state permeate flux in microfiltration enhanced by two-phase flows, Journal of Chemical Engineering, 97 (2004), 257-263.

[62] S. Chellam, Artificial neural network model for transient crossflow microfiltration of polydispersed suspensions, Journal of Membrane Science, 258 (2005), 35-42

[63] C. Aydiner , I. Demir, E. Yildiz, Modeling of flux decline in crossflow microfiltration using neural networks the case of phosphate removal, Journal of Membrane Science, 248 (2005), 53-62

[64] S. Kim, H. Park, Effective diameter for shear-induced diffusion for characterizing cake formation in crossflow microfiltration at polydisperse conditions, Journal of Environmental Engineering, 131 (2005), 865-873.

[65] J. Kromkamp, A. Bastiaanse, J. Swarts, A suspension flow model for hydrodynamics and concentration polarisation in crossflow microfiltration, Journal of Membrane Science, 253 (2005), 67-79.

[66] A. Malack, A. Bukhari, N. Abuzaid, Crossflow microfiltration of electrocoagulated kaolin suspension fouling mechanism, Journal of Membrane Science, 243 (2004), 143-153.

[67] W.F Blatt, A. David, L. Nelson, Solute polarisation and cake formation in membrane ultrafiltration Causes, consequences and control techniques, Membrane Science and Technology, Plenum Press, New York, (1970).

[68] A.L. Zydney, C.K. Colton, A concentration polarisation model for the filtrate flux in crossflow microfiltration of particulate suspensions, Chemical Engineering Communications, 47 (1986), 1-21.

[69] D.T. Leighton, A. Acrivos, Measurement of the shear induced coefficient of self-diffusion in concentrated suspensions of spheres, Journal of Fluid Mechanics, 177 (1987), 109-131.

[70] R.H. Davis, J.D. Sherwood, A similarity solution for crossflow microfiltration, Chemical Engineering Science, 45 (1990), 3203-3209.

[71] M. Stefanova, K. Markova, S. Marinov, B.R.T. Simoneit, Molecular indicators for coal-forming vegetation of the Miocene Chukurovo lignite Bulgaria, Fuel, 84 (2005), 1830-1838.

[72] Y. Li, R. Michels, L. Mansuy, S. Fleck, P. Faure, Comparison of pressurized liquid extraction with classical solvent extraction and microwave-assisted extraction application to the investigation of the artificial maturation of Mahakam coal, Fuel, 81 (2002), 747-755.

[73] F. Czechowski, M. Stolarski, B.R.T. Simoneit, Supercritical fluid extracts from brown coal lithotypes and their group components molecular composition of non-polar compounds, Fuel, 81 (2002), 1933-1944.

[74] A.B. Waugh, K.M. Bowling, Removal of mineral matter from bituminous coals by aqueous chemical leaching, Fuel Processing Technology, 9 (1984), 217-233.

[75] R.T. Yang, S.K. Das, B.M.C. Tsai, Coal demineralization using sodiumhydroxide and acid solution, Fuel, 64 (1985), 735-742.

[76] J. Wang, A. Tomita, Removal of mineral matter from Australian coals by $Ca(OH)_2$/HCl leaching, Fuel, 77 (1998), 1747-1753.

[77] S. Meffe, A. Perkson, O. Trass, Coal benefication and organic sulphur removal, Fuel, 75 (1996) 25-30.

[78] B.V. Bodengom, J.A.R.V. Veen, G.M.M.V. Kessel, M.W.A.S. Nijssen, H.C.M. Stuiver, The action of solvents on coal at low temperatures: 2. Medium-and high-rank coals, Fuel, 64 (1985), 59-63.

References

[79] N. Kashimura, T. Takanohashi, K. Masaki, T. Shishido, S. Sato, A. Matsumura, I. Saito, Relationship between thermal extraction yield and oxygen-containing functional groups, Energy & Fuels, 20 (2006), 2088-2092.

[80] S. Mishra, D.K. Sharma, Solvent extraction and extractive disintegration of coal in anthrancene oil, Fuel, 69 (1999), 1377-1380.

[81] M. Iino, T. Takanohashi, S. Obara, H. Tsueta, Y. Sanokawa, Characterization of the extracts and residues fromCS_2-N-methyl-2-pyrrolidinonemixed solvent extraction, Fuel, 68 (1989), 1588-1593.

[82] S. Jana, M.K. Purkait, K. Mohanty, Preparation and characterization of low-cost ceramic microfiltration membranes for the removal of chromate from aqueous solutions, Applied Clay Science, 47 (2010), 317-324.

[83] R.D. Colle, C.A. Fortulan, S.R. Fontes, Manufacture of ceramic membranes for application in demulsification process for cross-flow microfiltration, Desalination, 245 (2009), 527-532.

[84] B.K. Nandi, R. Uppaluri, M.K. Purkait, Preparation and characterization of low cost ceramic membranes for microfiltration applications, Applied Clay Science, 42 (2008), 102-110.

[85] Y. Dong, S. Chen, X. Zhang, J. Yang, X. Liu, G. Meng, Fabrication and characterization of low cost tubular mineral-based ceramic membranes for micro-filtration from natural zeolite, Journal of Membrane Science, 281 (2006), 592-599.

[86] P. Rai, G.C. Majumdar, S. Das Gupta, S. De, Effect of various pretreatment methods on permeate flux and quality during ultrafiltration of mosambi juice, Journal of Food Engineering, 78 (2007), 561-568.

[87] V. Gokmen, N. Artık, J. Acar, N. Kahraman, E. Poyrazoglu, Effects of various clarification treatments on patulin, phenolic compound and organic acid compositions of apple juice, European Food Research and Technology, 213 (2001), 194-199.

[88] D. Belhocine, H. Grib, D. Abdessmed, Y. Comeau, N. Mameri, Optimization of plasma proteins concentration by ultrafiltration, Journal of Membrane Science, 142 (1998), 159-171.

[89] G. Daufin, J.P. Escudier, H. Carrère, S. Bérot, L. Fillaudeau, M. Decloux, Recent and emerging applications of membrane processes in the food and dairy industry. Food and Bioproducts Processing, 79 (2001), 89-102.

[90] P. Onsekizoglu, K.S. Bahceci, M.J. Acar, Clarification and the concentration of apple juice using membrane processes: A comparative quality assessment, Journal of Membrane Science, 352 (2010), 160-165.

[91] K.B. Petrotos, P.C. Quantick, H. Petropakis, Direct osmotic concentration of tomato juice in tubular membrane module configuration. II. The effect of using clarified tomato juice on the process performance, Journal of Membrane Science, 160 (1999), 171-177.

[92] F. Tasselli, A. Cassano, E. Drioli, Ultrafiltration of kiwifruit juice using modified poly(ether ether ketone) hollow fibre membranes, Separation and Purification Technology, 57 (2007), 94-102.

[93] D. Saura, N. Marti, M. Valero, E. González, A. Carbonell, J. Laencina, Separation of aromatics compounds during the clarification of lemon juice by cross-flow filtration, Industrial Crops and Products, 36 (2012), 543-548.

[94] A.M. Ghosh, M. Balakrishnan, M. Dua, J.J. Bhagat, Ultrafiltration of sugarcane juice with spiral wound modules: on-site pilot trials, Journal of Membrane Science, 174 (2000), 205-216.

[95] N.A. Bastaki, A. Abbas, Permeate recycle to improve the performance of a spiral-wound RO plant, Desalination, 158 (2003), 119-126.

[96] F. Li, W. Meindersma, A.B. Haan, T. Reith, Optimization of commercial net spacers in spiral wound membrane modules, Journal of Membrane Science, 208 (2002), 289-302.

[97] M.F.A. Goosen, S.S. Sablani, H.A. Hinai, S.A. Obeidani, R.A. Belushi, D. Jackson, Fouling of reverse osmosis and ultrafiltration membranes: a critical review, Separation Science and Technology, 39 (2005), 2261-2297.

[98] D. Pepper, RO for improved products in the food and chemical industries and water treatment, Desalination, 77 (1990), 55-71.

[99] Z.R. Yu, B.H. Chiang, L.S. Hwang, Retention of passion fruit juice compounds by ultrafiltration, Journal of Food Science, 51 (1986), 841-844.

References

[100] P. Rai, G.C. Majumdar, S.D. Gupta, S. De, Modeling the performance of batch ultrafiltration of synthetic fruit juice and mosambi juice using artificial neural network, Journal of Food Engineering, 71 (2005), 273-281.

[101] J.P.S.G. Crespo, M.J. Moura, J.S. Almeida, M.J.T. Carrondo, Ultrafiltration membrane cell recycle for continuous culture of Propionibacterium, Journal of Membrane Science, 61 (1991), 303-314.

[102] A.I. Vogel, Textbook of practical organic chemistry, Longmans, London, second Edition, 1970.

[103] F.S. Manning, R.E. Thompson, Oil field processing of petroleum, Crude Oil Pennwell Corp Tulsa Oklahoma, First Edition, 1995.

[104] J.C. Chen, Q. Li, M. Elimelech, In situ monitoring techniques for concentration polarization and fouling phenomena in membrane filtration, Advances in Colloid and Interface Science, 107 (2004), 83-108.

[105] M. Belkacem, M. Bahlouli, A. Mraoui, K. Bensadok, Treatment of oil-water emulsion by ultrafiltration: A numerical approach, Desalination, 206 (2007), 433-439.

[106] X. Hu, E.B. Molnar, Study of modeling transmembrane pressure and gel resistance in ultrafiltration of oily emulsion, Desalination, 163 (2004), 355-360.

[107] G. Belfort, R.H. Davis, A.L. Zydney, The behaviour of suspensions and macromolecular solutions in crossflow microfiltration, Journal of Membrane Science, 96 (1994), 1-58.

[108] J. Kromkamp, M.V. Domselaar, K. Schoren, R.V. Sman, R. Boom, Shear-induced diffusion model for microfiltration of polydisperse suspension, Desalination, 146 (2002), 63-68.

[109] J. Kim, F.A. Digiano, Fouling models for low-pressure membrane systems, Separation and Purification Technology, 68 (2009), 293-304.

[110] J.M. Pope, S. Yao, A.G. Fane, Quantitative measurements of the concentration polarisation layer thickness in membrane filtration of oil-water emulsions using NMR micro-imaging, Journal of Membrane Science, 118 (1996), 247-257.

[111] A. B. Nordvik, J.L. Simmons, K.R. Bitting, A. Lewis, T.S. Kristiansen, Oil and water separation in marine oil spill clean-up operations, Spill Science and Technology Bulletin, 3 (1996), 107-122.

[112] E. Blomberg, C.M. Claeson, Oil spill clean-up technologies for rivers, ports and sheltered waters. Part I the hydrodynamic circus, Spill Science and Technology Bulletin, 4 (1997), 45-53.

[113] B. Chakrabarty, A.K. Ghoshal, M.K. Purkait, SEM analysis and gas permeability test to characterize polysulfone membrane prepared with polyethylene glycol as additive, Journal of Colloid and Interface Science, 320 (2008), 245-253.

[114] S.E. Klein, F.F. Holland, A. Donnaud, A. Lebeouf, K. Eberle, Diffusive and hydraulic permeabilities of commercially available cellulosic hemodialysis films and hollow fibers, Journal of Membrane Science, 2 (1977), 349-364.

[115] F. Shojai, T.A. Mantyla, Chemical stability of yttria doped zirconia membranes in acid and basic aqueous solutions: chemical properties, effect of annealing and ageing time, Ceramics International, 27 (2001), 299-307.

[116] Standard practice for proximate analysis of coal and coke by ASTM D3172-07 method.

[117] Standard Practice for Ultimate Analysis of Coal and Coke by ASTM D3176-09 methods.

[118] G. Pugazhenthi, A. Kumar, Enzyme membrane reactor for hydrolysis of olive oil using lipase immobilized on modified PMMA composite membrane, Journal of Membrane Science, 228 (2004), 187-197.

[119] N. Saffaj, S.A. Younssi, A. Albizane, A. Messouadi, M. Bouhria, M. Persin, M. Cretin, A. Larbot, Preparation and characterization of ultrafiltration membranes for toxic removal from wastewater, Desalination, 168 (2004), 259-263.

[120] A.A. Christy, Y.Z. Liang, O.M. Kvalheim, On-line pyrolysis of asphaltenes and kerogen studied by diffuse reflectance Fourier transform infrared spectroscopy, Fuel, 71 (1992), 125-127.

[121] M.F. Cai, R.B. Smart, Quantitative analysis of N-Methyl-2-pyrrolidinone in coal extracts by TGA-FTIR, Energy & Fuels, 7 (1993), 52-56.

[122] A. Krzton, D. Cagniant, R. Gruber, J. Pajak, F. Fortin, J.N. Rouzaud, Application of Fourier self-deconvolution to the FTIR. Characterization of coals and their N-methyl 2-pyrrolidinone extraction products, Fuel, 74 (1995), 217-225.

References

[123] B.D. Bhide, S.A. Stern, A new evaluation of membrane processes for the oxygen-enrichment of air. II. Effects of economic parameters and membrane properties, Journal of Membrane Science, 62 (1991), 37-58.

[124] W.J. Koros, R. Mahajan, Pushing the limits on possibilities for large scale gas separation: which strategies?, Journal of Membrane Science, 175 (2000), 181-196.

[125] M.A. Amerine, H.W. Berg, W.V. Cruess, The technology of wine making, AVI Publishing Company Westport, Third Edition, 1976.

[126] P.E. Nelson, D.K. Tressler, Fruit and vegetable juice processing technology, AVI Publishing Company Westport, Third Edition, 1980.

[127] V. Gokmen, O. Cetinkaya, Effect of pretreatment with gelatin and bentonite on permeate flux and fouling layer resistance during apple juice ultrafiltration, Journal of Food Engineering, 80 (2007), 300-305.

[128] N. Jacob, R.K. Sukumaran, P. Prema, Optimization of enzymatic clarification of sapodilla juice: A statistical perspective, Applied Biochemistry and Biotechnology, 151 (2008), 353-363.

[129] A.F.G. Bailey, A.M. Barbe, P.A. Hogan, R.A. Johnson, J. Sheng, The effect of ultrafiltration on the subsequent concentration of grape juice by osmotic distillation, Journal of Membrane Science, 164 (2000), 195-204.

[130] Z.J. Hua, W.U. Xiong, S.Z. Qiang, Viscous flow properties and viscosity average molecular mass of orange peel pectin. Journal of Central South University of Technology, 15 (2008), 520-524.

[131] B.K. Nandi, B. Das, R. Uppaluri, M.K. Purkait, Microfiltration of mosambi juice using low cost ceramic membrane, Journal of Food Engineering, 95 (2009), 597-605.

[132] H.N. Sin, S. Yusof, A.S.S. Hamid, A.R. Rahman, Optimization of enzymatic clarification of sapodilla juice using response surface methodology, Journal of Food Engineering, 73 (2006), 313-319.

[133] E. Sentandreu, C.M. Gurrea, N. Betoret, L.J. Navarro, Changes in orange juice characteristics due to homogenization and centrifugation, Journal of Food Engineering, 105 (2011), 241-245.

[134] P.D. Gurak, L.M.C. Cabral, M.H.M.R. Leao, V.M. Matta, S.P. Freitas, Quality evaluation of grape juice concentrated by reverse osmosis, Journal of Food Engineering, 96 (2010), 421-426.

[135] C. Das, P. Patel, S. De, S.D. Gupta, Treatment of tanning effluent using nanofiltration followed by reverse osmosis, Separation and Purification Technology, 50 (2006), 291-299.

[136] K.S. Youn, J.H. Hong, D.H. Bae, S.J. Kim, S.D. Kim, Effective clarifying process of reconstituted apple juice using membrane filtration with filter-aid pretreatment, Journal of Membrane Science, 228 (2004), 179-186.

[137] A. Yokozeki, Osmotic pressures studied using a simple equation of state and its applications, Applied Energy, 83 (2006), 15-41.

[138] S. De, Novel Separation Processes (Web) Module 3: Membrane Based Separation Processes, National programme on technology enhanced learning (NPTEL), 2012, pp. 75-120 (http://nptel.iitm.ac.in/courses/103105060/ Sde_pdf/Module-3.pdf) Accessed on 03.12.2013.

[139] S. De, P.K. Bhattacharya, Prediction of mass transfer coefficient with suction in the application of reverse osmosis and ultrafiltration, Journal of Membrane Science, 128 (1997), 119-131.

[140] V. Singh, M.K. Purkait, C. Das, Cross flow microfiltration of industrial oily wastewater: experimental and theoretical consideration, Separation Science and Technology, 46 (2011), 1213-1223.

[141] V. Singh, P.K. Jain, C. Das, Performance of spiral wound ultrafiltration membrane module for with and without permeate recycle: Experimental and theoretical consideration, Desalination, 322 (2013), 94-103.

[142] C. Fersi, M. Dhahbi, Treatment of textile plant effluent by ultrafiltration and/or nanofiltration for water reuse, Desalination, 222 (2008), 263-271.

[143] A. Cassano, J. Adzet, R. Molinari, M.G. Buonomenna, J. Roig, E. Drioli, Membrane treatment by nanofiltration of exhausted vegetable tannin liquors from the leather industry, Water Research, 37 (2003), 2426-2434.

[144] P. Rai, G.C. Majumdar, V.K. Jayanti, S.D. Gupta, S. De, Alternative pretreatment methods to enzymatic treatment for clarification of mosambi juice using ultrafiltration, Journal of Food Process Engineering, 29 (2006), 202-218.

References

[145] A. Zirehpour, M. Jahanshahi, A. Rahimpour, Unique membrane process integration for olive oil mill wastewater purification, Separation and Purification Technology, 96 (2012), 124-131.

[146] R. Jiraratananon, A. Chanachai, A study of fouling in the ultrafiltration of passion fruit juice, Journal of Membrane Science, 111 (1996), 39-48.

[147] V.B. Briao, C.R.G. Tavares, Pore blocking mechanism for the recovery of milk solids from dairy wastewater by ultrafiltration, Brazilian Journal of Chemical Engineering, 29 (2012), 393-407.

APPENDIX

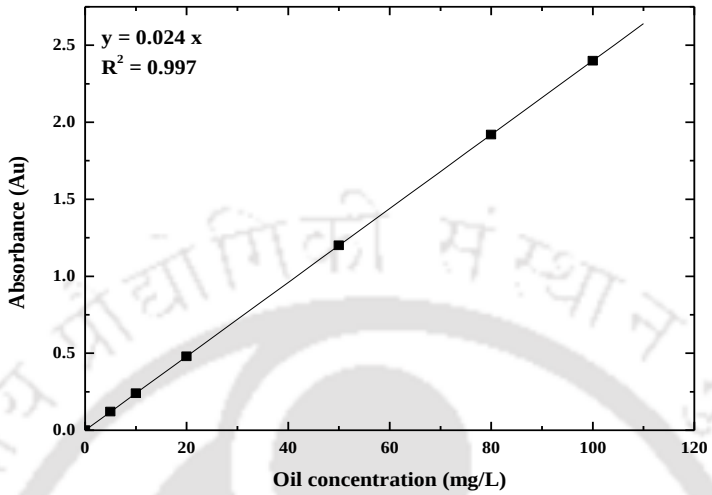

Figure A1. Calibration curve for determination of oil concentration.

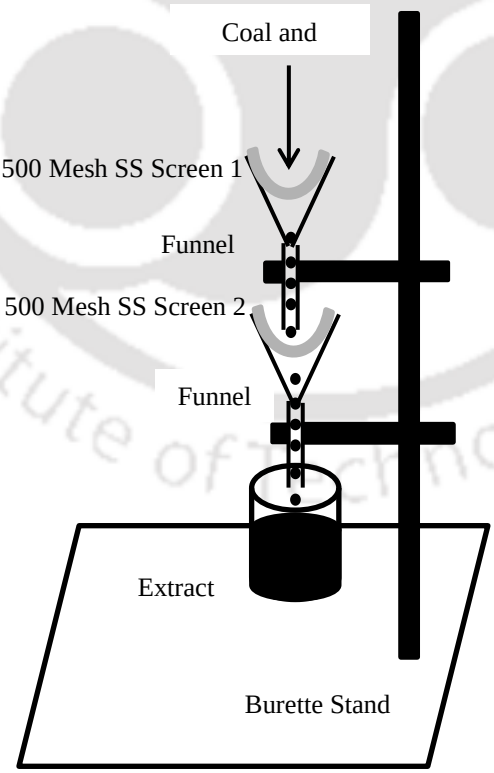

Figure A2: Extract filtration through stainless steel meshes.

Appendix

Reynolds number calculation for spiral wound membrane

Reynolds No for spiral wound membrane is estimated by using the Eq. (1), **[1A]**

$$\mathrm{Re} = \frac{\rho d_h u}{\mu} \tag{A1}$$

Hydraulic diameter (d_h) is defined as:

$$d_h = \frac{4\varepsilon}{(2/h)+((1-\varepsilon)S_{V,SP}} \tag{A2}$$

where,

ϵ is membrane channel porosity, $S_{V,SP}$ is specific surface of the spacer (m^{-1}) and h is membrane channel height.

Reynolds Number Calculation for Packed Column

The Reynolds No is defined as: [**2A**]

$$\mathrm{Re} = \frac{D_p V_s \rho}{(1-\varepsilon)\mu}$$

where

Re : Reynolds No

D_p : Equivalent diameter of particle (Glass beads 1 m, and molecular sieve 0.7 m)

V_s : Superficial velocity (Q/A)

Q : Volumetric flow rate

A : Cross sectional area of column (0.031557 m^2)

ρ : Density of mosambi juice (1100 kg/m^3)

μ : Viscosity of mosambi juice (3.30 kg/m.s)

ϵ : Void fraction of bed (0.68 for glass beads and 0.57 for molecular sieve)

For Glass Beads

Table A1. Calculation of Reynolds number for glass bead loaded packed bed

Sl.No.	Volumetric flow rate (cm^3/s)	Superficial velocity (m/s)	Reynolds No
1	50	4.39×10^{-7}	0.45
2	100	8.77×10^{-7}	0.91
3	200	1.75×10^{-6}	1.83
4	300	2.63×10^{-6}	2.74
5	400	3.50×10^{-6}	3.65
6	500	4.39×10^{-6}	4.57

For Molecular Sieve

Table A2. Calculation of Reynolds number for molecular sieve loaded packed bed

Sl.No.	Volumetric flow rate (cm^3/s)	Superficial velocity (m/s)	Reynolds No
1	50	4.39×10^{-7}	0.34
2	100	8.77×10^{-7}	0.68
3	200	1.75×10^{-6}	1.36
4	300	2.63×10^{-6}	2.04
5	400	3.50×10^{-6}	2.72
6	500	4.39×10^{-6}	3.40

Reference

[1A] Q. Yang, A. Drak, D. Hasson, R. Semiat, RO module RTD analyses based on directly processing conductivity signals, Journal of Membrane Science, 306 (2007), 355-364.

[2A] Perry's Chemical Engineers Handbook, McGraw-Hill, New York, Seventh Edition, 1997.

List of Publications from this Work

- **V. Singh**, M.K. Purkait, C. Das, Cross flow microfiltration of industrial oily wastewater: experimental and theoretical consideration, **Separation Science and Technology**, 46 **(**2011), 1213-1223.
- **V. Singh**, M.K. Purkait, V.K. Chandaliya, P.P. Biswas, P.K. Banerjee, C. Das, Development of membrane based technology for the separation of coal from organic solvent, **Desalination**, 299 (2012), 123-128.
- **V. Singh**, C. Das, Clarification of synthetic juice through spiral wound ultrafiltration module at turbulent flow region and cleaning study, **International Journal of Chemical Science and Engineering**, 7 (1) (2013), 945-949.
- **V. Singh**, P.K. Jain, C. Das, Performance of spiral wound ultrafiltration membrane module for with and without permeate recycle: Experimental and theoretical consideration, **Desalination**, 322 (2013), 94-103.
- **V. Singh**, C. Das, Comparison of spiral wound UF membrane performance between turbulent and laminar flow regimes, **Desalination** 337 (2014), 43-51.

Communicated

- **V. Singh**, N.K. Meena, A.K. Golder, C. Das, Fabrication of cost effective iron ore slime ceramic membrane for the recovery of organic solvent used in coke production, **Fuel** (Under review).
- **V. Singh**, C. Das, Detailed pretreatment studies for the clarification of mosambi juice, **Journal of Food Engineering** (Under review).

International Conferences

- **V. Singh**, M.K. Purkait, C. Das, “Ultrafiltration of oily wastewater" International conference of separation processes (ICSP-2009), 20-22nd Oct, 2009, IT BHU, Varanasi, India.

List of Publications

- **V. Singh**, C. Das, "Pretreatment of Mosambi juice by packed column and comparison with other methods", International Conference and Exhibition on Food Processing and Technology, 22-24th November, 2012 Hyderabad, India.
- **V. Singh**, C. Das, "Utilization of non-coking coal for the development of dense ceramic membrane", 4th International conference on Recent Advances in Composite Materials (ICRACM 2013), 18-21st February, 2013, Indian Institute of Technology, BHU.
- **V. Singh**, A. Saurav, C. Das "Membrane based separation of mosambi juice and it's degradation behaviour study during storage" Accepted in International Conference on Frontiers in Chemical Engineering (ICFCE-2013), December 9-11th, 2013, NIT Rourkela, Odisha, India.

National Conferences

- **V. Singh**, M.K. Purkait, C. Das, "Treatment of Industrial Wastewater by Membrane Separation Technology" Indian Chemical Engineering Congress (CHEMCON-2009), 27-30th December, 2009, Andhra University, Visakapattanam, India.
- **V. Singh**, M. K. Purkait, C. Das, "Low cost ceramic membrane prepared from iron ore slime" Indian Chemical Engineering Congress (CHEMCON-2010), 27-29th December, 2010, Annamalai University, Tamilnadu, India.
- **V. Singh**, N.K. Meena, A.K. Golder, C. Das, "Improvement of coal properties using organic solvent" Indian Chemical Engineering Congress (CHEMCON-2010), 27-29th December, 2010, Annamalai University, Tamilnadu, India.
- **V. Singh**, C. Das, "Study of different pretreatment methods for the clarification of mosambi juice" Indian Chemical Engineering Congress (CHEMCON-2011), 27-29th December, 2011, M S Ramaiah Institute of Technology, Bangalore, India.
- **V. Singh**, C. Das, "Study the Cleaning Performance for UF Module in Spiral Wound Membrane Fouled with Synthetic Juice" Indian Chemical Engineering Congress (CHEMCON-2012), 27-30th December, 2012, Dr. B.R. Ambedkar National Institute of Technology, Jalandhar, India.

- **V. Singh**, H. Rathore, A.K. Golder, C. Das "Fouling and cleaning performance of spiral wound reverse osmosis membrane module" Reflux 01, Annual Technical Festival, 6-7th April 2013, Dept. of Chemical Engg. IIT Guwahati, India.
- **V Singh**, S T Bhutia, C Das, "Spiral wound ultrafiltration treatment of synthetic fruit juice", Accepted in Indian Chemical Engineering Congress (CHEMCON-2013), 27-29th December, 2013, ICT, Mumbai, India.